NUCLEOSOME EPITOPES INFLUENCE THE ACTIVITY OF CHROMATIN REMODELERS

by
Robert F. Levendosky

A dissertation submitted to Johns Hopkins University in conformity with the requirements for the degree of Doctor of Philosophy

Baltimore, Maryland
January, 2019

Abstract

The association of DNA and histone proteins in the eukaryotic nucleus, called chromatin, impacts diverse aspects of biology including transcription, replication, and cell differentiation. The fundamental unit of chromatin is the nucleosome, in which DNA coils around a symmetric octamer of histones. Chromatin organization is maintained and modulated by molecular motors called chromatin remodelers, which guide the assembly, disassembly and repositioning of nucleosomes. As essential regulators of chromatin structure, chromatin remodelers are sensitive to different features of their nucleosome substrates, and in this dissertation I report on my work to characterize the actions of two chromatin remodelers called Chd1 and SNF2h.

By operating on alternating sides of the symmetric nucleosomes, both Chd1 and SNF2h can sense asymmetry in DNA flanking nucleosomes, and slide nucleosomes back and forth to form evenly spaced nucleosome arrays. Analogous to this spacing behavior, *in vitro*, Chd1 and SNF2h slide mononucleosomes away from DNA ends. Besides differences in flanking DNA lengths, nucleosomes can also contain asymmetries in histone content, mutations or modifications, and here I address how these asymmetries affect remodeler activity. Previously, the two-fold nucleosomal symmetry has complicated this endeavor, but I discovered a method for generating well-defined and oriented asymmetric nucleosomes containing histone mutations on one specific side. Using this tool, I demonstrated that asymmetric disruption of certain nucleosomal epitopes disfavors activity from one side of the nucleosome, promoting unidirectional sliding toward DNA ends.

In addition to sliding nucleosomes, Chd1 can unwrap DNA from the nucleosome edge. Using fluorescence techniques, I showed that the nucleotide state of Chd1 and the DNA

sequence influence the degree of unwrapping. I also explored various fluorescence techniques for monitoring nucleosome sliding, and here I describe how competing fluorescence effects and nucleosome unwrapping influence interpretations of sliding experiments. Finally, in collaboration with a single-molecule group, we leveraged these techniques and my experience with nucleosomes to developed a scheme to simultaneously monitor DNA movement on both sides of the nucleosome. An exciting outcome of this work was our discovery that Chd1 pulls between 1-4 bp of DNA onto the nucleosome prior to DNA exiting the other side.

Robert F. Levendosky

Thesis committee:

Gregory D. Bowman (advisor and primary reader)

Sua Myong (second reader)

Elijah Roberts

Evangelos Moudrianakis

Preface

This dissertation is the original work of Robert F. Levendosky and is based on research performed as a graduate student in the Laboratory of Gregory D. Bowman at Johns Hopkins University from 2014-2018. Portions of Chapter 2 have been published in Levendosky et al., 2016 and Qiu et al., 2017. A portion of Chapter 3 has been published in Tokuda et al., 2018. Data presented in Chapter 5 has been submitted to *Nature Communications* and is under review.

Acknowledgements

During my pursuit of a doctorate, I have been fortunate to receive support and encouragement from family, friends and colleagues. I am extremely grateful for the opportunity to practice and develop my understanding of the scientific discipline. This transformative experience has completely changed my perspective and deepened my love of science. Yet, it has been hard, and I could not have gotten through this alone.

First, I need to thank my parents for their unconditional love and support. They fostered my love of learning about the natural world. I grew up with my mother rattling off the names of birds, trees and flowers. My father, a science teacher, was always excited to explain some aspect of chemistry or physics. He showed me how to make electric motors from paper clips and wire, and we built a Van de Graaff generator together. Mom and Dad, you taught me that science was fun and exciting.

I want to thank my brother and sisters for being there when I needed an extra hand, an ear to bend or a shoulder to cry on. Susie, Ted and Kate, your counsel and friendship have helped to keep me sane these last few years. I love you guys. And Ted, you're like a brother to me.

I wish to thank the staff, students and community of Johns Hopkins University for welcoming me and creating a positive environment in which to learn and work. In particular, I want to thank the program in Cellular, Molecular, Developmental Biology and Biophysics (CMDB aka the biology program) for taking a chance on an unusual student (but everything worked out pretty well). I also wish to thank the Program in Molecular Biophysics, which has been my adopted home.

I especially want to thank all the members of the Bowman Lab, past and present. Greg, thank you for welcoming me into your lab. I appreciate how you immediately started brainstorming with me, allowing me to see your thought process. You have been a great mentor and collaborator, setting a good example in your work ethic and scientific rigor. I thoroughly enjoyed our discussions. Ilana, thank you for training me and for offing continued advice and guidance through the years. Kyle, it was great to get to know you before you graduated. I learned a lot from watching you, and we had some laughs too. Jessica, we started the same year and I talked you into rotating in the Bowman lab. Hopefully you don't fault me, but it sure was nice to have another student in the lab. We were lucky to have each other to brainstorm with, laugh with, and commiserate. You have been a valuable companion the last five years and I wish you good luck.

I wish to thank the Laboratories of Sua Myong, Sarah Woodson, Geeta Narlikar, Sebastian Deindl, Lois Pollack and Cynthia Wolberger for collaboration, reagents and advice. I also want to thank the Center for Molecular Biophysics and Katie Tripp for instrument use and technical advice.

I want to thank the members of my thesis committee, past and present: Sua Myong, Elijah Roberts, Van Mourianakis, Bertrand Garcia-Moreno and Xin Chen.

To my kids, Jaya and Xander, thanks for believing in your dad. You guys offered a wonderful escape from my academic pressures, a chance to feel connected, and get a little oxytocin boost from some snuggles. You two have asked some of the most difficult questions ever posed to me, but I love it. Keep asking! Jaya, when you were born, you inspired me to go back to school, and your work ethic still inspires me. Xander, you were just six months old when I started grad school, so watching you grow has been a constant reminder of how long this

endeavor has taken. But seriously, when I see how positively you both respond to watching me work hard to become a scientist, I know I made the right choice to pursue a PhD. I look forward to watching you both grow up. I am so proud of you both.

And last, but certainly not least, I am eternally grateful for my wonder wife. Mette, you are my love, my partner; and we make a pretty great team. I am constantly amazed by what a caring, supportive person you are. You inspire me to be a better person. Obviously, I couldn't have made it through graduate school without you, but you made it enjoyable. I love you, and I look forward to raising these wonderful children you have given me. But first, you need to read my whole dissertation. Enjoy!

Table of Contents

List of Figures

Chapter 1: Introduction

Overview

In this introductory chapter, I present some basic concepts to establish a context for the research presented in this dissertation and convey its relevance to biology. I begin with a brief explanation of chromatin and its roles in eukaryotic biology. The structure and features of the fundamental unit of chromatin, the nucleosome, is discussed. Chromatin remodelers maintain the characteristic positioning of nucleosomes found within genes. Current thoughts on higher order chromatin structure and how that may relate to nucleosome positioning are examined. Finally, I introduce the Chd1 chromatin remodeler that is the focus of much of this dissertation, and describe its features and current ideas about its regulation and activity.

Chromatin is a central factor in eukaryotic biology

Within the eukaryotic nucleus, DNA associates with histone proteins to form a complex referred to as chromatin. Chromatin facilitates the packaging of roughly two meters of DNA into a nucleus only 6 μm wide. Although such compaction seems daunting, since the DNA is only two nm wide, with perfect packing the volume of the DNA would fill less than ten percent of the nuclear volume. Instead, the stiffness of the DNA (Brinkers et al., 2009) and self-repulsion of the negatively charged DNA phosphate backbone poses greater problems by limiting how much DNA folds back upon itself (Bloomfield, 1996). To overcome these challenges, the negatively charged DNA is associated with positively charged histone proteins that form tightly coiled structures in chromatin.

In addition to compacting the eukaryotic genome into the nucleus, chromatin presents a scaffold for epigenetic information, playing a role in transcription, replication and DNA repair.

The organization of chromatin is a critical link in the chain connecting the genome to phenotype and this connection remains a focus of biological investigation. The fundamental unit of chromatin is the nucleosome, in which DNA is wrapped tightly around histone spools. By occluding access to the DNA, the nucleosome is primarily a repressive element, and the organization and modification of nucleosomes within genes help guide proper gene expression, for example, by defining the transcription start site.

The structure of the nucleosome

The distinctive structure of the nucleosome underlies every aspect of chromatin, from DNA charge neutralization to how chromatin factors access DNA. At the core of the nucleosome the histone octamer is composed of a central tetramer of $(H3/H4)_2$ flanked by two H2A/H2B heterodimers (Moudrianakis and Arents, 1993). The nucleosome is composed of 145-147 bp of DNA tightly wound ~1 ⅔ times around an octamer of histone proteins containing two copies each of H2A, H2B, H3 and H4 (Luger et al., 1997) (Figure 1.1). During nucleosome assembly by salt dialysis or histone chaperones, the tetramer is first deposited on the DNA, followed by one H2A/H2B heterodimer, and then the other (Böhm et al., 2011; Hansen et al., 1991; Mazurkiewicz et al., 2006). The histone core of the nucleosome forms a positively charged ramp that guides the DNA into a left handed superhelix. The DNA is held in place by strong histone-DNA contacts every ~10 bp where basic arginine residues protrude into the DNA minor groove. The nucleosome is symmetric about a central dyad axis that runs through the central DNA base pair and bisects the interface of the two H3 histones in the tetramer. To provide points of reference, the nucleosomal DNA is divided into sections demarcated by superhelical locations (SHLs) where the major groove faces in towards the histone octamer. The numbering emanates out from the central dyad (SHL 0) in either direction to the edge of the nucleosome (SHL ±7).

Other than serving as a protein spool for DNA, the histones form an epigenetic scaffold with key features for regulating chromatin compaction and transcriptional accessibility. Beyond the core nucleosome, histone tails extend to interact with linker DNA, chromatin factors and other nucleosomes. *In vivo*, the tails are heavily modified with moieties with the most common being acetylation, methylation, phosphorylation, and ubiquitination, among others (Bannister and Kouzarides, 2011; Wozniak and Strahl, 2014). These post translational modifications (PTMs) can both serve as epitopes recognized by specific chromatin readers and also alter physical properties of the nucleosome, affecting how tightly DNA wraps around the histone core and the compaction of chromatin (Bowman and Poirier, 2015). For example, acetylation of lysine residues removes a positive charge and generally promotes more open chromatin. One mode of chromatin compaction relies on association of a basic stretch of the H4 N-terminal tail (H4-tail) with the nucleosome acidic patch on H2A/H2B of adjacent nucleosomes (Kalashnikova et al., 2013). The acetylation of H4 K16 disrupts this interaction, which interferes with the packing of chromatin strands (Dorigo et al., 2003; Shogren-Knaak et al., 2006).

While nucleosomes are usually found with the full complement of histones, there is evidence for subnucleosomal species. Genomic chromatin immunoprecipitation-exonuclease (ChIP-exo) experiments reveal nucleosome sites where some histones are not pulled down, suggesting the presence of nucleosome constructs that are missing histones (Rhee et al., 2014) or sites where chromatin factors are disrupting DNA-histone contacts (Ramachandran et al., 2015). The hexasome, missing one of the H2A/H2B heterodimers, wraps only ~110 bp of DNA (Arimura et al., 2012; Levendosky et al., 2016). Hexasomes missing the downstream H2A/H2B heterodimer are found in the wake of transcription by RNA polymerase II (Kireeva et al., 2002). These post-transcriptional hexasomes may not be very long lived *in vivo* due to rapid

replacement of H2A/H2B by the FACT complex (Hsieh et al., 2013). Though hexasomes are a necessary intermediate in nucleosome assembly (Bohm et al., 2011), it is not known if hexasomes persist in the cell or what role they play in chromatin structure and regulation. As suggested in **Chapter 2**, hexasomes may contribute to packing of nucleosomes up against the transcription start site (Levendosky et al., 2016).

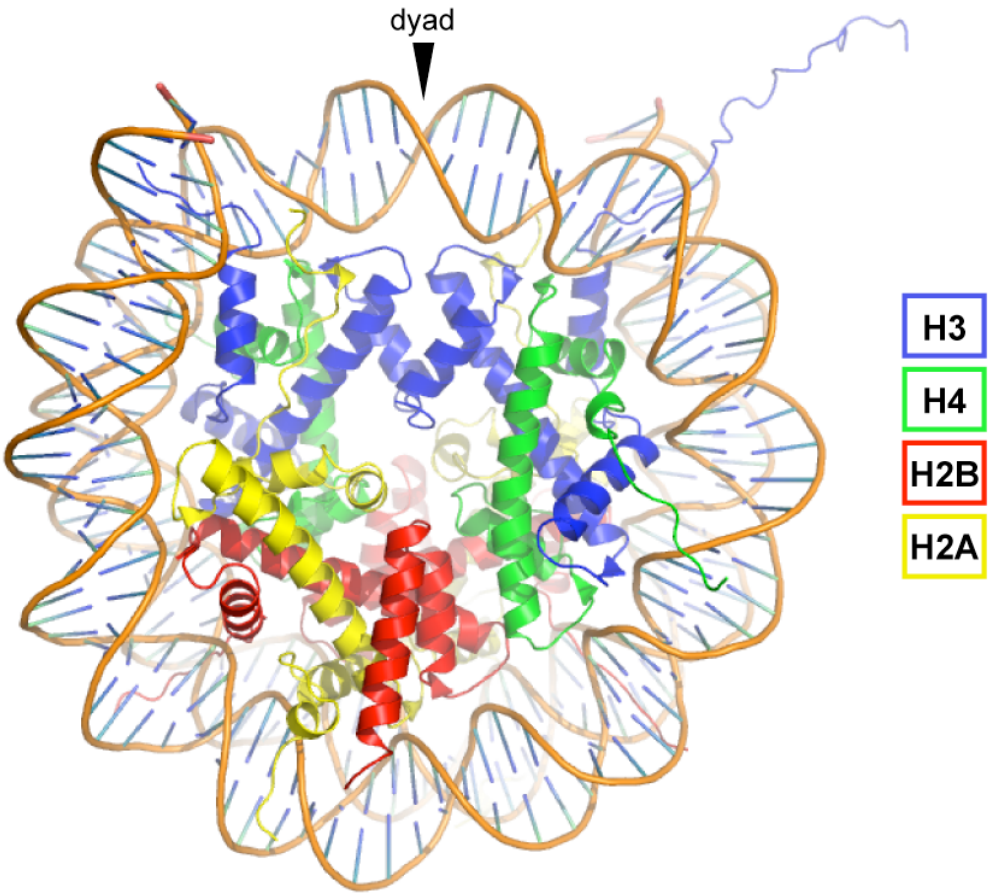

Figure 1.1: The crystal structure of the nucleosome
In this structure of the nucleosome, 146 bp of DNA (orange) wrap an octamer of histones. The dyad bp is indicated (black triangle).
pdb: 1AOI (Luger et al., 1997)

Nucleosome positioning is determined by both DNA sequence and chromatin remodelers

The organization of nucleosomes in gene bodies is important for defining promoters and the transcription start site (TSS). Promoters are characterized by a 5' nucleosome free region (NFR) flanked by two well-positioned nucleosomes. The downstream nucleosome, known as the +1 nucleosome, overlaps the TSS and often contains the histone variant H2A.Z and ubiquitination of H2B (Rhee et al., 2014) and acetylation of H3 and H4 (Reinke et al., 2001). Beyond the TSS an array of evenly spaced nucleosomes covers the rest of the gene with the orderly phasing of nucleosome positions decreasing towards the 3' end, where another 3' NFR is thought to facilitate transcription termination (Mavrich et al., 2008). Disruption of this organization of nucleosomes can lead to leaky transcription resulting in developmental defects and cancer (Bagchi et al., 2007; Gao et al., 2008; Huang et al., 2011; Liu et al., 2012).

Nucleosome occupancy is affected by both DNA sequence and active positioning by ATP-dependent motor proteins called chromatin remodelers. DNA sequence plays a large role in nucleosome positioning with histones preferentially depositing on regions of curved DNA (Lowary and Widom, 1997). Accordingly, the NFR is often rich in stiff poly dA:dT stretches that exclude nucleosomes. Computational studies based on the deformation energy of specific DNA sequences bending around the histone core are capable of predicting nucleosome placement with great accuracy (Cui and Zhurkin, 2010). However, while deposition of histones onto yeast genomic DNA by salt gradient dialysis approximately reproduces the NFR, +1 and -1 nucleosomes, it does not accurately reproduce the evenly-spaced nucleosome arrays observed *in vivo* (Zhang et al., 2011). Instead, ATP-dependent remodelers are necessary to maintain nucleosome arrays (Gkikopoulos et al., 2011).

ATP-dependent remodelers help establish and maintain nucleosome organization. Remodelers all share an SF2 helicase-like ATPase and are broadly categorized into four primary families based on domain architecture: SWI/SNF, ISWI, CHD, and INO80 (Clapier and Cairns, 2009; Flaus et al., 2006). Different families of remodelers have specialized functions. The SWI/SNF remodeling complex catalyzes the eviction of nucleosomes by sliding adjacent nucleosomes together (Dechassa et al., 2010; Gkikopoulos et al., 2009). Another SWI/SNF remodeler, Remodels Structure of Chromatin (RSC), maintains the NFR by destabilizing nucleosomes on poly dA:dT regions and actively maintaining the position of the +1 nucleosome (Kubik et al., 2018; Lorch and Kornberg, 2015; Lorch et al., 2018). RSC sliding is inhibited by acetylation of the +1 nucleosome, which indicates that RSC may be holding the +1 nucleosome in place (Lorch et al., 2018). The related SWR1 and INO80 remodeling complexes catalyze the deposition and removal of H2A.Z, respectively (Brahma et al., 2017; Gerhold and Gasser, 2014; Mizuguchi et al., 2004). INO80 is also capable of positioning the +1 nucleosome (Krietenstein et al., 2016). Chd1 and ISWI remodelers both slide nucleosomes to space them ~160-170 bp apart in nucleosome arrays (Gkikopoulos et al., 2011), and have been shown to assemble nucleosomes *in vitro* (Lusser et al., 2005). Thus a variety of remodelers contribute to nucleosome localization, but how remodelers are regulated to perform these functions is not understood.

Higher-order chromatin structure

Arrays of nucleosomes along DNA, like beads on a string, represent the primary structure of chromatin; the 10 nm fiber (Olins and Olins, 2003). Beyond this, the secondary structure of chromatin must involve additional interactions within and/or between 10 nm fibers as they coil and fold back across themselves, but what form this takes is a subject of debate (Hansen et al., 2018; van Holde and Yager, 1985; Maeshima et al., 2010; Tremethick, 2007). The term higher-

order chromatin structure is used liberally in the literature to represent a more condensed and repressive form of chromatin. Nucleosome arrays and linker histones are both credited with facilitating the formation of higher order chromatin structures. But what is higher order chromatin?

It has been proposed that multiple 10 nm fibers come together to form the 30 nm chromatin fiber (Grigoryev and Woodcock, 2012), which then compact further to create the mitotic chromosome. The 30 nm fiber was first observed in chromatin spreading assays (Gall, 1966), and it stood to reason that this structure represented an intermediate sub-structure between the 10 nm fiber and condensed chromatin. By modulating ionic conditions, the condensation of 10 nm fibers into 30 nm fibers has been observed by electron microscopy (Huynh et al., 2005; Robinson et al., 2006; Song et al., 2014) and sedimentation experiments (Hansen, 2002) The structure of the 30 nm fiber has been modeled as a one start solenoid or a two start zigzag (Dorigo et al., 2004; Grigoryev et al., 2009) with the two start model supported by EM structures and the crystal structure of the tetra nucleosome (Schalch et al., 2005; Song et al., 2014).

So the 30 nm fiber can form under certain conditions, but are these biologically relevant? The 30 nm fiber has been conspicuously absent from EM experiments performed *in situ* (Eltsov et al., 2008; McDowall et al., 1986). Smaller clusters of nucleosomes resembling the tetranucleosome were visible, but no extended 30 nm fibers were evident (Ou et al., 2017). In oligonucleosome sedimentation assays, nucleosome arrays titrated with Mg^{2+} oligomerize as the divalent ions neutralize the negatively charged DNA and promote chromatin compaction. Removal of the histone tails prevent oligomerization even at high Mg^{2+} concentrations (Schwarz et al., 1996) and histone tails participate additively during this self association (Gordon et al., 2005). These observations indicate that nucleosome arrays are intrinsically self-interacting.

Species consistent with 30 nm fibers form at Mg^{2+} concentrations below 2 mM (Schwarz and Hansen, 1994; Schwarz et al., 1996). Larger structures of heterogeneous size form at higher, more physiologically relevant Mg^{2+} concentrations (Hansen, 2002; Schwarz et al., 1996). From these experiments, it was not clear whether the larger oligomers were composed of individual self-associating 30 nm fibers or if another structure formed from the oligonucleosomes. SAXS experiments revealed the heterogeneous larger structures to be globular and found no evidence of the 30 nm fiber (Maeshima et al., 2016). These results indicate that instead of being made up of a rigid hierarchy of nesting structures, chromatin is more of a molten-globule or polymer-melt of interdigitated 10 nm fibers that associate through interactions involving the histone tail (Hansen et al., 2018). Even spacing of nucleosomes by chromatin remodelers would be expected to facilitate the interdigitation of nucleosomes between parallel 10 nm fibers.

Chd1 is self regulated to slide nucleosomes away from barriers

Our lab studies the regulation and activity of chromatin remodelers and how they sense and respond to nucleosome features. We primarily study the monomeric yeast Chd1 remodeler that, like ISWI remodelers, preferentially moves nucleosomes away from barriers such as other nucleosomes and DNA binding proteins. In this way, Chd1 contributes to generating evenly spaced nucleosome arrays *in vivo*. *In vitro,* Chd1 also slides mononucleosomes away from DNA ends, creating a distribution of nucleosome positions near the center of short DNA fragments (Levendosky et al., 2016; McKnight et al., 2011; Nodelman et al., 2017; Stockdale et al., 2006).

While the molecular mechanism by which Chd1 can slide and space nucleosomes is not completely understood, some pieces of the puzzle are coming together. Chd1 and other remodelers contain a conserved helicase-like ATPase composed of two RecA-like domains (Figure 1.2). The ATPase motor uses energy from ATP hydrolysis to translocate primarily along

one strand (called the tracking strand) of dsDNA in the 3' to 5' direction (Nodelman et al., 2017; Saha et al., 2005). The motor most likely operates as a Brownian ratchet, using energy from ATP hydrolysis to impart directionality to random thermal fluctuations. As predicted by previous studies (Nodelman et al., 2017; Saha et al., 2005), recent cryo-EM structures of remodelers bound to the nucleosome show the ATPase motor positioned at SHL 2 (Farnung et al., 2017; Li et al., 2017; Sundaramoorthy et al., 2018) (Figure 1.3). From this position, Chd1 and other remodelers pull DNA on one side of the nucleosome and push it out the other. Though there are different models for how remodelers can catalyze the propagation of DNA around the nucleosome (discussed in **Chapter 5**), I favor the twist-diffusion model in which DNA moves around the nucleosome in a corkscrewing motion, which maintains the orientation of the major and minor groove locations around the histone core during movement (van Holde and Yager, 1985). This model makes the role of the remodeler motor very simple: it is a DNA translocase. During translocation, the remodeler winds around the DNA minor groove. Based on available structures (Farnung et al., 2017; Li et al., 2017; Sundaramoorthy et al., 2018) and from biochemical studies that used ssDNA gaps in the tracking strand to restrict ATPase movement (McKnight et al., 2011; Saha et al., 2005), the ATPase motor is oriented at SHL 2 to move away from the nucleosome dyad. The motor winds around the DNA and bumps up against the face of the histone core, pushing the octamer forward and driving DNA back towards the dyad.

The activity of the Chd1 motor is regulated by twin N-terminal chromodomains and a C-terminal SANT/SLIDE DNA binding domain (DBD) (Delmas et al., 1993; Marfella and Imbalzano, 2007; Ryan et al., 2011) (Figure 1.2**A**). The chromodomains increase substrate specificity by auto inhibiting the ATPase motor when Chd1 is not bound to the nucleosome. In the crystal structure of the isolated chromodomain-ATPase unit, the chromodomains lie across

the two lobes of the ATPase, appearing to hold them in an open, inactive conformation that would not be conducive to ATP hydrolysis (Hauk et al., 2010). In this arrangement, an acidic wedge from the chromodomains (chromo-wedge) contacts a basic surface of lobe two of the ATPase. In cryo-EM structures of an active conformation of Chd1 bound to the nucleosome, the chromodomains are displaced and the basic surface of lobe two closes around the DNA (Farnung et al., 2017). In this state, the basic H4-tail contacts an acidic region on the back of lobe two, which most likely stabilizes the active state of the remodeler, explaining the requirement for the H4-tail for full activity (Farnung et al., 2017; Ferreira et al., 2007; Hauk et al., 2010). This rearrangement suggests that the chromo-wedge prevents the lobes from closing when not bound to the nucleosome. Mutations of the chromo-wedge result in higher ATPase activity on naked DNA than WT Chd1 and partially rescue sliding on nucleosomes with H4-tail truncations (Hauk et al., 2010) or hexasomes missing one H2A/H2B heterodimer (discussed in **Chapter 2**). The chromodomains are not entirely repressive however, and deletion of the entire domain results in poor sliding (Hauk et al., 2010). This may be due to interactions between the chromodomains and DNA at SHL 1 that could promote binding (Farnung et al., 2017; Nodelman et al., 2017; Sundaramoorthy et al., 2018).

The Chd1 DBD plays essential roles in tethering Chd1 to nucleosomes and sensing linker DNA. The Chd1 DBD contributes to nucleosome sliding by tethering the remodeler to linker DNA adjacent to the nucleosome (McKnight et al., 2011; Patel et al., 2013). Without the DBD, Chd1 remodels poorly, yet this activity can be rescued by fusing another DNA binding protein in place of the DBD, indicating that tethering represents a significant role for the DBD (McKnight et al., 2011; Patel et al., 2013). When tethered directly to histones, Chd1 readily slides nucleosomes off DNA ends without regard for linker DNA, confirming the DBD's role in linker

sensing and nucleosome spacing (Patel et al., 2013). Since linker DNA typically emanates from both sides of the nucleosome, the DBD can either bind to DNA that is entering or exiting the nucleosome due to activity of the ATPase at SHL 2. Thus, two distinct arrangements are possible for Chd1: one with the DBD bound to the entry side DNA, on the same DNA gyre but across the face of the nucleosome disc from where the ATPase is active; and the other with the DBD bound to the exit side DNA, on the opposite DNA gyre but close in space to the ATPase (Figure 1.2**B**). Extensive crosslinking experiments (Nodelman et al., 2017) and recent cryo-EM structures revealed the cross-gyre arrangement in the presence of the ATP mimic ADP•BeF_3^- (Farnung et al., 2017; Sundaramoorthy et al., 2018) (Figure 1.3). Some class averages of negative stain and cryo-EM structures show two Chd1 remodelers bound to the nucleosome, one at each SHL 2 (Nodelman et al., 2017; Sundaramoorthy et al., 2018). In this cross-gyre conformation, the DBD contacts the regulatory chromodomains, which in turn contact the ATPase, suggesting that this arrangement may communicate the presence of linker DNA to the ATPase. To determine whether this cross-gyre interaction was stimulator or inhibitory, Chd1 ATPase activity was compared between nucleosomes with linker DNA on one side and both sides of the nucleosome (Nodelman et al., 2017). ATPase was significantly higher when linker DNA was only available to form the cross-gyre interaction on one side. This suggests that the cross gyre interaction is inhibitory. Mutations that disrupted the interface between the DBD and the chromodomains (Chd1 D1201A P1202A) resulted in similar ATPase activity regardless of linker DNA (Nodelman et al., 2017). This suggests this interface plays a role in communicating the presence of the DBD to the chromodomains, which then inhibit the ATPase. This concept also fits with earlier observations that the presence of a DNA binding protein on the exit side DNA, which would block association of the DBD, increased the rate of Chd1 sliding away from that site

(Nodelman et al., 2016). These results support a model in which, instead of being stimulated by entry DNA, Chd1 is inhibited by the presence of exit DNA.

In EM structures, Chd1 unwraps two turns of DNA from the exit side of the nucleosome (Farnung et al., 2017; Sundaramoorthy et al., 2017, 2018). The DBD is bound to the unwrapped DNA and appears to be driving this unwrapping, but as discussed in **Chapter 3**, the nucleotide state dependent conformations of the ATPase also affects unwrapping in the absence of the DBD (Tokuda et al., 2018), suggesting a key role for the ATPase motor.

Outline of research presented in this dissertation

In **Chapter 2**, I describe how hexasomes generated on the Widom 601 and 603 sequences are oriented to retain the lone H2A/H2B dimer on the TA-rich side of the sequence. I found that Chd1 requires the entry-side H2A/H2B dimer for robust activity and that the Chd1 chromodomains limit hexasome remodeling. The presence of ubiquitinated H2B on the entry side H2A/H2B promotes faster nucleosome sliding by Chd1.

In **Chapter 3**, I explore the use of various fluorescence techniques to monitor the unwrapping and sliding of nucleosomes. I find that Chd1 unwraps nucleosomes in a sequence and nucleotide-dependent manner. I note that certain labeling schemes can produce signals with convoluted fluorescence effects and present alternate strategies.

In **Chapter 4**, I probe how mutations in the nucleosome acidic patch on each side of the nucleosome affect remodeling by Chd1 and Snf2h. I find that Chd1 is sensitive to mutations in either or both acidic patches. Strikingly, SNF2h requires the entry-side acidic patch for robust remodeling and asymmetric acidic patch mutations lead to unidirectional sliding off DNA end.

Finally, in **Chapter 5,** I discuss the propagation of DNA around the histone octamer during remodeling by Chd1. Using a novel approach, my collaborators and I find that Chd1 pulls

entry DNA onto the nucleosome before pushing DNA off the exit. I conclude that 1-4 bp of DNA is transiently absorbed by the nucleosome during remodeling.

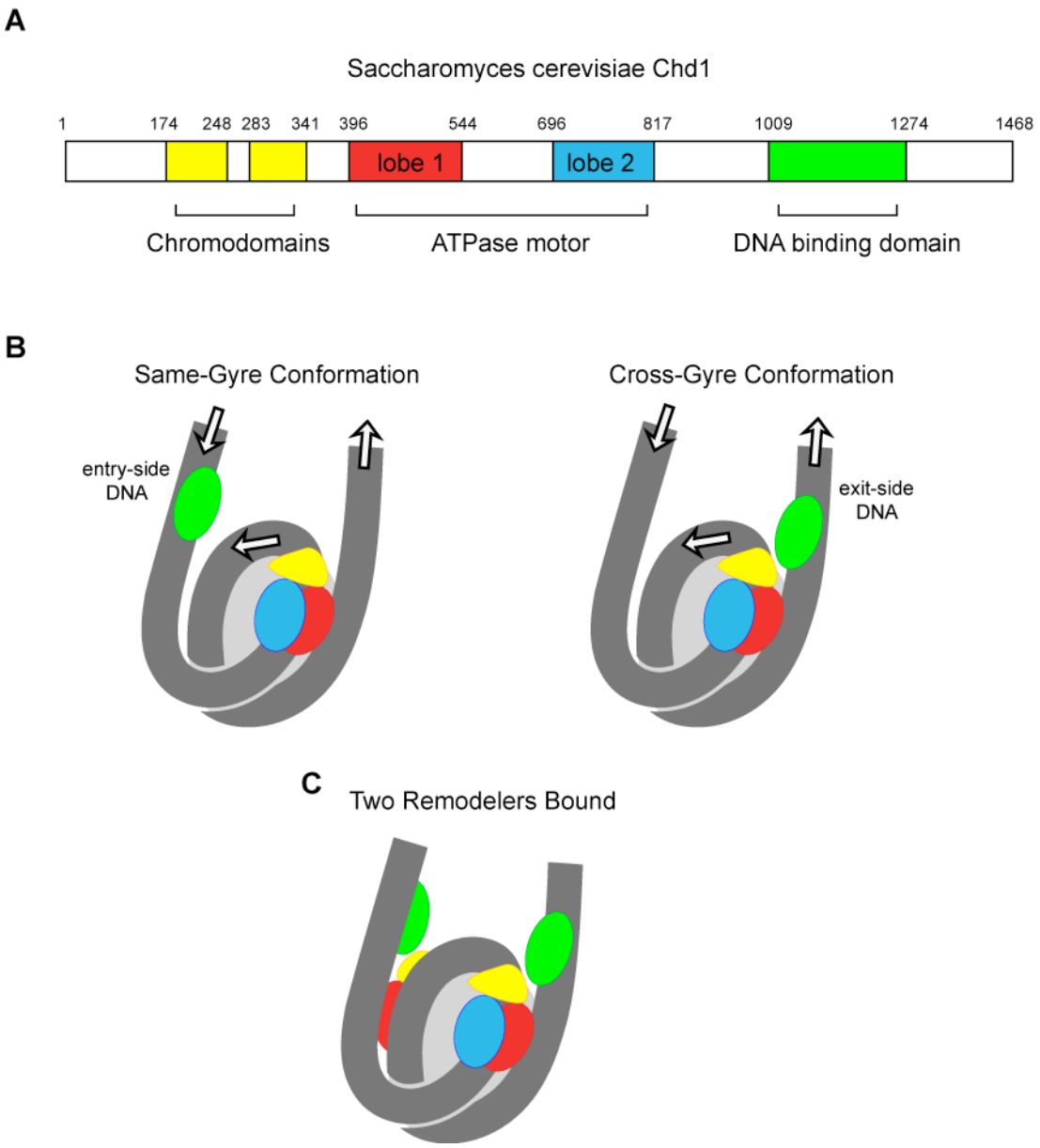

Figure 1.2: The Chd1 chromatin remodeler engages the nucleosome in various arrangements

(**A**) The domain architecture of full length Chd1 from Saccharomyces cerevisiae is depicted with the twin chromodomains (yellow), the two lobes of the ATPase motor (red and blue), and the DBD (Green).

(**B**) This cartoon shows the ATPase bound to the nucleosome at SHL 2 with the DBD either bound to the same gyre on entry DNA or to the opposite gyre on exit DNA. The arrows represent to movement of DNA catalyzed by the ATPase bound to this side of the nucleosome.

(**C**) This cartoon illustrates how two Chd1 remodelers can be bound to the nucleosome at the same time. In this arrangement, the activity of the remodelers on opposite SHL 2 sites would slide DNA in opposite directions.

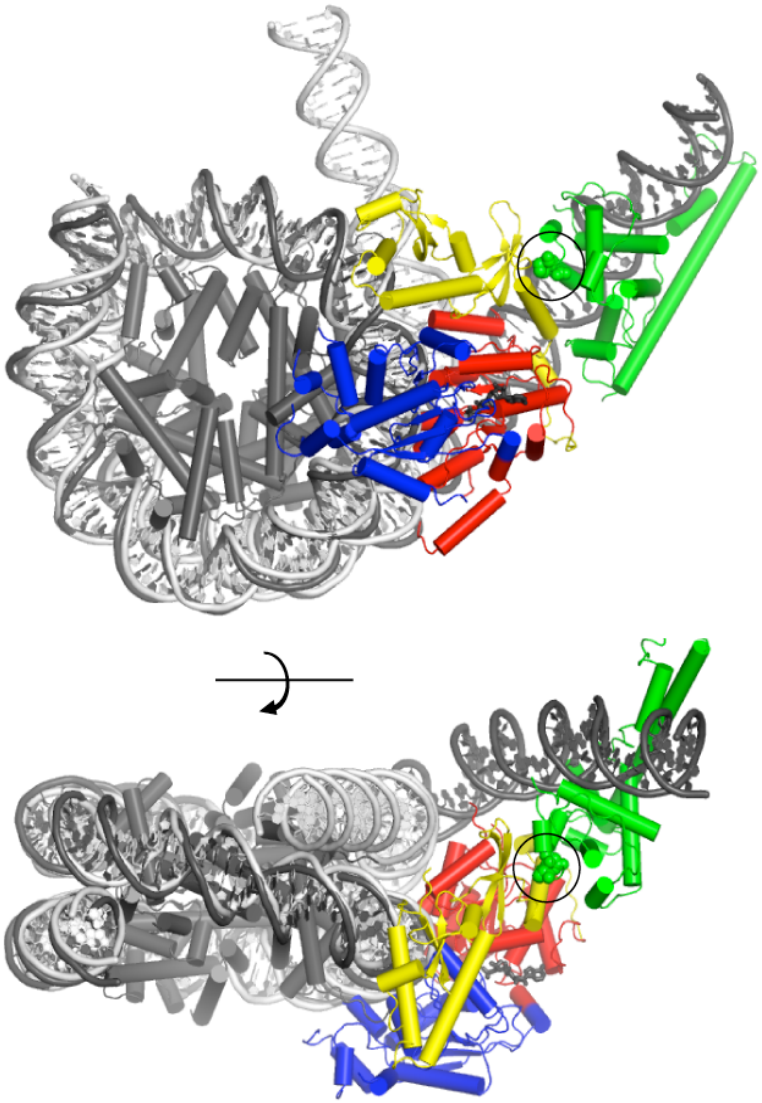

Figure 1.3: Chd1 unwraps DNA from the edge of the nucleosome
Cryo-EM structure of Chd1 bound to the nucleosome (black DNA and histones) is superimposed on DNA from the nucleosome crystal structure with linker DNA modeled on one side (white). The domains of Chd1 are colored as in Figure 1.2. The location of the DBD/chromodomains interaction is circled with the DBD residues that were mutated to disrupt this interface (D1201A P1202A) shown as spheres.
EM structure is from PDB code 5O9G (Farnung et al., 2018) and DNA crystal structure is based on PDB code PDB code 1KX5 (Davey et al., 2002)

Chapter 2: The Chd1 Chromatin Remodeler Moves Hexasomes Unidirectionally

ABSTRACT

Despite their canonical two-fold symmetry, nucleosomes in biological contexts are often asymmetric: functionalized with post-translational modifications (PTMs), substituted with histone variants, and even lacking H2A/H2B dimers. Here I show that the Widom 601 nucleosome positioning sequence can produce hexasomes in a specific orientation on DNA, which provide a useful tool for interrogating chromatin enzymes and allow for the generation of precisely defined asymmetry in nucleosomes. Using this methodology, I demonstrate that the Chd1 chromatin remodeler from *Saccharomyces cerevisiae* requires H2A/H2B on the entry side for sliding, and thus, unlike the back-and-forth sliding observed for nucleosomes, Chd1 shifts hexasomes unidirectionally. Chd1 takes part in chromatin reorganization surrounding transcribing RNA polymerase II (Pol II), and using asymmetric nucleosomes I show that ubiquitin-conjugated H2B on the entry side stimulates nucleosome sliding by Chd1. We speculate that biased nucleosome and hexasome sliding due to asymmetry contributes to the packing of arrays observed *in vivo*.

Most of the research in this chapter was originally published in Levendosky et al., 2016, with the exception of Figure 2.18, which was published in Qiu et al., 2017, and Figure 2.5 and Figure 2.19, which have not been published.

INTRODUCTION

As the repeating unit of chromatin, the nucleosome is the canvas upon which the epigenetic histone code is written. A fundamental characteristic of the histone code is the combinatorial diversity achieved from multiple marks, which may or may not reside on the same histone tail (Ruthenburg et al., 2007; Tee and Reinberg, 2014). Both through post-translational modifications (PTMs) and substitution of histone variants, additional chemical diversity arises from asymmetric modifications of nucleosomes. Since the nucleosome is pseudo-symmetric with two copies of each core histone (H2A, H2B, H3 and H4), asymmetry occurs when each copy possesses distinct epigenetic modifications. Recent advances have revealed asymmetry at the single nucleosome level (Rhee et al., 2014; Voigt et al., 2012), yet with challenges in synthesizing uniform populations of asymmetrically modified nucleosomes (Lechner et al., 2016; Liokatis et al., 2016), the biological significance of the vast majority of asymmetric marks remains unclear.

A dramatic example of asymmetry is the pairing of activating H3K4me3 and repressive H3K27me3 marks, known as bivalency (Voigt et al., 2013). Trimethylation of H3K27 is carried out by PRC2, and while H3K4me3 blocks modification of K27 on the same H3 tail, PRC2 can deposit a H3K27me3 mark on the opposing H3 tail of the same nucleosome (Lechner et al., 2016; Voigt et al., 2012). In addition to generating nucleosomes with asymmetric H3K4me3/H3K27me3, PRC2 is also activated by the mark it deposits, with substrate preference for asymmetric nucleosomes containing one H3K27me3 (Lechner et al., 2016; Margueron et al., 2009). While recognition of asymmetric H3K27me3 is believed to be important for maintenance and spreading of heterochromatin, and the bivalent H3K4me3/H3K27me3 signature has been well established for stem cell identity, there is relatively little biological understanding for most

other epigenetic marks that are prominently asymmetric. Genome-wide studies have revealed that the +1 nucleosome is strikingly asymmetric with regards to H3K9 acetylation, H2B ubiquitination, and residency of H2A.Z (Rhee et al., 2014). Asymmetric marks of the +1 nucleosome correlate with asymmetric localization of the RSC, INO80, and SWR1 chromatin remodelers (Ramachandran et al., 2015; Yen et al., 2012), and a major question is how these and other enzymes generate and read-out the asymmetric distribution of these marks.

Nucleosomes can also exhibit asymmetry with respect to histone content, with the lack of one H2A/H2B dimer defining the hexasome. The existence of hexasomes *in vivo* has been supported by ChIP-exo and MNase-seq experiments (Rhee et al., 2014), and *in vitro*, hexasomes have been shown to be generated by the RSC remodeler with the NAP1 histone chaperone (Kuryan et al., 2012) and also by RNA polymerase II (Pol II) transcribing through nucleosomes (Kireeva et al., 2002, 2005). Intriguingly, Pol II successfully transcribes through hexasomes oriented with the promoter-distal H2A/H2B dimer missing, but stalls in the absence of the promoter-proximal dimer (Kulaeva et al., 2009). Whether the orientation of hexasomes may affect other enzymes that act on chromatin has not previously been addressed.

Transcription requires local disruption and reassembly of nucleosomes, which is achieved by elongation factors, histone chaperones, and chromatin remodelers such as Chd1 and ISWI (Venkatesh and Workman, 2015). Chd1 and ISWI reposition nucleosomes into evenly spaced arrays, and are required for packing arrays of nucleosomes against the +1 nucleosome (Gkikopoulos et al., 2011; Lusser et al., 2005; Pointner et al., 2012; Tsukiyama et al., 1999). Although specific binding of H3K4me3 by the chromodomains of mouse Chd1 has been correlated with its localization to the promoter (Lin et al., 2011), Chd1 and ISWI remodelers have been shown to participate in resetting the chromatin barrier in coding regions after passage

of Pol II, required for preventing cryptic transcription (Cheung et al., 2008; Pointner et al., 2012; Radman-Livaja et al., 2012; Smolle et al., 2012). Chd1 has been linked to elongating Pol II through interactions with the transcriptional elongation factors FACT and Spt4-Spt5, and with the Rtf1 subunit of the PAF complex (Kelley et al., 1999; Krogan et al., 2002; Simic et al., 2003). To aid passage of Pol II, the machinery that travels along with the transcription bubble alters local chromatin structure, yet it is not known how changes to nucleosomes might influence Chd1 or other chromatin remodelers. In addition to potentially generating hexasomes, passage of Pol II is also coupled to transient ubiquitination of H2B (Fleming et al., 2008; Xiao et al., 2005). Interestingly, the H2B-Ubiquitin (H2B-Ub) mark is required for FACT-assisted disruption of the chromatin barrier (Pavri et al., 2006). Chd1 has been shown to be required for high levels of transcription-coupled ubiquitination of H2B *in vivo* (Lee et al., 2012), yet a direct connection between Chd1 and transcriptionally altered nucleosomes has remained elusive.

In this work, I report the discovery that the Widom 601 nucleosome positioning sequence can generate oriented hexasomes, with the sole H2A/H2B positioned in a sequence-defined location. Using oriented hexasomes, I show that Chd1 requires H2A/H2B on the entry side for robust sliding and preferentially shifts hexasomes unidirectionally. I observe that mutations in the auto-inhibitory chromodomains of Chd1 improve the sliding of hexasomes missing the entry side H2A/H2B dimer, suggesting the chromodomains play a role in preventing hexasome sliding. Hexasomes can be transformed into nucleosomes upon addition of H2A/H2B dimers, and I demonstrate that oriented hexasomes are an ideal substrate for generating uniform populations of asymmetric nucleosomes with uniquely modified H2A/H2B dimers. I find that nucleosomes with an asymmetric H2B-Ub modification can stimulate nucleosome sliding by Chd1, revealing an unexpected activating role for H2B-Ub in remodeling.

RESULTS

The Widom 601 sequence allows for generation of oriented hexasomes

Since the nucleosome consists of two copies each of the four canonical histones – H2A, H2B, H3 and H4 – *in vitro* nucleosome reconstitutions that deviate from equi-molar histone stoichiometries can result in sub-nucleosomal products. Curiously, during the course of nucleosome reconstitutions by salt dialysis, I noticed that native PAGE migration of a smaller species changed depending on the location of flanking DNA. I use the strong Widom 601 positioning sequence (Lowary and Widom, 1998), with the X-601-Y naming convention, where X and Y refer to the number of base pairs flanking the core 145 bp 601 sequence. Consistently, observed that the subspecies from 0-601-80 preps migrated faster than that of 80-601-0 preps (Figure 2.1**A**). I purify nucleosomes, free DNA, and subnucleosomal species away from each other using native polyacrylamide gel electrophoresis (PAGE) (Figure 2.1**B,C**), allowing for isolation of homogeneous material. The hexasome is a stable sub-nucleosomal particle lacking one of the two H2A/H2B dimers (Arimura et al., 2012; Kireeva et al., 2002; Mazurkiewicz et al., 2006), and I confirmed by SDS-PAGE analysis that the faster migrating species in my nucleosome preparations were in fact hexasomes (Figure 2.1**D**).

Nucleosomes migrate differently in native gels depending on whether flanking DNA is present only on one or both sides of the histone core (Eberharter et al., 2004; Pennings et al., 1991). With one H2A/H2B dimer missing, hexasomes have ~40 bp of DNA unwrapped from the core, resulting in DNA lifting off the histone core prematurely at superhelical location 3 (SHL3), three helical turns from the nucleosome dyad, on the side lacking the H2A/H2B dimer. For end-positioned 601 constructs, where nucleosomes lack flanking DNA on one side, hexasomes would be expected to migrate differently depending on whether unwrapping occurred on the side with

or without flanking DNA. I reasoned that the differences in hexasome migration might therefore be due to a systematic loss of H2A/H2B from one side of the Widom 601 sequence (Figure 2.2**A**). To test this idea, I probed the accessibility of DNA using Exonuclease III (ExoIII) (Figure 2.2**B**). On nucleosomes, ExoIII digestion showed the expected protection at the edge of the histone core, with preferential cleavage in ~10-11 nt increments (lanes 2-4 and 14-16). The 80-601-0 hexasome, in contrast, was digested more internally by ~30-40 nt on the 0 bp side, while showing full nucleosome protection on the 80 bp side (lanes 6-8 and 18-20). Relative to the orientation of the 601 sequence, the 0-601-80 hexasome showed an analogous pattern, with ~30-40 nt more extensive ExoIII digestion on the 80 bp side and similar protection on the 0 bp side compared to nucleosomes (Figure 2.3). Thus, the preferred location of the remaining H2A/H2B dimer in the hexasome was not influenced by flanking DNA, but instead was determined in a sequence-specific fashion based on the orientation of the Widom 601.

Previous work by several labs has revealed asymmetry in the Widom 601 sequence with respect to the strength of histone-DNA contacts. Single-molecule DNA unzipping experiments demonstrated that one side of the 601 forms more stable contacts with histones (Hall et al., 2009), and the asymmetry of the 601 was found to form a polar barrier to passage of RNA polymerase II (Bondarenko et al., 2006). One feature that has been pointed out as a key determinant of stable histone-DNA contacts are periodic TA dinucleotide steps (Lowary and Widom, 1998). The Widom 601 is notably asymmetric in TA steps on either side of the dyad where binding affinity is expected to be highest, with four TA steps on one side opposite a single TA step on the other side (Chua et al., 2012). Symmetric derivatives of 601 have shown that the TA-rich side is much more salt stable than the TA-poor side (Chua et al., 2012), and single molecule experiments have found that the TA-poor side preferentially unwraps under force (Ngo

et al., 2015). I orient the Widom 601 with the TA-rich side on the left, which means that the side lacking the H2A/H2B dimer in hexasomes corresponds with the TA-poor side of the 601 sequence (Figure 2.4**A**).

If the asymmetry of TA dinucleotides in the Widom 601 was directing hexasome orientation, I reasoned that asymmetric sequences other than the 601 might also form oriented hexasomes. The Widom 603 is another strong positioning sequence uncovered in the same screen as the 601 that also has an asymmetric distribution of TA dinucleotides (Lowary and Widom, 1998) (Figure 2.4**B**). On the TA-rich side, the 603 has three sets of TA steps at SHL 0.5, SHL 1.5 and SHL 2.5 compared to the 601, which has TA steps at all four contacts on the tetramer. On the TA-poor side, the 603 has no TA steps over the tetramer, and instead contains one over the H2A/H2B dimer at SHL 5.5. Though the pattern of TA steps is different, like the 601, the 603 contains an asymmetric distribution of TA steps.

As for the Widom 601, I used Exo III digestion to analyze the orientation of hexasomes formed on the Widom 603. Due to my observations that flanking DNA does not contribute to the orientation of hexasomes, I generated hexasomes and nucleosomes on the centered of 40-603-40 DNA fragments (Figure 2.5**A**). On nucleosomes, digestion with Exo III proceeded up to either edge of the 603 sequence (lanes 1-4 and 13-16), consistent with protection from the histone octamer (Figure 2.5**B**). On the TA-rich side of hexasomes, for most of the hexasomes digestion penetrated into the footprint of the H2A/H2B dimer by only 5-24 bp, which suggests unwrapping from the edge and not complete loss of the H2A/H2B dimer (lanes 5-8). For a small population of hexasomes, digestion penetrated the TA-rich side of the hexasome by 43 bp, suggesting the H2A/H2B dimer is absent from the TA-rich side. On the TA-poor side, Exo III digestion proceeded through the footprint of the H2A/H2B dimer by 34-45 bp for the majority of

hexasomes (lanes 17-20). Thus, as for the Widom 601, the majority of hexasomes formed on the Widom 603 are missing the H2A/H2B dimer on the TA-poor side of the sequence. This consistency between the 601 and 603 could be coincidental and other sequences and variations need to be analyzed to definitively determine what sequence features contribute to the orientation of hexasomes. Since the 601 is better characterized and exhibits more resolved digestion boundaries than the 603, I performed subsequent analyses with the Widom 601.

Others have shown that hexasomes can generate nucleosome-like products upon addition of H2A/H2B dimer (Kireeva et al., 2002). To investigate this step-wise method of generating nucleosomes, I incubated hexasomes with a 2-fold molar excess of H2A/H2B dimer and monitored ExoIII digestion. As shown in Figure 2.2 and Figure 2.3, addition of H2A/H2B dimer to hexasomes formed on the Widom 601 yielded a protection pattern indistinguishable from nucleosomes (lanes 22-24). A similar effect was observed after addition of H2A/H2B dimer to hexasomes formed on the Widom 603 (Figure 2.5; lanes 22-24). Therefore, even in the absence of histone chaperones or elevated salt, addition of H2A/H2B dimer to hexasomes was sufficient for recovering nucleosome-like protection patterns.

As an alternative method for characterizing hexasomes and nucleosomes generated from H2A/H2B dimer addition, I used histone mapping. With this technique, labeling a single cysteine variant of H2B (S53C) with photo-reactive 4-azidophenacyl bromide (APB) allows for UV-induced cross-linking to nucleosomal DNA (Kassabov and Bartholomew, 2004; Kassabov et al., 2002). Importantly, cross-linking reduces the chemical stability of the modified base, and therefore favors abasic sites that in turn result in cleavage of the DNA backbone. By separating such site-specifically cleaved fragments on a sequencing gel, the DNA base that reacted with the APB-labeled cysteine can be identified. For chromatin remodelers, changes in positioning of the

cross-linked site is interpreted as a shift in the position of the histone core along DNA. In nucleosomes, each H2B cross-links to only one DNA strand, and therefore doubly-labeled fluorescent DNA is needed to report on both sides of the 601 sequence. In agreement with ExoIII experiments, H2B cross-linking for hexasomes was virtually absent on the TA-poor side of the 601, whereas cross-linking on the TA-rich side was equivalent for hexasomes and nucleosomes (Figure 2.6; compare lane 1 with 2 and 4 with 5). Strikingly, addition of H2A/H2B fully recovered the H2B cross-link on the TA-poor side (compare lanes 5 and 6), demonstrating that dimer addition generates correctly organized nucleosomes that are indistinguishable from those obtained by salt dialysis reconstitution. Similar results were obtained with 0-601-80 hexasomes (Figure 2.7), reinforcing the conclusion that salt dialysis deposits limiting H2A/H2B on the TA-rich side of the Widom 601.

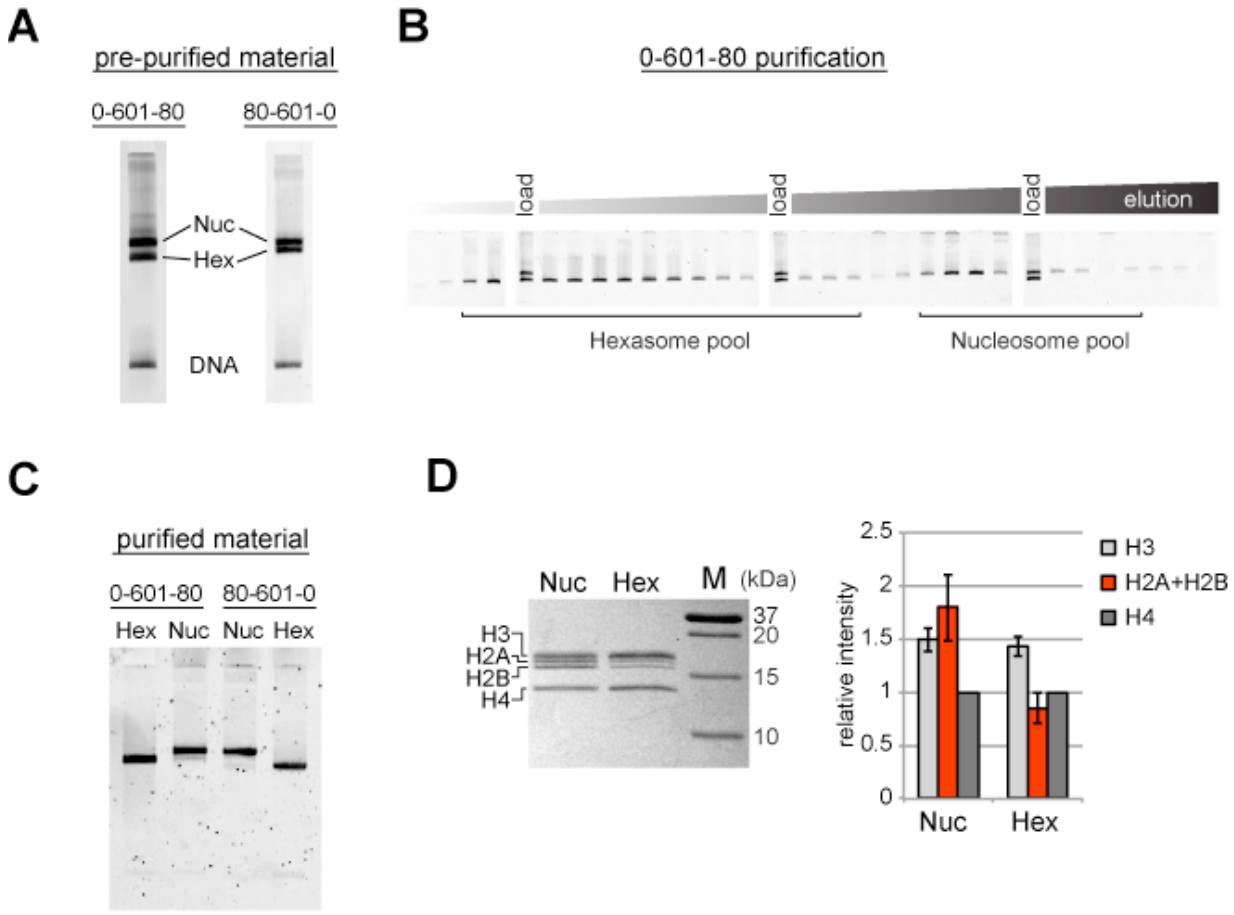

Figure 2.1: Separation of nucleosomes and hexasomes made with the Widom 601 sequence.
(A) Hexasomes but not nucleosomes migrate differently by native PAGE when flanking DNA is on the left or right of the 601 sequence. These two gels, poured from the same solution, are representative of 0-601-80 and 80-601-0 reconstitutions made using histone octamer.
(B) Separation of hexasomes from nucleosomes. Shown is a representative purification over a 7% native acrylamide column using a Prep Cell apparatus. The elution fractions were analyzed by native PAGE.
(C) Purified nucleosome and hexasome pools, analyzed by native PAGE.
(D) As shown by SDS-PAGE, the hexasome species lack one H2A/H2B dimer. The bar graph is a quantification of gel band intensities from three different nucleosome/hexasome purifications. All histone bands were normalized to histone H4. The H2A and H2B bands often migrate close together, and therefore the relative intensities of H2A/H2B bands are shown summed together. Within each nucleosome/hexasome pair, the intensity of H2A/H2B in hexasomes was 47 ± 6% of that of nucleosomes.

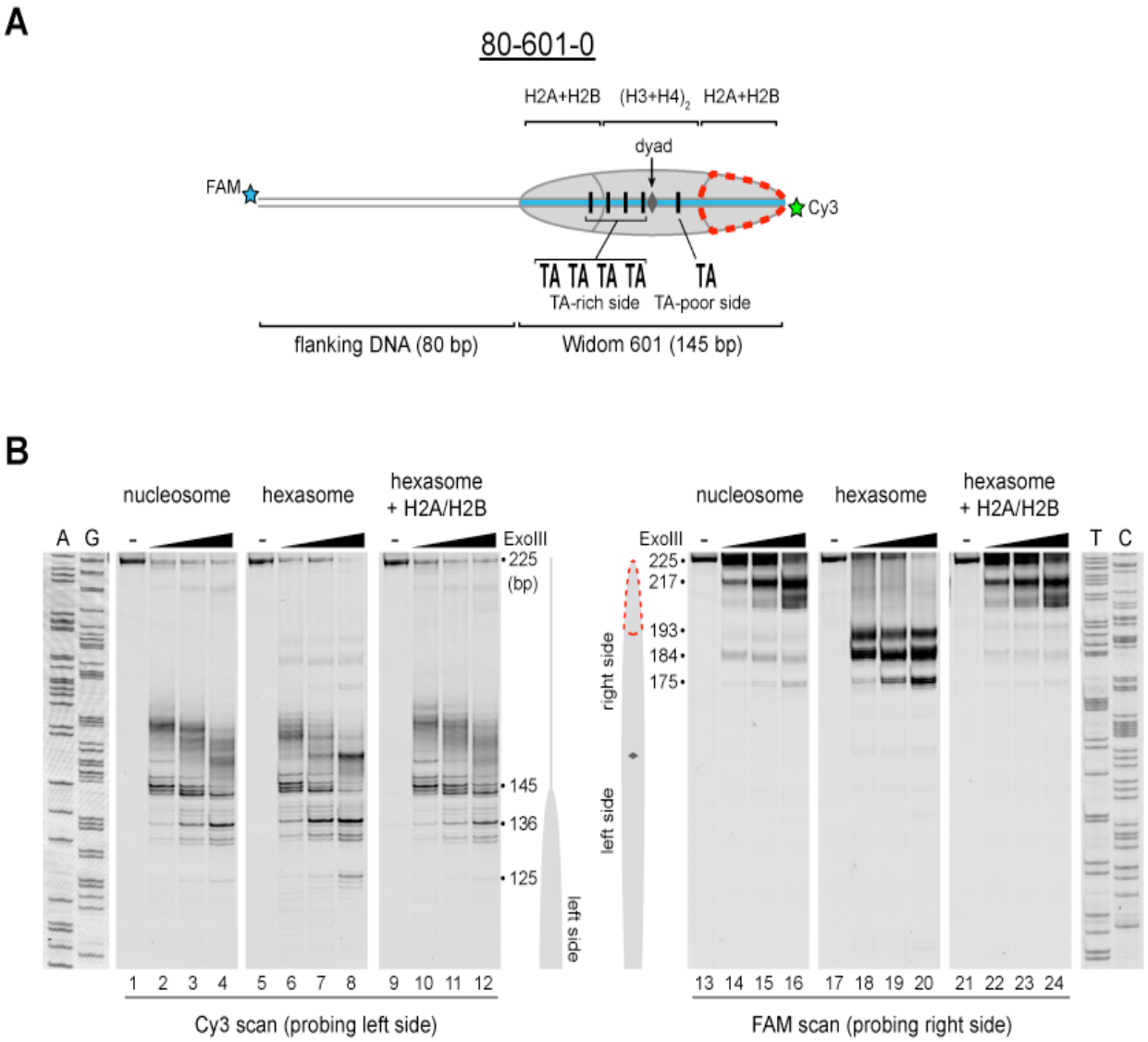

Figure 2.2: Oriented hexasomes can be generated using the Widom 601 sequence.
(**A**) Schematic representation of the 80-601-0 nucleosome and hexasome. With limiting amounts of H2A/H2B dimer, the side of the hexasome lacking the dimer (red dotted outline) corresponds with the TA-poor side of the Widom 601 sequence.
(**B**) ExoIII analysis of 80-601-0 demonstrates that hexasomes specifically retain the H2A/H2B dimer on the TA-rich side of the 601 sequence. Purified nucleosomes, hexasomes, and hexasomes plus H2A/H2B were incubated with 0, 10, 40, and 160 units of ExoIII and resolved on urea denaturing gels. Lanes 9-12 and 21-24 show addition of 200 nM H2A/H2B dimer to 100 nM hexasomes, which recovered nucleosome digestion patterns. The size (bp) of major products are indicated. These gels are representative of two independent experiments. Dideoxy sequencing lanes (A, G, T, C) were run on the same gel as the samples shown.

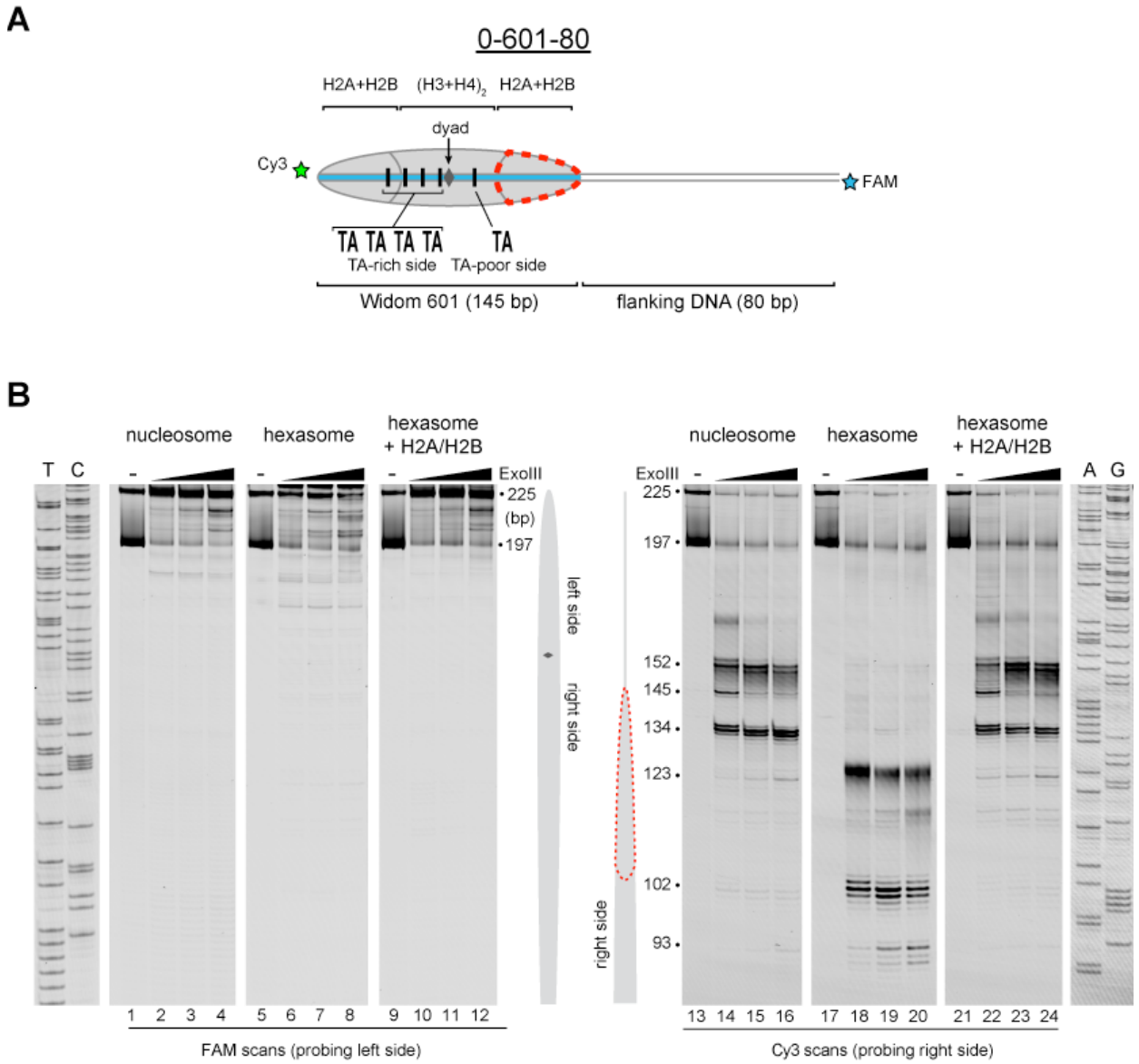

Figure 2.3: Flanking DNA does not influence the orientation of the hexasome.
(**A**) Schematic representation of the 0-601-80 nucleosome and hexasome. As shown for 80-601-0 in Figure 2.2, limiting amounts of H2A/H2B favors a hexasome that lacks the dimer on the TA-poor side of the Widom 601 sequence.
(**B**) ExoIII digestions performed as in Figure 2 except using purified 0-601-80 nucleosomes and hexasomes, where flanking DNA was on the opposite (right) side of the 601. Comparing digestion patterns of 0-601-80 and 80-601-0 hexasomes revealed that hexasomes lacked H2A/H2B on the TA-poor side of the 601 regardless of flanking DNA. Addition of two-fold molar excess H2A/H2B to hexasomes restored nucleosome digestion patterns (lanes 21-24). ExoIII digestions of 0-601-80 and 80-601-0 hexasomes and nucleosomes were performed in parallel, run on the same gel and are each representative of two independent experiments.

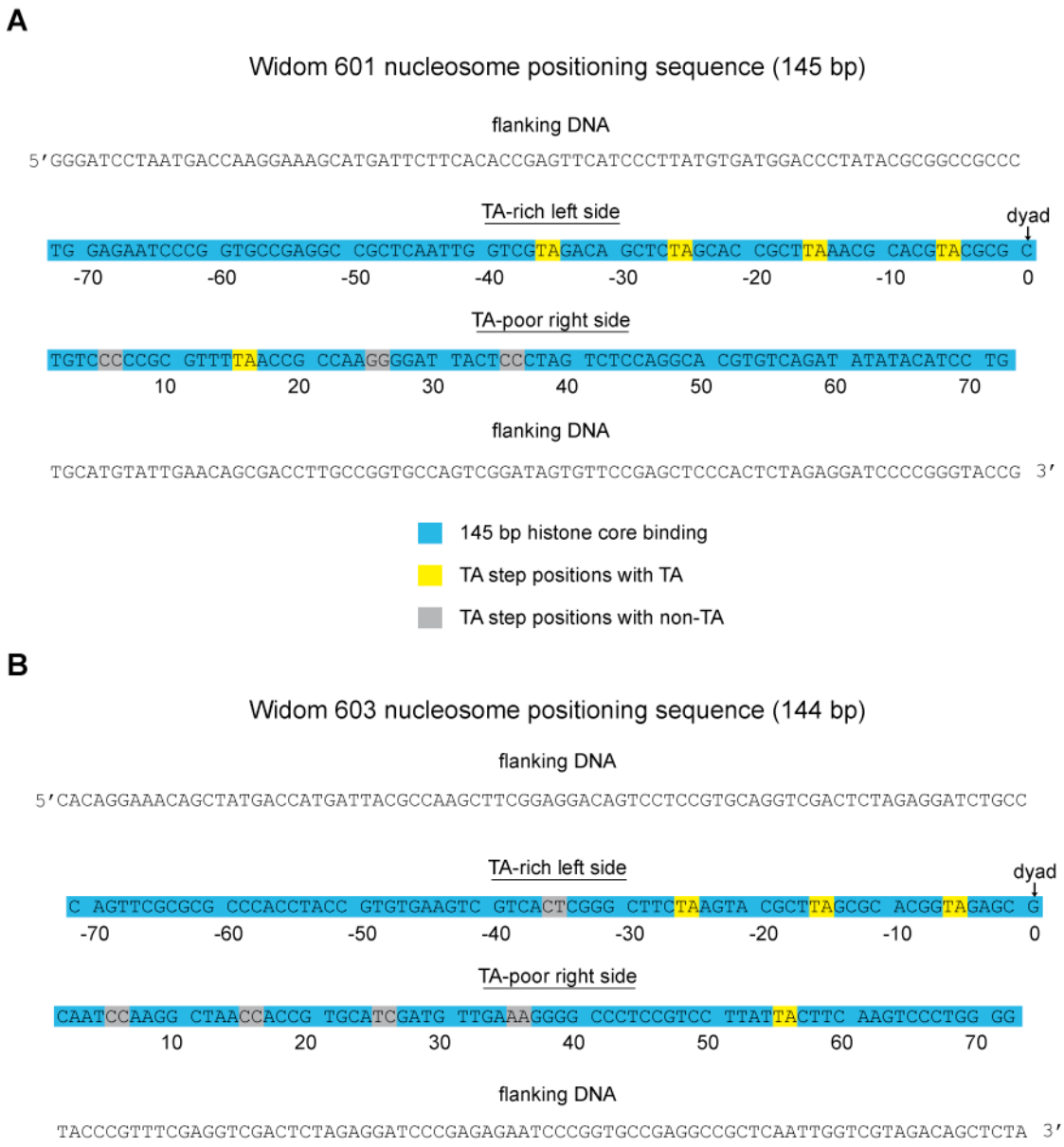

Figure 2.4: Sequence and orientation of the Widom 601 and Widom 603 sequences used in this study.
(**A**) Shown is the core 145 bp histone binding region of the 601 (blue) with flanking DNA. Numbering gives the distances from the dyad (zero). TA step positions are highlighted in yellow
(**B**) The 144 bp Widom 603 nucleosome positioning sequence is shown with the location of TA steps.

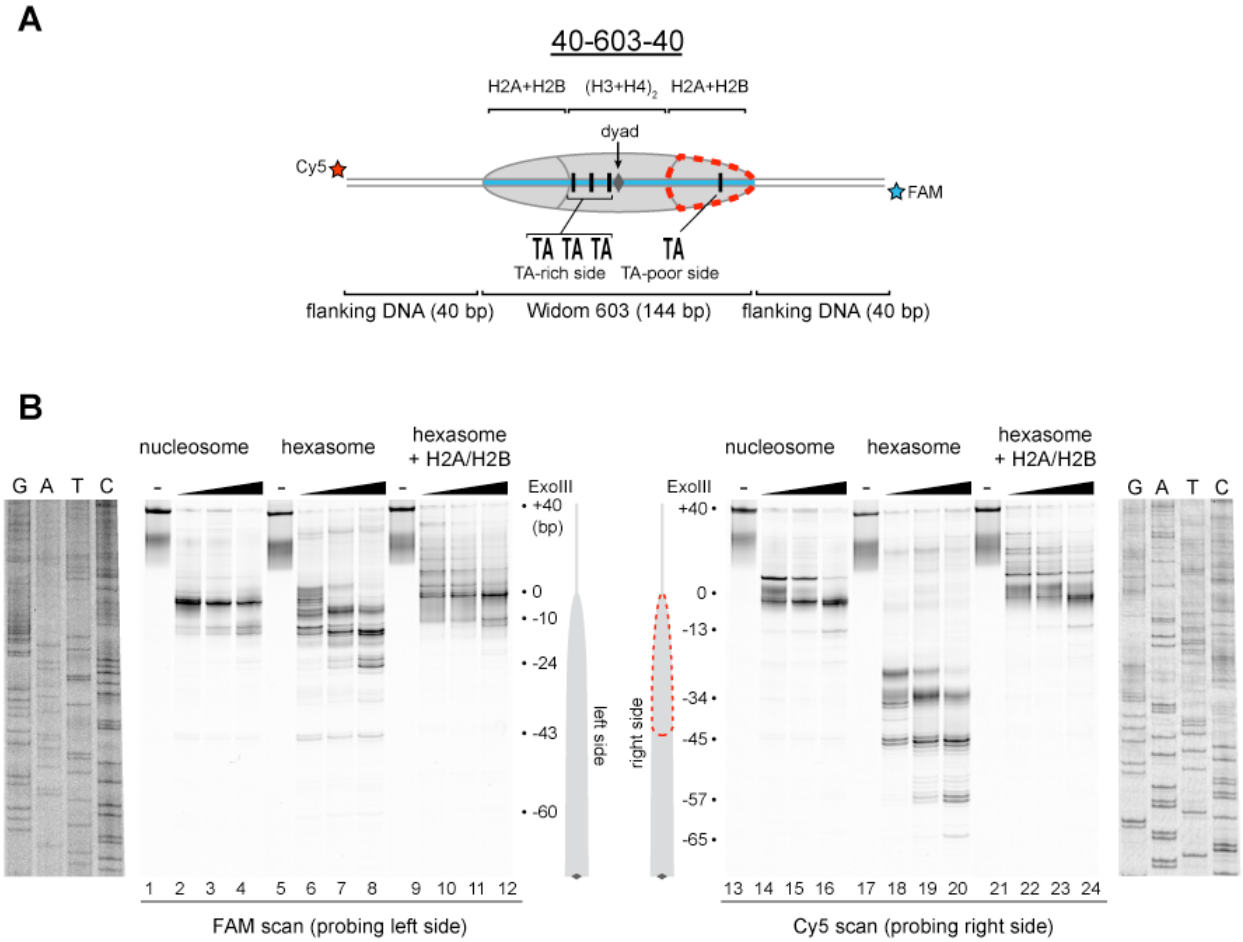

Figure 2.5: Hexasomes generated on the Widom 603 lack the H2A/H2B dimer on the TA-poor side

(**A**) Schematic representation of the 40-603-40 nucleosome and hexasome. As for the Widom 601, limiting dimer favors a hexasome lacking H2A/H2B on the TA-poor side of the 603. (**B**) ExoIII digestions performed as in Figure 2.2 except using purified 40-603-40 nucleosomes and hexasomes. Digestion patterns were similar to those of hexasomes formed on the 601. Addition of two-fold molar excess H2A/H2B to hexasomes restored nucleosome digestion patterns (lanes 21-24).

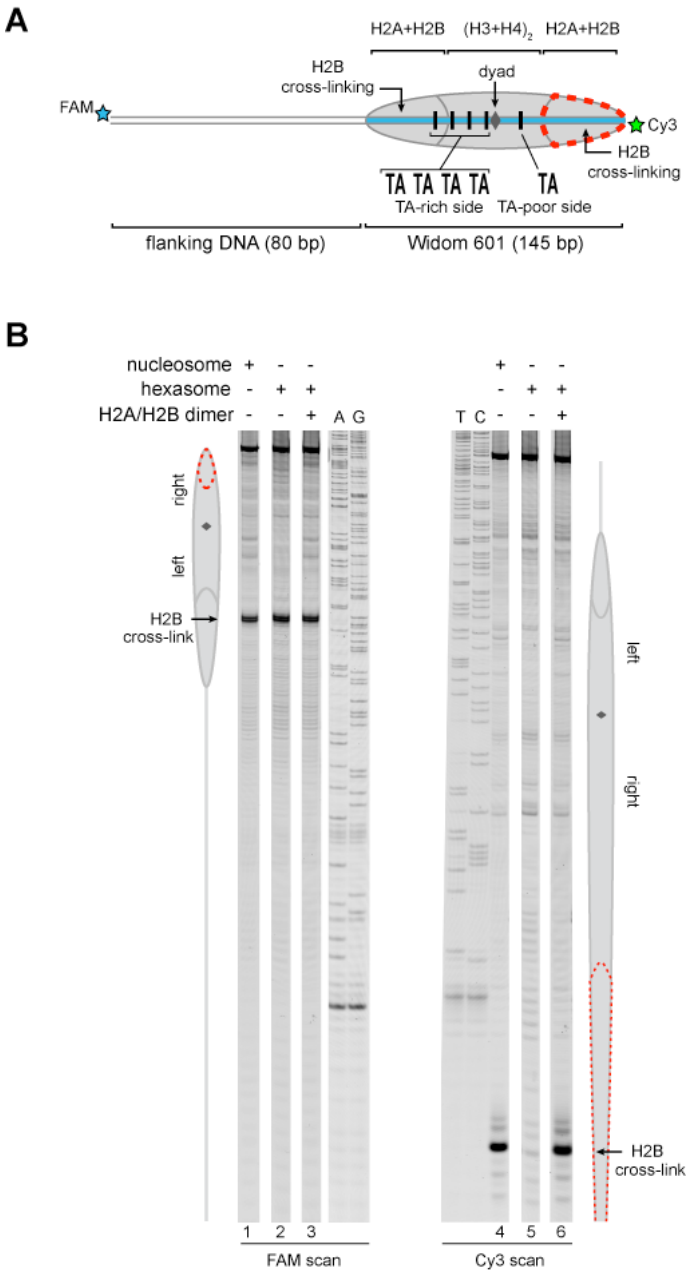

Figure 2.6: Addition of H2A/H2B dimer to hexasomes produces canonical nucleosomes.
(**A**) Schematic representation of the 80-601-0 nucleosome and hexasome, highlighting the locations where H2B-S53C cross-links to DNA. Due to the absence of one H2A/H2B dimer, H2B cross-linking with hexasomes is limited to the TA-rich side of the Widom 601.
(**B**) Histone mapping demonstrates that canonical nucleosomes can be generated by addition of H2A/H2B dimer to hexasomes. For reactions containing hexasomes plus H2A/H2B, the hexasomes (150 nM) were incubated for 2-3 minutes with H2A/H2B (300 nM) prior to labeling with APB. Nucleosome and hexasome alone were subjected to the same brief incubation. Following UV cross-linking and DNA extraction, the DNA was cleaved at the crosslinking site and the products separated on a denaturing gel alongside a sequencing ladder to determine the cross-linking position. Results are representative of three or more independent experiments.

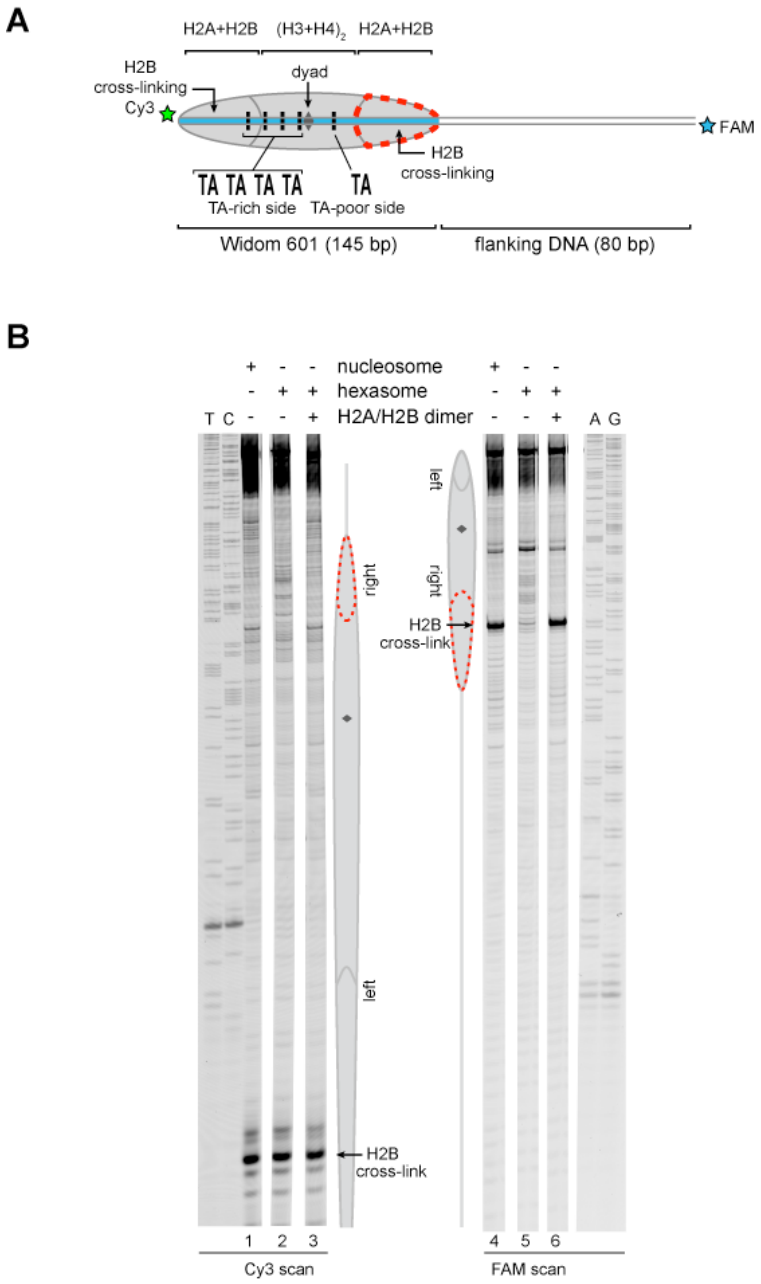

Figure 2.7: Addition of H2A/H2B dimer to hexasomes produces canonical nucleosomes, regardless of flanking DNA location.
(**A**) Schematic representation of the 0-601-80 nucleosome and hexasome, highlighting the location where the hexasome lacks one H2A/H2B dimer.
(**B**) Histone mapping experiments using 0-601-80 nucleosomes, hexasomes, and hexasomes plus excess H2A/H2B dimer. Reactions were carried out as described for Figure 2.6. Sequencing ladder markers (T, C, A, G) were run in the same gel as the samples. This gel is representative of three or more experiments.

Chd1 requires the entry-side H2A/H2B dimer for robust sliding

Given the strong sequence-defined placement of limiting H2A/H2B dimer, I refer to hexasomes produced by the Widom 601 as "oriented hexasomes." By having a defined orientation on DNA, these hexasomes offer a unique tool for probing requirements of nucleosome-interacting enzymes. Despite the two-fold pseudo-symmetry of the nucleosome, factors binding off the central dyad axis encounter the two halves of the nucleosome at distinct distances and orientations. The two H2A/H2B dimers and the DNA they coordinate are therefore likely to play unequal roles in nucleosome recognition and enzyme regulation. Chromatin remodelers such as Chd1 shift DNA past the histone core by acting at SHL2, an internal DNA site located ~20 bp from the dyad (McKnight et al., 2011; Saha et al., 2005; Schwanbeck et al., 2004; Zofall et al., 2006). Relative to the SHL2 site of DNA translocation, one H2A/H2B dimer is positioned to bind DNA that is pulled onto the nucleosome, and is therefore considered to be on the entry side, whereas the other H2A/H2B binds DNA that shifts off the histone core, and thus is on the exit side. *In vitro*, Chd1 slides mononucleosomes away from DNA ends (McKnight et al., 2011; Stockdale et al., 2006). By using end-positioned nucleosomes, one can restrict the direction of sliding, thereby defining H2A/H2B adjacent to the long flanking DNA as the entry-side dimer. Since the placement of the single H2A/H2B dimer relative to 601 is maintained regardless of flanking DNA (Figure 2.6 and Figure 2.7), I can generate hexasomes with the H2A/H2B dimer on either the entry or exit side, which allows me to determine the extent that Chd1 relies on H2A/H2B at each position.

As a standard technique for visualizing repositioning of mononucleosomes along DNA, I first investigated movement of oriented hexasomes using native PAGE (Figure 2.8). I used 0-601-80 and 80-601-0 constructs described above, which lacked one of the H2A/H2B dimers on

either the entry side (0-601-80) or exit side (80-601-0). For nucleosomes, electrophoretic mobility decreased upon addition of Chd1 and ATP, signifying movement away from DNA ends (lanes 1-8). In contrast, under the same conditions the hexasomes failed to show analogous changes in migration patterns (lanes 9-16).

Since the loss of one H2A/H2B dimer in the hexasome dramatically alters the location where DNA extends away from the histone core and thus the geometry of flanking DNA with respect to the core, I considered the possibility that native PAGE may not accurately report on changes in hexasome positioning. I therefore investigated the ability of Chd1 to reposition hexasomes using histone mapping (Figure 2.9). In agreement with previous work (Patel et al., 2013; Stockdale et al., 2006), Chd1 shifted end-positioned mononucleosomes to more central locations on DNA, with the majority of nucleosomes repositioned ~20 to ~60 bp from their starting locations (lanes 1-3, 7-18). For hexasomes, however, the ability of Chd1 to reposition was strongly dependent on the location of the single H2A/H2B dimer. The 0-601-80 hexasomes, which lacked the entry-side H2A/H2B dimer, failed to show robust repositioning, with the majority of products remaining at the starting position (lanes 4-6). In marked contrast, the 80-601-0 hexasomes shifted robustly onto flanking DNA, demonstrating that Chd1 activity can be supported by an H2A/H2B dimer on only the entry side (lanes 19-30). Interestingly, instead of generating more centrally positioned products, Chd1 shifted 80-601-0 hexasomes to the opposite end of DNA, farther than observed for nucleosomes (Figure 2.9**B**). This biased movement of 80-601-0 toward the entry H2A/H2B dimer, even after the hexasome had shifted away from its starting position on the 601 sequence, was consistent with much poorer sliding toward the side lacking the H2A/H2B dimer and indicated that it was the absence of H2A/H2B rather than the DNA sequence that blocked efficient sliding of 0-601-80 hexasomes. Thus, Chd1 can reposition

hexasomes, but the requirement for entry-side H2A/H2B yields a strong directional bias for hexasomes that contrasts with the back-and-forth sliding observed for nucleosomes.

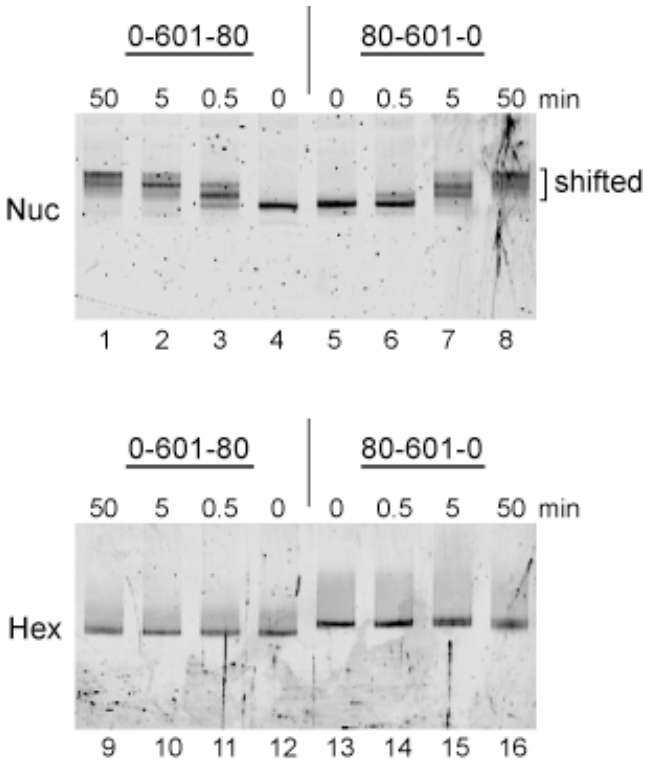

Figure 2.8: Chd1 remodeling dramatically alters nucleosome but not hexasome mobility as assessed by native PAGE.
Purified nucleosomes (top) or hexasomes (bottom), each 150 nM, were incubated with yeast Chd1 (50 nM) and 2.5 mM ATP in sliding buffer for 0, 0.5, 5, and 50 min. After quenching with EDTA and competitor DNA, reaction products were separated by native PAGE. Shown is a representative of four independent experiments.

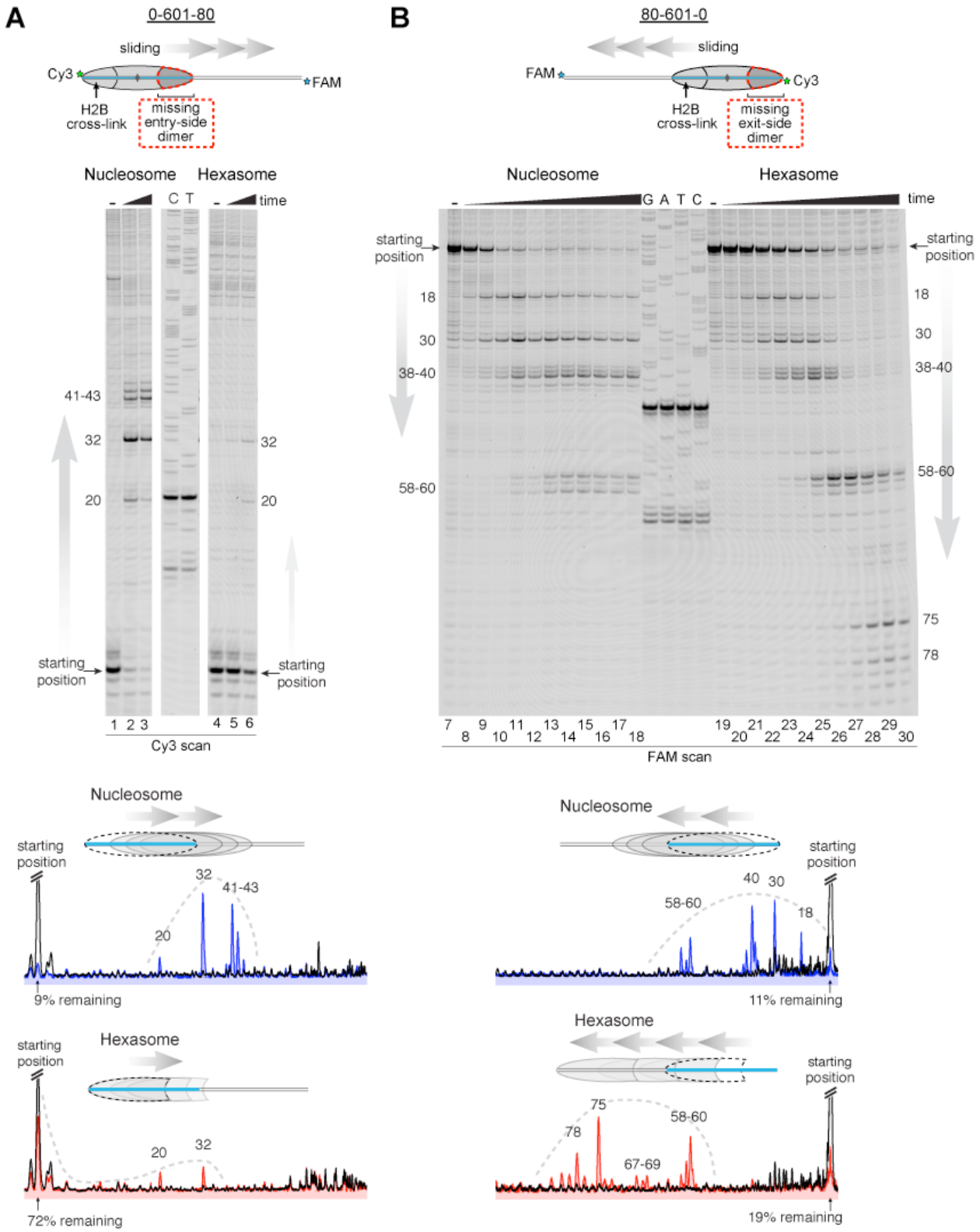

Figure 2.9: Chd1 requires entry side H2A/H2B for robustly repositioning hexasomes.
(*Figure legend on next page*)

(Figure 2.9 *legend continued from previous page*)
(**A**) Nucleosome and hexasome sliding reactions, visualized through histone mapping. For 150 nM hexasome and nucleosome 0-601-80 constructs (left), sliding reactions were monitored after incubation with 50 nM Chd1 and 2 mM ATP for 0, 1, and 64 min. Reactions were quenched at time points with the addition of EDTA and competitor DNA. Comparison of intensity profiles for histone mapping reactions are shown below. Samples before ATP addition (0 min) are black, nucleosome sliding reactions after 64 min are blue, and hexasome sliding reactions after 64 min are red.
(**B**) Sliding reactions and intensity profiles carried out with 80-601-0 constructs as described for (A). Time points were 0, 0.25, 0.5, 1, 2, 4, 8, 16, 32, and 64 min. Sliding experiments for 0-601-80 and 80-601-0 were each performed six or more times with similar results.

Oriented hexasomes allow for precisely designed asymmetric nucleosomes

The discovery of oriented hexasomes opens up a simple means for producing asymmetric nucleosomes, where unique modifications in the two H2A/H2B dimers can be directed to specific sides of the nucleosome. One powerful technique that can benefit from generating asymmetric nucleosomes is single molecule FRET (smFRET). Though many variations are possible, fluorescent dye labeling of nucleosomes commonly involves both histones and DNA, which allows for detection of DNA unwrapping and DNA translocation relative to the histone core (Blosser et al., 2009; Li and Widom, 2004; Yang et al., 2006). The FRET signal, however, can be complicated by the two-fold symmetry of the nucleosome, since dyes at the two related histone positions are typically not equidistant from the DNA-tethered dye, and therefore lead to a mixture of FRET levels (Deindl et al., 2013). A standard solution to this issue has been to dilute the labeled histone with an excess of unlabeled histone during nucleosome reconstitution, and select out the desired FRET signal from a single donor/acceptor pair. I expected that the unique placement of a single H2A/H2B dimer relative to the DNA sequence should allow the generation of nucleosomes with a single, uniform FRET pair.

To examine this idea, I labeled H2A-T120C with Cy3-maleimide and generated 3-601-80 hexasomes and nucleosomes containing a DNA-tethered Cy5 dye on the 3 bp side. As previously described (Deindl et al., 2013), the nucleosomes gave rise to two major FRET populations corresponding to single Cy3 dyes on the distal or proximal H2A (Figure 2.10**A**). A mid-FRET population is expected between these two major species, where nucleosomes contain Cy3 on both copies of H2A. Here, due to extensive dilution of labeled H2A-Cy3, that population was minimal. In contrast, the oriented hexasomes yielded a single, high-FRET population as expected for the H2A/H2B dimer located on the exit side, proximal to the DNA label (Figure 2.10**B**). To see whether these hexasomes would behave as nucleosomes upon H2A/H2B dimer addition, Chd1 and ATP were added to stimulate nucleosome sliding. After a 10 min incubation, all nucleosomes had shifted to a low FRET state, as expected for a ≥ 20 bp shift of the histone core away from the labeled DNA end. Hexasomes, in contrast, maintained a significant population of high-FRET species after incubation, consistent with the poor movement observed by histone mapping in the absence of entry-side H2A/H2B dimer. Addition of H2A/H2B dimer to hexasomes did not significantly alter the starting high-FRET population, yet incubation with Chd1 and ATP yielded a low-FRET profile similar to that observed for nucleosomes (Figure 2.10**C**). These results show that oriented hexasomes offer a defined methodology for producing uniformly labeled nucleosomes that should benefit smFRET experiments.

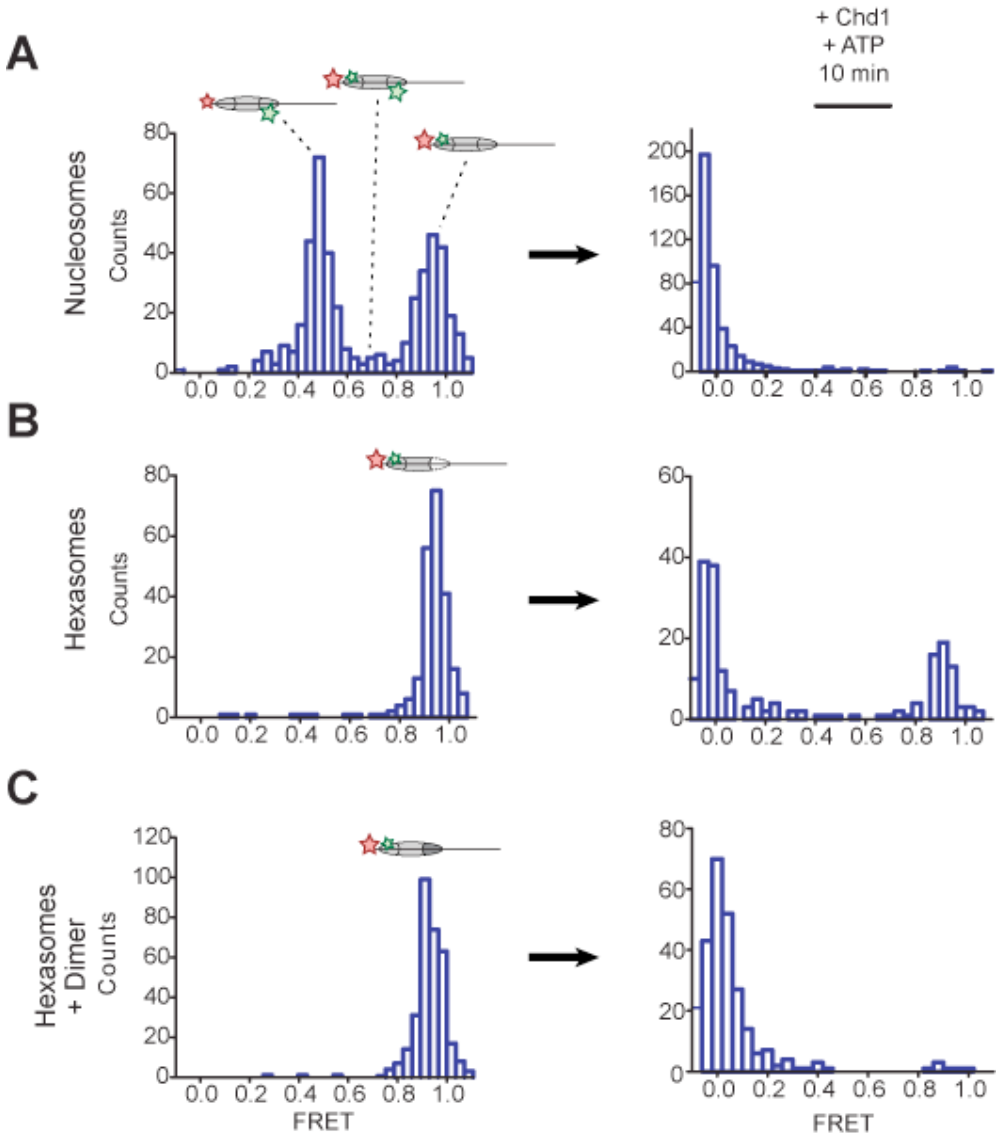

Figure 2.10 Oriented hexasomes allow targeted placement of modified H2A/H2B dimers on the nucleosome

(**A**) Analysis of dual labeled 3-601-80 nucleosomes (H2A T120C-Cy3 and DNA-Cy5) by single-molecule FRET (smFRET) reveals multiple species prior to nucleosome sliding by Chd1. Nucleosomes were surface-immobilized by biotin on the 80 bp flanking DNA. Infusion of 300 nM Chd1 and ATP initiated remodeling.

(**B**) Oriented 3-601-80 hexasomes (H2A-Cy3 and DNA-Cy5) uniformly show one dye pair that yields high FRET. Right panel shows relatively poor mobilization of hexasomes by Chd1.

(**C**) Incubation of a two-fold molar excess of unlabeled H2A/H2B dimer with the labeled 3-601-80 hexasomes yielded asymmetric nucleosomes, only possessing the high FRET dye pair. After remodeling with Chd1 and ATP, the FRET population was similar to nucleosome. Data collected and analyzed by Anton Sebantsev and Sebastian Deindl

Chd1 requires entry side H2A/H2B for sliding but not binding

From the experiments presented above, it was unclear whether the asymmetric sliding of hexasomes simply reflected much poorer binding of Chd1 to the side lacking the H2A/H2B dimer. To see whether the remodeler engaged with hexasomes differently than nucleosomes, I utilized single cysteine variants of Chd1 that allow for site-specific cross-linking to nucleosomal DNA. In the presence of the ATP analog ADP·BeF_3, both lobes of the ATPase motor of Chd1 bind to DNA at SHL2, which can be monitored by APB labeling of the Chd1 variants N459C (lobe 1) and V721C (lobe 2) (Nodelman et al., 2017). Using 300 nM of either Chd1 variant with 150 nM 40-601-40 nucleosomes, cross-linking was observed to SHL2, 15 to 19 bp from the dyad on either side of the nucleosome as expected (Figure 2.11, lanes 2, 5, 8 and 11). Strikingly, the same cross-linking pattern was also observed with 40-601-40 hexasomes (lanes 3, 6, 9 and 12), indicating that this ATP-bound state of the ATPase motor was not hindered by the lack of H2A/H2B on one side. These results suggest that the deficiency in sliding hexasomes lacking entry side H2A/H2B was likely a catalytic rather than a binding defect.

To quantitatively analyze the impact of entry side H2A/H2B dimer on Chd1 sliding, I monitored repositioning of the histone core using a real-time assay based on static quenching of fluorescence (SQOF). Using the same labeling positions described above for FRET, I found that quenching can be achieved using either a donor (Cy3B) and quencher (Dabcyl) pair, or two cyanine dyes (Cy3-Cy3). As with FRET, movement of exit DNA away from the histone core separates donor-quencher pair and results in increased donor fluorescence. Since quenching requires direct contact, SQOF likely provides higher sensitivity than FRET at shorter distances. With Dabcyl as a quencher on exit DNA, I monitored fluorescence of 0-601-80 hexasomes containing a single H2A-Cy3B label in the absence and presence of an additional, unlabeled

H2A/H2B dimer. Reactions were performed with saturating ATP (1 mM) and excess Chd1 (600 nM) relative to hexasome (10 nM) to reduce the likelihood that defects in sliding might be attributed to binding. Under these conditions, Chd1 shifted the hexasome much more rapidly when excess H2A/H2B was added to generate nucleosomes (Figure 2.12). Both reactions were fit to double exponentials, with hexasome alone dominated by a slower rate of 0.0017 s^{-1}, whereas hexasome plus H2A/H2B dimer yielded a dominant, >300-fold faster rate of 0.57 s^{-1}. The hexasome reactions also yielded a ~three-fold lower change in fluorescence intensity compared to nucleosomes, consistent with an inability to shift all hexasomes away from the DNA end under equilibrium conditions and indicating that even the slow hexasome rate is likely an overestimate. Taken together, these experiments demonstrate that the ability of Chd1 to shift hexasomes lacking the entry side H2A/H2B dimer is extremely poor.

I also compared sliding reactions for hexasome plus H2A/H2B dimer versus salt-dialyzed nucleosomes. As expected, these two substrates yielded similar progress curves, though hexasome plus dimer was slightly faster. This difference arose from a modest (~15%) decrease in the fast rate (0.49 s^{-1} vs 0.57 s^{-1}) and a larger contribution of the slow rate to the fits (11% vs 1%) for salt dialyzed nucleosome compared with hexasome plus H2A/H2B dimer. Previous kinetic analysis of nucleosome sliding by the ACF remodeler using FRET reported that a ~10-fold slower phase contributed 10% of the signal, which the authors suggested was due to a distinct population of nucleosome substrates (Yang et al., 2006). This explanation matches the behavior I observed for nucleosomes here, and suggests that the faster shifting population of nucleosomes is more favored with H2A/H2B dimer addition to hexasomes. I also repeated comparison of nucleosomes versus hexasome plus dimer substrates at a lower (25 μM) ATP concentration (Figure 2.13). Under these conditions, I found no significant difference in the fast

rate of sliding, again with the slow rate contributing more to the amplitude of the progress curve for nucleosome (10%) compared to hexasome plus H2A/H2B (3%). These results suggest that adding H2A/H2B to hexasomes produces nucleosomes that are similar to and apparently more homogeneous than those produced by salt dialysis.

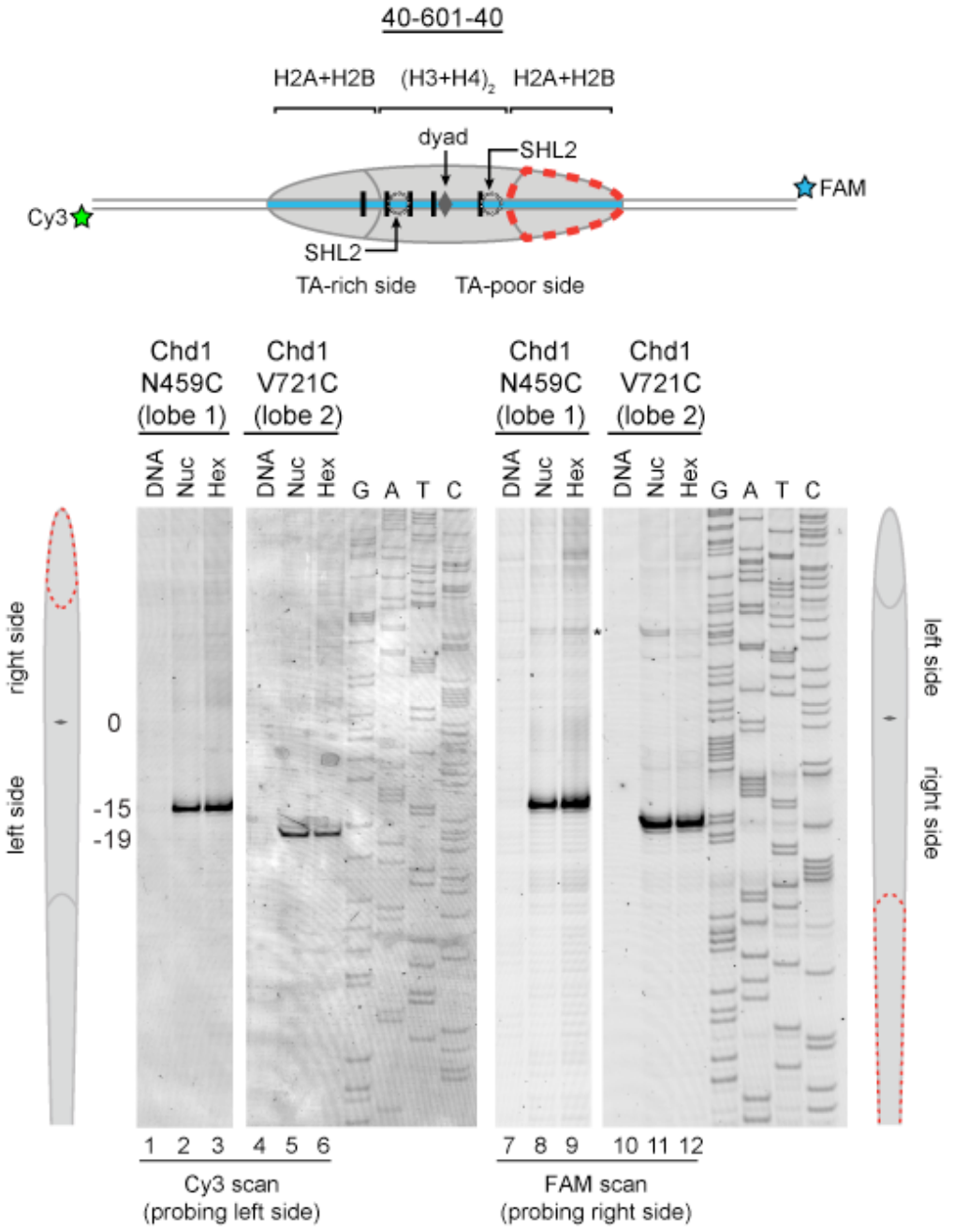

Figure 2.11: Chd1 does not require entry side H2A/H2B for binding
Chd1 cross-linking to 40-601-40 nucleosomes and hexasomes. Single cysteine variants on lobe 1 (N459C) and lobe 2 (V721C) of the Chd1 ATPase cross-linked to DNA 15 and 19 bp from the dyad, respectively, on both sides of nucleosomes and hexasomes. Chd1 was labeled with APB and incubated in a 2:1 ratio with DNA, nucleosomes, or hexasomes in the presence of ADP·BeF_3. After UV irradiation, DNA extraction and cleavage, cross-linking sites were determined by separating DNA fragments on a denaturing gel alongside a sequencing ladder. The gel shown is representative of two independent experiments. Asterisk marks cross-linking from a non-cysteine residue (Nodelman et al., 2017).

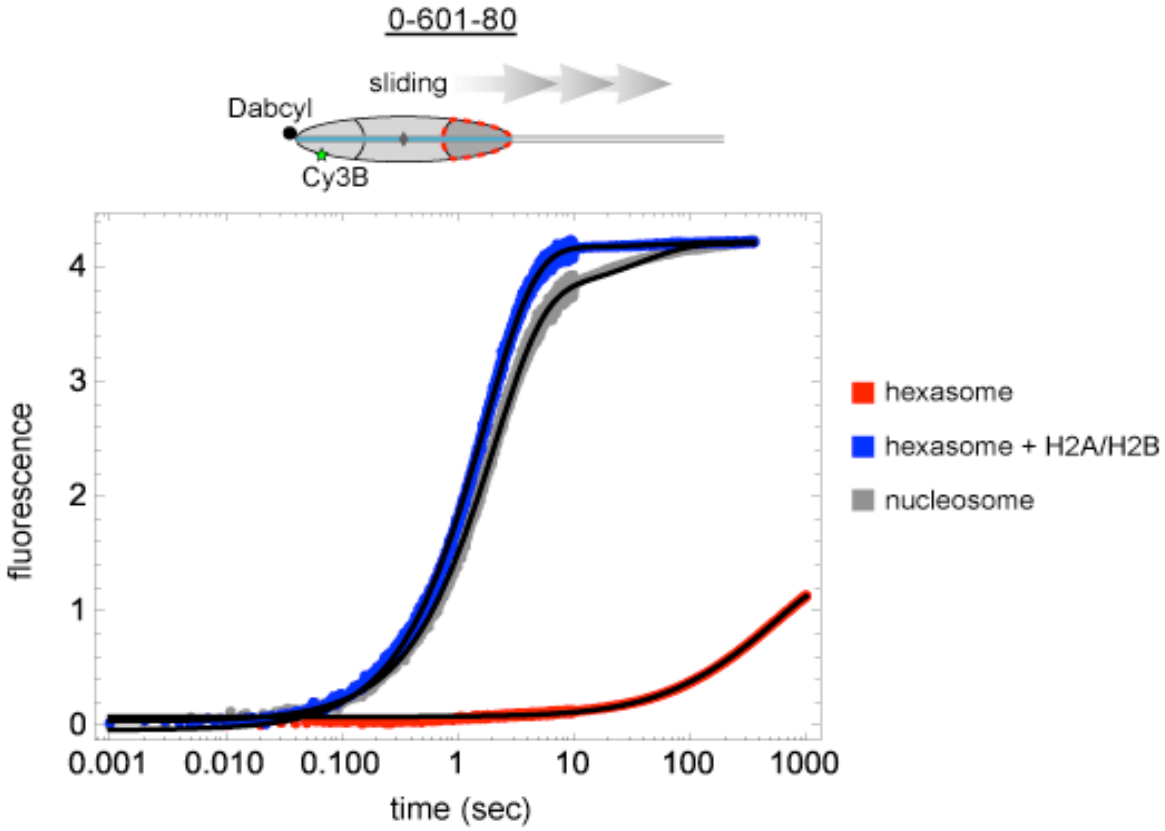

Figure 2.12: Chd1 requires entry side H2A/H2B for sliding
Stopped flow sliding reactions comparing the activity of Chd1 on 10 nM 0-601-80 nucleosomes, hexasomes, and hexasomes plus 12 nM dimer. Nucleosomes and hexasomes were labeled with Cy3B on H2A-T120C and with Dabcyl quencher on the zero end of the DNA. Reactions were initiated with the addition of saturating (600 nM) Chd1 and 1 mM ATP. Black lines represent double exponential fits of the data. Each progress curve is an average of 3-6 replicate injections, and representative of two independent experiments.

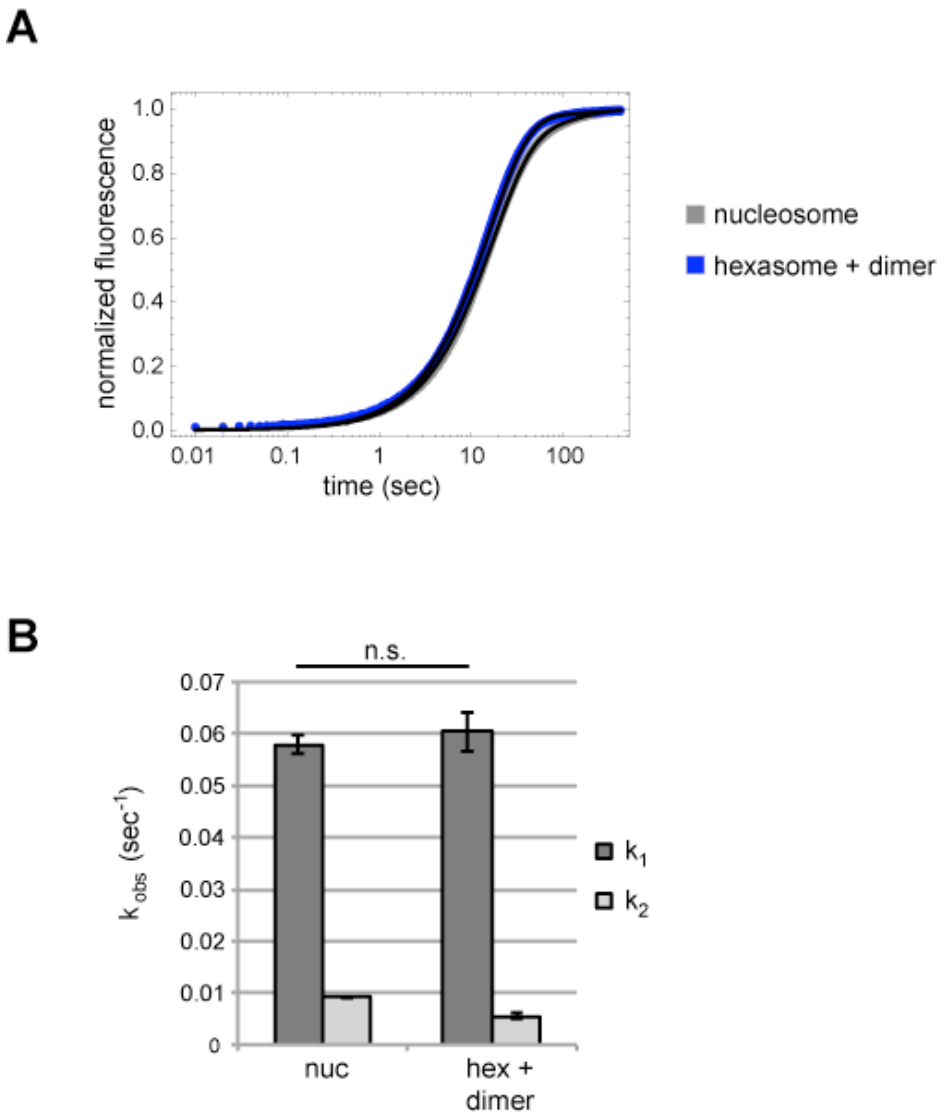

Figure 2.13: Chd1 repositions nucleosome and hexasome plus dimer at similar rates with limiting ATP

(**A**) Progress curves from stopped flow experiments performed with 400 nM Chd1 on 10 nM 0-601-80 nucleosomes (gray) or 10 nM hexasomes plus 12 nM dimer (blue) in the presence of 25 µM ATP. Reactions were monitored by Cy3B-Dabcyl SQOF. Black lines depict double exponential fits of the data. Each progress curve is the average of 3-6 technical replicates and is representative of three independent experiments.

(**B**) Comparison of sliding rates. The bar chart shows observed fast and slow rates (k1, k2) from the fits as means ± standard deviations from three independent experiments. n.s. = not significant.

The H2A acidic patch is not essential for nucleosome sliding by Chd1

One possible explanation for the sliding defect of hexasomes is that Chd1 makes a critical contact with the entry side H2A/H2B dimer. To see if I could identify an important epitope required for sliding, I generated five H2A/H2B variants that could be used to transform hexasomes containing one wild type H2A/H2B into a nucleosome with an altered H2A/H2B on the entry side. Since each of the H2A/H2B variants were generated in distinct preparations, however, I was concerned about two possible complications associated with H2A/H2B dimer addition: too little dimer would allow a significant fraction of hexasome to remain in the reaction, which might compete with the nucleosome, whereas too much dimer could create off-products that might interfere with nucleosome sliding.

To evaluate the potential effects of dimer concentration on sliding, I used Cy3-Cy3 SQOF to monitor sliding of 0-601-80 hexasomes in the presence of increasing amounts of wild type H2A/H2B dimer. Relative to the constant hexasome concentration used (10 nM), addition of unlabeled H2A/H2B dimer stimulated sliding at all concentrations, from undersaturating (4 nM) to saturating (24 nM) (Figure 2.14**A**). The total change in fluorescence intensity increased with dimer concentration, consistent with only the fraction of hexasomes converted to nucleosomes being readily shifted by Chd1. A maximum change in fluorescence was observed with a 1.6-fold molar ratio of dimer to hexasome (Figure 2.14**B**), which is in agreement with others who have reported requiring ~2-fold molar equivalent of dimer to convert all hexasome to nucleosome (Kireeva et al., 2002).

Interestingly, the reaction rates were maximal and remained constant over a wide range of H2A/H2B concentrations, from subsaturating up to the 1.6-fold molar equivalent that yielded the maximum change in fluorescence intensity (Figure 2.14**C**). Thus, under the conditions used

here, the presence of hexasome due to limited H2A/H2B dimer addition did not influence rates for Chd1 remodeling. Beyond this saturating amount, both the rates and range of fluorescence intensity decreased. These reductions likely resulted from improper H2A/H2B deposition on flanking DNA that interfered with Chd1 action. I also monitored nucleosome formation by native PAGE, which showed a dimer-mediated shift of the hexasome species to nucleosomes and aggregation with excessive H2A/H2B (Figure 2.14**D**). As the most consistent rates were observed below the two-fold molar equivalent, I used only a slight molar excess of dimer for the remainder of my dimer addition experiments (10 nM hexasome plus 12 nM H2A/H2B).

In an attempt to identify a critical epitope required for Chd1 sliding, I introduced site-specific disruptions in three locations of the H2A/H2B dimer: (1) a potential binding surface on H2B; (2) the C-terminus of H2A; and (3) the H2A acidic patch (Figure 2.15**A**). I used Cy3B-Dabcyl SQOF to compare the activity of Chd1 on nucleosomes containing disruptions at these sites on the entry side H2A/H2B.

Histone H2B possesses a conserved hydrophobic patch that was recently shown to be recognized independently by both Spt16 and Pob3 subunits of FACT (Kemble et al., 2015). Interestingly, the residues bound by FACT (Y45 and M62 in yeast) are also recognized by the catalytic subunit of the SWR1 remodeler (Hong et al., 2014), highlighting the importance of this patch in H2A/H2B dimer recognition. To see if this region is also important for Chd1, I substituted both H2B residues (Y39 and M56 in *Xenopus*) with alanine. Nucleosome sliding rates with this H2B variant (Figure 2.15, cyan) were indistinguishable from wild type, indicating that Chd1 does not require these residues on the entry side dimer for normal activity.

Another epitope on H2A/H2B that has been shown to be important for a chromatin remodeler is the H2A C-terminal tail. In previous work, nucleosomes lacking H2A C-terminal

residues 115-129 were repositioned more poorly by ISWI remodelers, even though this C-terminal deletion was reported to facilitate heat shifting of histone octamers (Vogler et al., 2010). Since the H2A C-terminus was reported to not be required for octamer stability (Bao et al., 2004), I used a truncated H2A lacking residues 110-129. Interestingly, Chd1 mobilized nucleosomes containing this truncated H2A on the entry dimer 2.5-fold faster than wild type (Figure 2.15, green). Thus, the H2A C-terminus does not contain a critical epitope for Chd1, and faster sliding may have been achieved by altered histone-histone or histone-DNA dynamics.

Finally, the H2A acidic patch, which differs among H2A variants, has been found to be a critical epitope for several nucleosome-interacting factors (Kalashnikova et al., 2013). In fact, direct interactions with the H2A acidic patch occur in all of the nucleosome co-crystal structures solved to date: the LANA peptide from Kaposi's sarcoma-associated herpesvirus (Barbera et al., 2006), the Sir3 BAH domain (Armache et al., 2011), RCC1 (Makde et al., 2010), the ubiquitylation module of PRC1 (McGinty et al., 2014), and the SAGA deubiquitinating module (Morgan et al., 2016). I introduced three combinations of amino acid substitutions of the H2A acidic patch: H2A-E64R, H2A-D90R/E92R, and H2A-E61A/E64A/D90A/E92A. In comparison to wild type H2A, each of these H2A mutations resulted in a two-fold decrease in Chd1 nucleosome sliding rates (Figure 2.15, brown, orange, and magenta). These modest rate decreases suggest that the entry-side H2A acidic patch is not a critical epitope required for Chd1 sliding. However, it is interesting to note that these reactions were performed with saturating Chd1 (Figure 2.16), and therefore the reduced rate, while modest, suggests a catalytic rather than a binding defect.

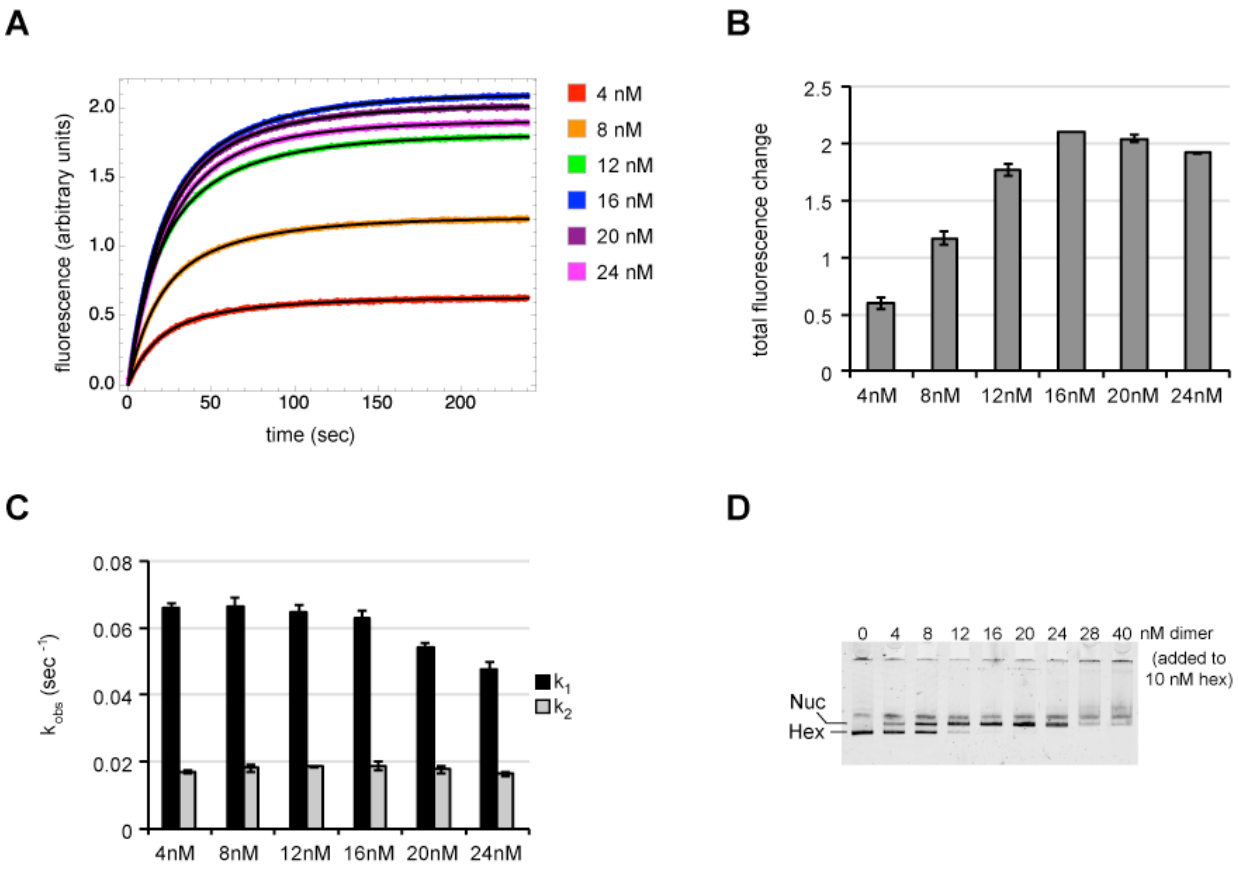

Figure 2.14: With subsaturating H2A/H2B dimer addition, rates of nucleosome sliding by Chd1 are not sensitive to nucleosome:hexasome ratios.
(**A**) Stopped flow nucleosome sliding reactions monitored by Cy3-Cy3 fluorescence quenching. The legend indicates the amount of H2A/H2B dimer in each reaction, which contained 10 nM 0-601-80 hexasome, 50 nM Chd1, and 25 μM ATP. Each trace is an average of 4 or more injections from the same stopped flow experiment. The black curves represent double exponential fits to the data.
(**B**) Graph of overall intensity changes at each H2A/H2B dimer concentration added to hexasomes, with higher intensity reflecting a greater proportion of nucleosomes that were shifted. Error bars indicate the range from two independent sets of experiments.
(**C**) Graph of sliding rates for stopped flow H2A/H2B dimer addition. The observed rates (given as k1 and k2) were determined from double exponential fits to the data. Error bars indicate the range from two independent sets of experiments.
(**D**) Native PAGE visualization of nucleosomes generated by addition of H2A/H2B dimer to hexasomes. Shown is a representative of ten similar titrations performed using wild-type or modified H2A/H2B dimers.

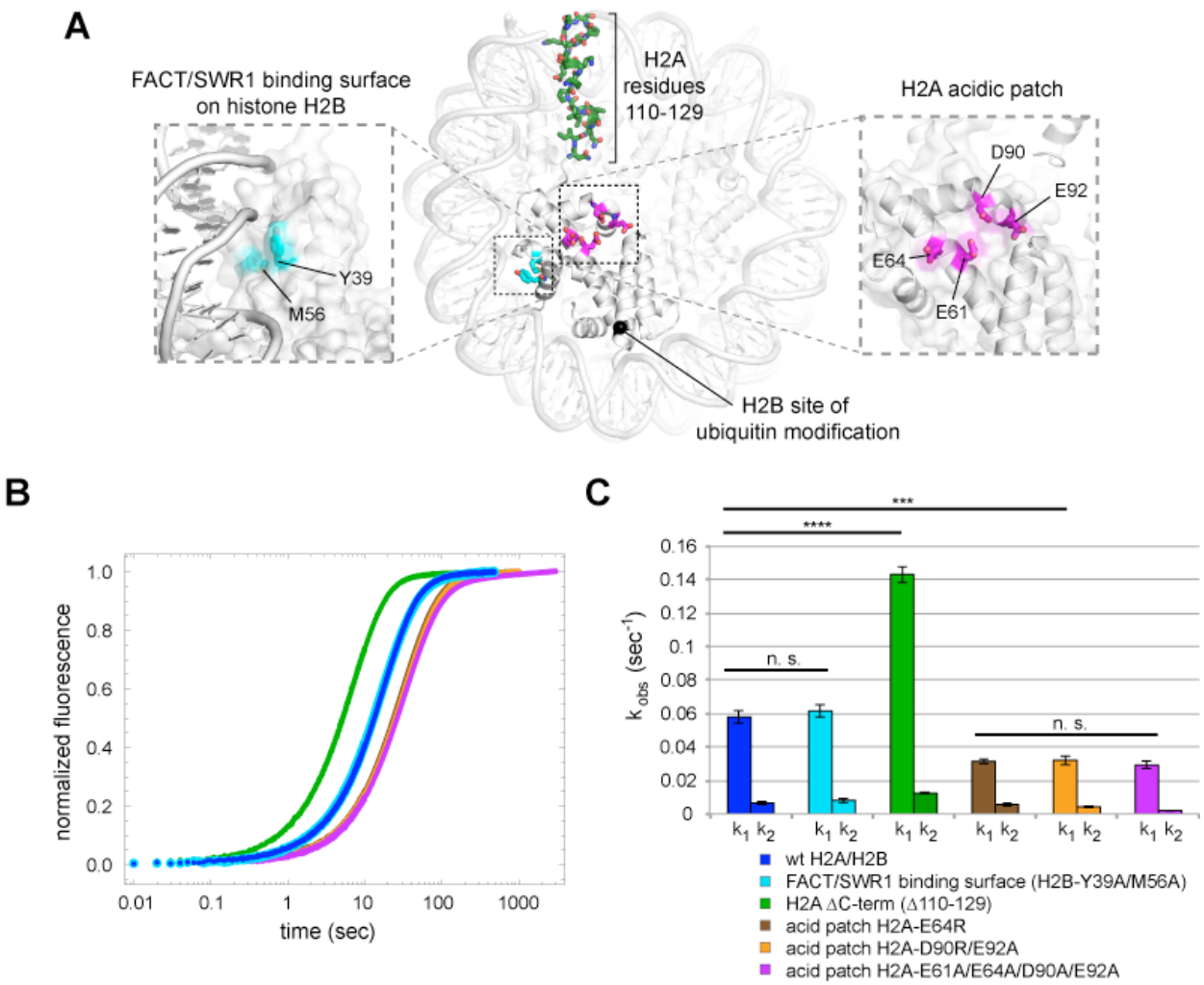

Figure 2.15: Disruptions in the nucleosome acid patch only moderately decrease sliding by Chd1

(**A**) Overview of disruptions introduced on H2A/H2B. Nucleosome crystal structure shown is PDB code 1KX5 (Davey et al., 2002).

(**B**) Stopped flow sliding reactions using asymmetric nucleosomes containing H2A or H2B disruptions on the entry side H2A or H2B. Asymmetric nucleosomes were generated by incubating 10 nM 0-601-80 hexasomes with 12 nM H2A/H2B containing one of the following sequence variants: Wt (blue); FACT/SWR1 binding surface disruption (H2B-Y39A/M56A) (cyan); H2A C-terminal tail truncation (Δ110-129) (green); acid patch single mutant (H2A-E64R) (brown); acid patch double mutant (H2A-D90R/E92A) (orange); acid patch quadruple mutant (H2A-E61A/E64A/D90A/E92A) (magenta). Reactions were performed with 400 nM Chd1 and 25 μM ATP and followed by Cy3B-Dabcyl SQOF. Each progress curve is an average of 3-6 technical replicates.

(**C**) Summary of observed rates (k_1, k_2) obtained from double exponential fits to stopped flow data as shown in (A). In every case the observed fast rate (k_1) contributes >90% of the amplitude of the progress curve. Error bars represent standard deviation from three (six for Wt) independent experiments. Statistics compare k_1 rates for indicated constructs: *** P-value < 0.00001; **** P-value <0.0000001; n.s., not significant.

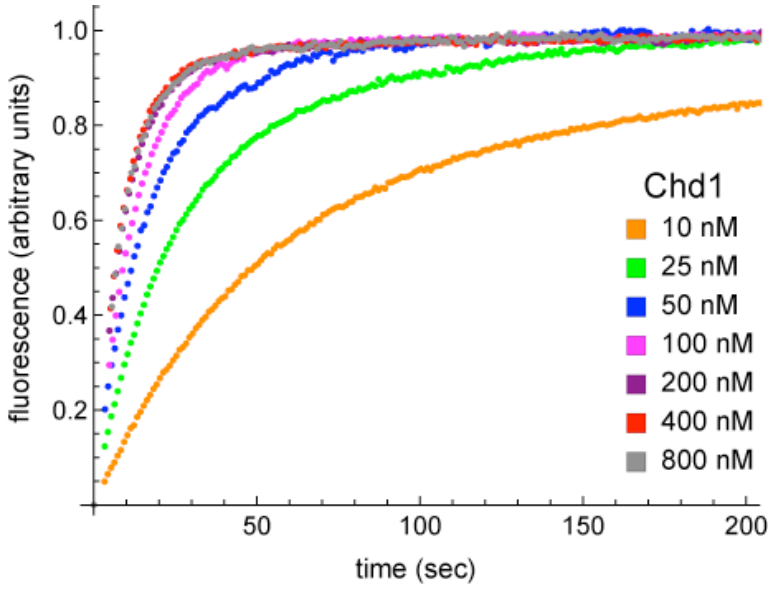

Figure 2.16: With limiting ATP, remodeling saturates at 400 nM Chd1

Nucleosomes formed by adding 12 nM dimer to 10 nM 0-601-80 hexasomes were titrated with 10, 25, 50, 100, 200, 400, and 800 nM Chd1 and 25 μM ATP. Reactions were monitored by Cy3-Cy3 SQOF via fluorometer, and show that remodeling plateaued at 400 nM Chd1. The progress curves shown are representative of two independent Chd1 titrations using unmodified H2B (Wt-Wt). Similar results were observed for duplicate titrations using Ub-Wt, Wt-Ub, and Ub-Ub nucleosomes.

Chd1 is specifically stimulated by ubiquitinated H2B on the entry-side dimer

As an alternative to disrupting a surface of H2A/H2B, I explored the addition of a ubiquitin modification to H2B. It was reasonable to expect that the large ubiquitin moiety may block access of Chd1 to a critical dimer epitope required for robust Chd1 sliding. Additionally, based on the close ties of both Chd1 and H2B ubiquitination with transcribing Pol II (Kelley et al., 1999; Krogan et al., 2002; Simic et al., 2003; Xiao et al., 2005), Chd1 likely encounters ubiquitinated nucleosomes, and it would therefore be biologically relevant to understand the impact of H2B-ubiquitination on Chd1 activity.

I used oriented hexasomes to produce nucleosomes with the four combinations of modified and unmodified H2A/H2B dimers. To assemble nucleosomes with different placements of ubiquitin, I first generated 0-601-80 hexasomes with the exit dimer either unlabeled (Wt) or chemically crosslinked to ubiquitin (Ub) via a cysteine introduced at the H2B C-terminus (Long et al., 2014). To each of these hexasomes, H2A/H2B dimer (Wt or Ub) was then added to produce the four combinations of Wt/Ub nucleosomes. Since ubiquitin significantly alters the sizes and shapes of hexasomes and nucleosomes, analysis by native gel clearly demonstrated that each reaction possessed a unique nucleosome with the desired placement of modified and unmodified H2A/H2B dimers (Figure 2.17**A**).

With these four nucleosome species, sliding reactions monitored by Cy3-Cy3 SQOF were carried out to determine whether H2B-Ub affected Chd1 activities. Despite the significant size of ubiquitin and potential to block access to H2A/H2B, the presence of this modification did not impede nucleosome sliding by Chd1. In fact, the two nucleosomes containing entry-side H2B-Ub (Wt-Ub and Ub-Ub) yielded faster rates than nucleosomes with unmodified entry-side H2B

(Figure 2.17**B**). These results reinforce the finding that Chd1 activity is sensitive to the entry-side dimer, and reveal that Chd1 is stimulated by H2B-Ub.

I used the Cy3B-Dabcyl pair to measure the rates of Chd1 sliding for nucleosomes with and without H2B-Ub on the entry side, generated from oriented hexasomes. In agreement with a preferential stimulation of Chd1, nucleosomes containing entry-side H2B-Ub consistently showed faster rates of sliding (Figure 2.17**C,D**). These experiments were conducted with saturating Chd1 (400 nM) indicating that H2B-Ub did not merely improve Chd1 binding but increased catalytic turnover. The presence of the ubiquitin moiety could accomplish this either by helping to retain Chd1 on the nucleosome thereby increasing processivity/productivity from one enzyme-binding event, or by predisposing Chd1 to adopt an active conformation on the nucleosome.

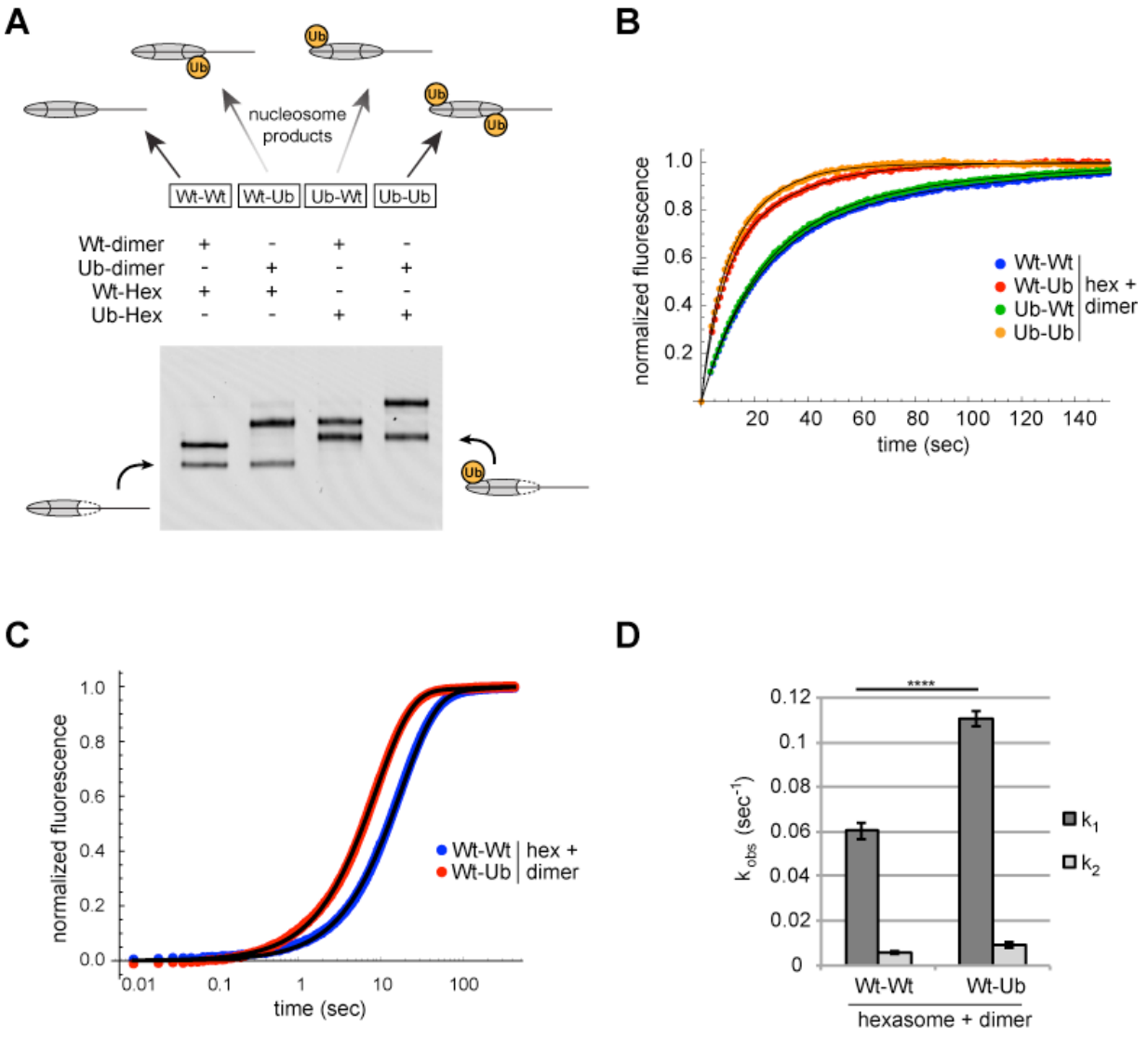

Figure 2.17: Entry-side H2B-Ubiquitin stimulates nucleosome sliding by Chd1.
(**A**) Generation of symmetric and asymmetric nucleosomes with site-specific placement of H2B-Ubiquitin. Nucleosomes were formed from subsaturating H2A/H2B dimer (12 nM) addition to 0-601-80 hexasomes (10 nM). Hexasomes and H2A/H2B dimer contained either unmodified (Wt) or ubiquitinated (Ub) H2B as indicated, and resulting nucleosome and hexasome species were visualized by native PAGE. Shown is a representative from six independent dimer addition experiments.
(**B**) Comparison of remodeling reactions with subsaturating (25 nM) Chd1, using hexasomes (10 nM) and H2A/H2B dimers (12 nM) containing unmodified or Ub-conjugated H2B. Shown are progress curves for remodeling reactions monitored using a Cy3-Cy3 pair at 25 µM ATP. Black traces represent fits to the data. Progress curves are representative of two independent experiments.
(**C**) Representative progress curves of nucleosome sliding reactions monitored by stopped flow using Cy3B-Dabcyl at 25 µM ATP and saturating (400 nM) Chd1. Each progress curve is an average of 3-6 technical replicates. Black traces represent fits to the data.
(**D**) Comparison of observed sliding rates monitored with Cy3B-Dabcyl at 25 µM ATP and saturating Chd1 (400 nM). Error bars show standard deviations from three independent experiments. **** P-value <0.0001.

The Chd1 chromodomains prevent hexasome remodeling

The H2A/H2B modifications and mutations explored in this work affected rates of nucleosome sliding even at saturating levels of Chd1, indicating these effects are not due to differences in binding of Chd1, but are catalytic or regulatory in nature. Therefore, I decided to test whether disrupting the regulatory chromodomains would affect remodeling of hexasomes.

The crystal structure of the Chd1 chromodomains and ATPase revealed a contact between an acidic wedge formed from two alpha helices in the chromodomains and a basic DNA binding patch on lobe two of the ATPase (Hauk et al., 2010). This interaction appears to stabilize the ATPase in an open conformation that inhibits ATP hydrolysis when Chd1 is not bound to the nucleosome. In Chd1 KAK (E265K/D266A/E268K), mutations in the acidic wedge disrupt this inhibitory interaction, resulting in reduced substrate specificity (Hauk et al., 2010) (Figure 2.18**A)**. For example, though deletion of the H4-tail is known to reduce remodeler activity, Chd1 KAK is able to remodel H4-tailess nucleosomes better than WT Chd1 (Hauk et al., 2010). In addition Chd1 KAK exhibits much higher ATPase activity and stronger binding on naked DNA than WT Chd1 (Hauk et al., 2010; Qiu et al., 2017). These results indicate that the chromodomains limit Chd1 activity when it is not associated with normal nucleosomes. I hypothesized that this tendency might also apply to hexasomes; suggesting Chd1 KAK may remodel hexasomes better than Chd1 WT does.

I again used histone mapping to compare hexasome sliding by Chd1 WT to Chd1 KAK (Qiu et al., 2017). On 0-601-80 nucleosomes, both Chd1 WT and Chd1 KAK shifted the majority of the end positioned nucleosomes by 32 and 41-43 bp to more central positions (Figure 2.18**B**). As I observed earlier, Chd1 WT failed to shift hexasomes missing the entry-side H2A/H2B heterodimer towards the center, though the starting material decreased for the 64’ time

point. I attribute this decrease to hexasomes sliding in the opposite direction off the end of the DNA, which would be consistent with the directional bias observed in Figure 2.9. In contrast, Chd1 KAK successfully shifted hexasomes in the direction of the missing H2A/H2B heterodimer towards the center of the DNA (Figure 2.18**B**). This movement was not as robust as for nucleosome alone, indicating that Chd1 KAK did not fully rescue sliding activity on hexasomes.

Next, I used SQOF to quantify how much autoinhibition by the chromodomains was affecting sliding rates of Chd1 on hexasomes. I first compared Chd1 WT to Chd1 KAK on hexasomes (10 nM) plus WT H2A/H2B heterodimer (20 nM) with excess, but not saturating remodeler (50 nM). I used 25 μM ATP to start the reactions, which is below Chd1's K_m for ATP and slows the reaction enough to collect kinetic information. With these conditions Chd1 KAK remodeled nucleosomes approximately 2.5 fold faster than WT (0.0213 ± 0.0005 sec^{-1} for Chd1 WT versus 0.0521 ± 0.0001 sec^{-1} for Chd1 KAK) (Figure 2.19**A**). This advantage may result from moderately tighter binding or higher overall activity by Chd1 KAK, which is unencumbered by inhibition from the chromodomains. Chd1 slides hexasomes missing the entry-side H2A/H2B heterodimer slowly, requiring the use of 1 mM ATP to observe a signal change. Even with higher ATP, Chd1 WT shifted hexasomes about 30-fold slower than nucleosomes (Figure 2.19**B**). Chd1 KAK shifted hexasomes about 20 times faster than Chd1 WT (0.00065 ± 0.00007 sec^{-1} for Chd1 WT versus 0.0127 ± 0.0019 sec^{-1} for Chd1 KAK). Even adjusting for the faster sliding observed for Chd1 KAK on nucleosome, Chd1 KAK shifted hexasomes 8-fold faster than Chd1 WT. These results indicate that the advantage that Chd1 KAK has over Chd1 WT when remodeling nucleosomes is larger when remodeling hexasomes.

These observations agree with data published by my collaborators, single molecule experts Sua Myong and Peggy Qiu from Johns Hopkins University. Using an smFRET system,

they showed that while Chd1 WT fails to shift hexasomes, Chd1 KAK does so successfully (Qiu et al., 2017).

These results suggest that the chromodomains reduce the activity of Chd1 on hexasomes. This likely prevents Chd1 from further destabilizing an incomplete construct, which may permit reassemble of the nucleosome through dimer addition.

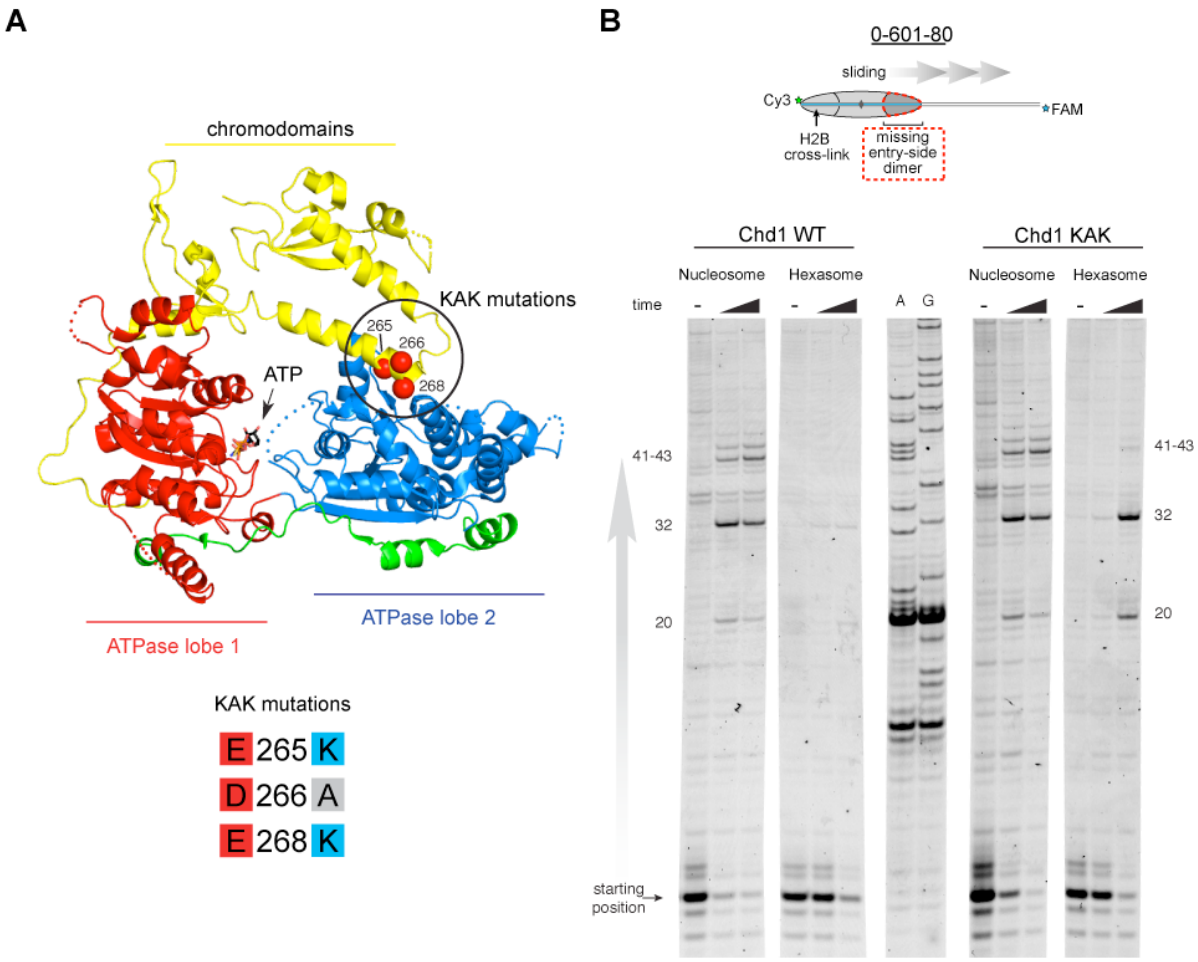

Figure 2.18: Disruption of the chromodomains permits hexasome sliding
(**A**) Structure of the Chd1 chromodomains and ATPase are shown in an autoinhibited conformation with the chromodomains contacting ATPase lobe 2. This interaction is perturbed in Chd1 KAK (red spheres). PDB code: 3MWY
(**B**) Histone mapping comparing Chd1 WT and Chd1 KAK (each 50 nM) sliding nucleosomes and hexasomes (each 150 nM) with 2.5 mM ATP. Reaction time points were taken at 0', 1' and 64'. The starting position and the distance shifted (bp) are indicated beside prominent bands. This gel is representative of three or more experiments.
(*Originally published in Qiu et al., 2018*)

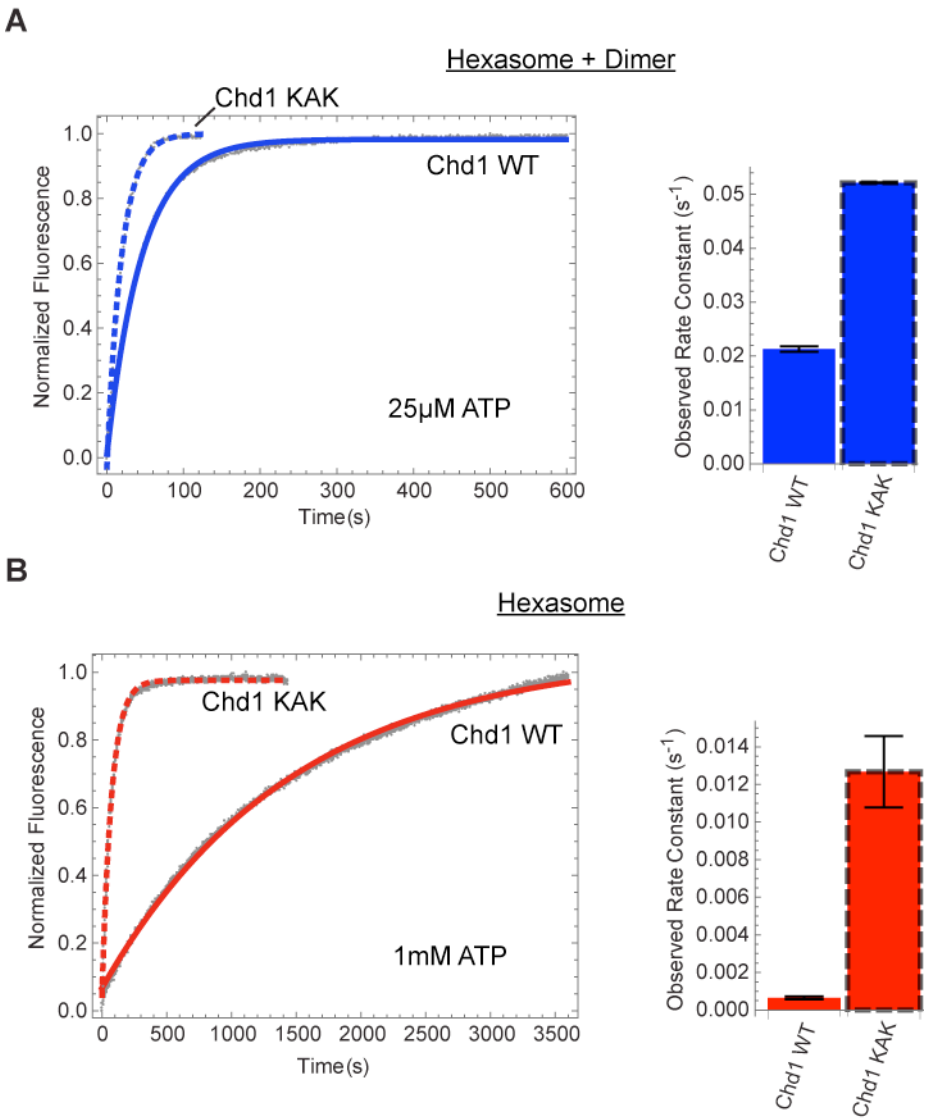

Figure 2.19: Chd1 KAK slides hexasomes faster than Chd1 WT
(**A**) SQOF experiments comparing sliding activity of Chd1 WT and Chd1 KAK (each 50 nM) with 25 μM ATP on nucleosomes made from 10 nM hexasome and 20 nM H2A/H2B dimer. Single exponential fits of Chd1 WT (solid line) and Chd1 KAK (dotted line) reveal ~2.5-fold higher rates for Chd1 KAK.
(**B**) As in (A) but with 1 mM ATP on hexasomes alone. Chd1 KAK slides hexasomes ~20-fold faster than Chd1 WT. Traces are representative of three independent experiments. Bar charts show mean ± standard deviation of three replicates.

DISCUSSION

Here I show that the Widom 601 and the Widom 603 can be used to make oriented hexasomes, a unique and powerful tool for studying chromatin-interacting factors. I generated hexasomes from nucleosome reconstitutions in the presence of limiting H2A/H2B dimer, and my work indicates that one side of both the 601 and 603 has a much higher affinity for H2A/H2B than the other, resulting in preferential salt-deposition of the dimer in a sequence-specific fashion (Figure 2.2, Figure 2.3 and Figure 2.5). While identification of sequence elements responsible for preferred H2A/H2B deposition requires further investigations, I speculate that the biased orientation of hexasomes may arise from the asymmetric distribution of inward-facing minor groove TA steps flanking the nucleosome dyad. The Widom 601 is well known for its marked asymmetry in strength of histone-DNA contacts (Hall et al., 2009), and higher salt resistance of the TA-rich side of the 601 (Chua et al., 2012) is consistent with the preferential H2A/H2B deposition that yields oriented hexasomes. Although primarily associated with H3/H4 on the most internal portion of nucleosomal DNA, the periodic TA steps also correlate with interactions between H2A/H2B and the adjacent segments of DNA. In force pulling experiments, the periodic TA steps were shown to influence unwrapping, with a strong preference for unwrapping the TA-poor side of the Widom 601 (Ngo et al., 2015). The sequence and structural properties of the DNA segment directly contacting H2A/H2B should be important for dimer affinity, and notably, one of the four TA-step positions is located at SHL3.5, a minor groove site contacted directly by H2A/H2B dimer, which is 'TA' on the TA-rich side and 'CC' on the TA-poor side (Figure 2.4). However, this contact is missing in the Widom 603, which still forms hexasomes lacking H2A/H2B on the TA-poor side (Figure 2.5). Therefore, I believe that, while DNA that directly contacts H2A/H2B likely plays a role, the stability of the adjacent H3/H4-DNA

interactions, dictated by the presence or absence of periodic TA steps surrounding the dyad may be just as important in determining H2A/H2B occupancy. The strength of histone-DNA interactions also depends on the nature of the histones themselves. Here, I focused on the widely used canonical histones from *Xenopus laevis*, and it will be interesting to discover the extent that histone variants and canonical histones of other species respond to DNA sequence elements of the Widom 601 and 603 and in naturally occurring nucleosome positioning sequences.

For chromatin remodelers, each H2A/H2B dimer is in a unique position, engaging with DNA either entering or exiting the nucleosome. Like other remodelers, the ATPase motor of Chd1 shifts DNA toward the dyad (McKnight et al., 2011), which means that the SHL2 site where the motor acts is adjacent to the entry-side H2A/H2B dimer. I show that the entry-side dimer is critical for robust sliding by Chd1, which results in a strongly biased repositioning of hexasomes toward the side with the H2A/H2B dimer (Figure 2.9). As shown by cross-linking, the absence of one H2A/H2B dimer does not appear to diminish binding of the Chd1 ATPase motor to either SHL2 site of the hexasome (Figure 2.11), strongly suggesting that the defect in sliding occurs after engagement of the remodeler. This defect could be regulatory or mechanical in nature.

While disruption of the entry-side H2A acidic patch modestly decreased Chd1 sliding, I was unable to identify an epitope on the entry side H2A or H2B that mimicked the dramatic loss of sliding activity seen with hexasomes. In these studies, I was principally concerned with disrupting the entry-side dimer, since Chd1 slides hexasomes missing that H2A/H2B dimer so poorly. Since publication of this data, I found that Chd1 activity is also reduced on nucleosomes containing disruptions in the exit-side acidic patch and both acidic patches (discussed in **Chapter 4**). Even with mutations in both acidic patches, Chd1 remodeling was only ~10 fold

slower than on WT nucleosomes, which is minor compared to the >300-fold decrease in activity on hexasomes missing the entry-side H2A/H2B dimer.

Rather than requiring a specific interaction with the entry side H2A/H2B dimer, Chd1 may instead be responding to DNA unwrapping. DNA unwrapping could affect remodeling either through a regulatory interaction where Chd1 decreases activity in response to an aberrant form of the nucleosome, or due to mechanical factors that limit translocation from the unwrapped side of the hexasome. EM structures of Chd1 bound to the nucleosome show the Chd1 ATPase at SHL 2 with the DBD contacting the opposite gyre and unwrapping two turns of exit DNA (Farnung et al., 2017; Sundaramoorthy et al., 2018). It is not completely understood how this cross-gyre unwrapping interaction might affect sliding. An smFRET investigation found that a subset of sliding events were preceded by motions that appear to be unwrapping, but more studies need to be performed to be sure this is meaningful (Kirk et al., 2018). The cross gyre interaction is associated with lower ATPase activity indicating this interaction may down-regulate ATPase activity when exit DNA is available the DBD to bind (Nodelman et al., 2017). This observation suggests that the directional sliding of hexasomes could be due to a bias toward remodeler activity on the side of the hexasome that cannot form the inhibitory cross-gyre interaction. Without the H2A/H2B dimer, DNA would be expected to make its last contact with the hexamer at SHL 2.5, adjacent to the SHL 2 site where I observe weaker remodeler activity on hexasomes. The cross-gyre arrangement is still possible from this SHL 2 site because the exit side DNA is wrapped by the remaining dimer on the other gyre. However, a remodeler positioned on the opposing SHL 2 site would not be able to make the same inhibitory cross-gyre interactions because the exit DNA is unwrapped from that side of the hexasome. As I observe, this difference in remodeling activity would bias hexasome sliding towards the side with

H2A/H2B. One caveat to this interpretation is that while Chd1 repositions hexasomes missing the exit-side H2A/H2B dimer much faster than those missing entry-side H2A/H2B, it does so slower than nucleosomes (Figure 2.9). The regulatory explanation of hexasome sliding is consistent with my observations that disruption of the autoinhibitory chromodomains in Chd1 KAK improves hexasome sliding (Figure 2.18). However, Chd1 KAK still slides hexasome far slower than nucleosomes, suggesting there are other difficulties in hexasome sliding (Figure 2.19). Another possibility to explain the reliance of Chd1 on the entry-side H2A/H2B dimer is that Chd1 has difficulty catalyzing DNA translocation from the SHL 2 site adjacent to the unwrapped side of the hexasome. Any transient unwrapping from the last histone contact at SHL 2.5 would detach the DNA bound by the ATPase from the histones. It follows that detaching this segment of DNA would prevent the ATPase from moving the histone core. Spontaneous DNA unwrapping has been observed at the edge of the nucleosome (Li and Widom, 2004), and DNA strain generated by action of the ATPase at SHL 2 could make unwrapping at the edge of the hexasome even more likely.

Sensitivity to DNA unwrapping is consistent with slower nucleosome sliding activity of Chd1 when a transcription factor is bound on the entry side of the nucleosome (Nodelman et al., 2016). Transcription factors compete with histone-DNA contacts and can dramatically unwrap nucleosomal DNA when their binding sites are located within the histone footprint (Li and Widom, 2004; North et al., 2012). By slowing nucleosome sliding by Chd1, analogously to what I observe here with hexasomes, DNA unwrapping could provide a means for sensing a transcription factor at the nucleosome edge, which in turn would help avoid pulling transcription factors further onto the nucleosome. Although experiments performed here were limited to the Chd1 remodeler, we expect that the biochemically similar ISWI remodelers, which slide

nucleosomes directionally away from bound transcription factors and generate evenly spaced nucleosome arrays (Kang et al., 2002; Li et al., 2015; Lusser et al., 2005), should also exhibit a strong directional bias in sliding hexasomes.

The directional sliding of hexasomes by Chd1 contrasts with the back-and-forth movement typical for nucleosomes and likely influences chromatin organization *in vivo*. *In vitro*, both transcription through nucleosomes by Pol II and remodeling by RSC along with the NAP1 chaperone have been shown to generate hexasomes (Kireeva et al., 2002). Although histone chaperones such as FACT would be expected to replace the missing H2A/H2B dimer during transcription, the passage of Pol II has been shown to specifically displace the H2A/H2B dimer distal to the promoter (Hsieh et al., 2013; Kulaeva et al., 2009), which would orient hexasomes for biased sliding toward the 5' end. One speculative idea is that nucleosome array packing against the +1 nucleosome, which is dependent on Chd1 and ISWI chromatin remodelers (Gkikopoulos et al., 2011; Zhang et al., 2011), would be favored by directional hexasome sliding (Figure 2.20). Even with relatively few or transient hexasomes, directional sliding toward the transcriptional start site would be expected to corral upstream nucleosomes, similar to the phasing of nucleosome arrays against transcription factor-targeted nucleosomes (McKnight et al., 2011; Wiechens et al., 2016). Consistent with this idea, it has been shown that inactivation of Pol II relaxes nucleosome packing in coding regions, resulting in a nucleosome drift of ~10 bp toward the 3' end of yeast genes (Weiner et al., 2010).

This work also demonstrates how hexasomes made using the Widom 601 are a useful tool for generating specifically oriented asymmetric nucleosomes. To extract meaningful information on nucleosome dynamics, single molecule FRET experiments require a single, specifically positioned donor-acceptor pair (Blosser et al., 2009; Deindl et al., 2013; Ngo et al.,

2015). However, due to the pseudo two-fold symmetry of the nucleosome, labeling any of the histones with a FRET fluorophore (donor or acceptor) typically yields three different labeling configurations (Deindl et al., 2013). The presence of multiple FRET pairs, each with distinct and potentially closely spaced FRET values substantially complicates such analyses and at the same time limits throughput by decreasing the population of nucleosomes with the desired labeling configuration. Here, we show how oriented hexasomes can yield a homogeneously labeled population (Figure 2.10) that greatly facilitates smFRET experiments.

I furthermore demonstrate the utility of oriented hexasomes for generating asymmetric nucleosomes containing a uniquely positioned H2A/H2B PTM (Figure 2.17**A**). This method complements a recent procedure described for generating nucleosomes with distinct H3 tails (Lechner et al., 2016), and has the added advantage that the standard nucleosome reconstitution is sufficient for making oriented hexasomes, which can then be readily transformed into asymmetric nucleosomes with H2A/H2B dimer addition. Given the prevalence of asymmetric histone modifications and variants, this methodology should aid further investigation into how spatial cues contribute to the histone code, especially when used in conjunction with recent advances in detecting modifications on asymmetric nucleosome substrates (Liokatis et al., 2016).

Using this methodology, I demonstrate that ubiquitin-modified H2B stimulates Chd1, but only when present on the entry-side dimer (Figure 2.17). Unexpectedly, the stimulatory effect of ubiquitin was observed even with saturating remodeler concentrations, indicating that it is not merely the result of improved Chd1 binding. A recent cryo-EM structure of Chd1 in complex with a nucleosome does not show a direct interaction between Chd1 and ubiquitin (Sundaramoorthy et al., 2018). However, since this structure was solved in the presence of the post-hydrolysis ATP mimic, ADP•BeF_3^-, other conformations may exist during remodeling with

ATP where ubiquitin interacts with Chd1. While we favor the idea of a direct interaction, where ubiquitin stabilizes an active conformation of Chd1 on the nucleosome, it is also possible that H2B-Ub alters the structure or dynamics of the nucleosome itself. Interestingly, H2B-Ub is required for maximum stimulation of Pol II transcription by FACT, potentially through aiding displacement of H2A/H2B (Pavri et al., 2006).

The stimulatory effect of ubiquitin raises new questions regarding how histone modifications bias chromatin remodelers, and more broadly, the discovery of oriented hexasomes should be a valuable tool for deepening our understanding of chromatin biology.

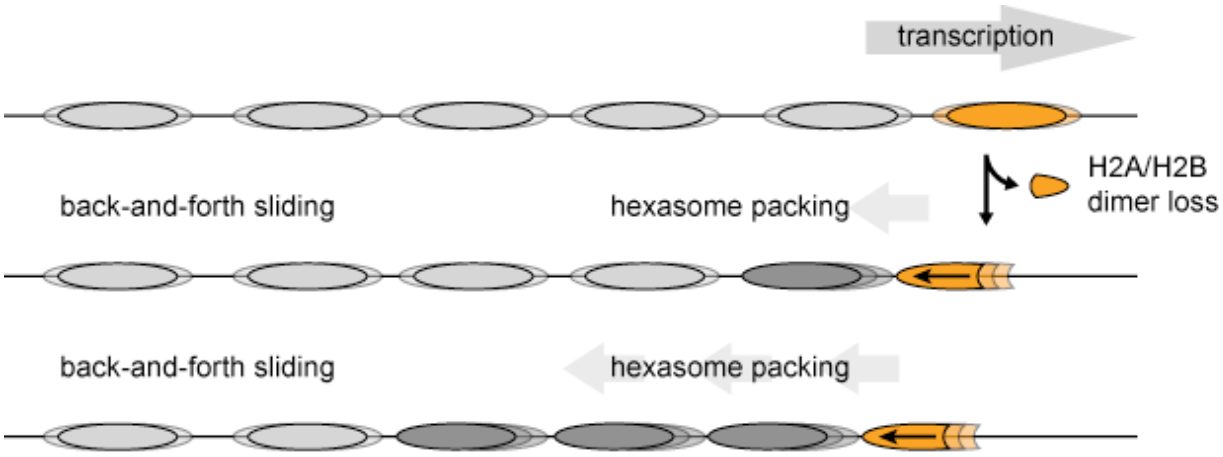

Figure 2.20 Model for nucleosome packing by oriented hexasomes
As others have shown, transcription by Pol II through nucleosomes is facilitated by removal of the promoter-distal H2A/H2B dimer (Kulaeva et al., 2009). My results indicate that Chd1 would slide a hexasome of this orientation upstream. We propose that one or more hexasomes would corral intervening nucleosomes toward the promoter. Alternately, if every transcribed nucleosome were briefly converted to a hexasome, unidirectionally sliding of each hexasome would maintain tight nucleosome packing.

Chapter 3: Probing Nucleosome Movement with Fluorescence: Options and Obstacles

ABSTRACT

Fluorescent probes are valuable tools for determining the location, separation and movement of biomolecules. Fluorescent probes have been harnessed to study rearrangements of the nucleosome; including DNA unwrapping from the edge of the nucleosome and sliding of the histone octamer along DNA. Here, I use FRET between fluorescent labels on the histone core and DNA near the entry exit region to monitor nucleosome unwrapping by Chd1. I find that Chd1 unwraps DNA in a nucleotide and sequence-dependent manner and does not rely on the DBD for unwrapping. I discover that the intrinsic fluorescence of the histone label is sensitive to the unwrapped state of the nucleosome. In nucleosome sliding assays, I find that labeling arrangement that place the FRET pair in close proximity can lead to quenching of both donor and acceptor, consistent with static quenching. I discuss different fluorescence approaches to monitor nucleosome remodeling, and how to separate competing fluorescence responses.

INTRODUCTION

Methods employing fluorescent probes are widely used in biological studies, providing information about the localization, separation and environment of biomolecules. Though these methods are powerful, care must be taken to control the competing processes affecting fluorophores.

Fluorophores are molecules capable of absorbing light energy and re-emitting that energy at a longer wavelength. Fluorophores include many kilodalton fluorescent proteins, such as the ubiquitous green fluorescent protein (GFP) and its many derivatives, and also small molecules closer to the size of a nucleotide, including the cyanine dyes, rhodamine and fluorescein, among others. These small fluorophores generally share structural themes of highly conjugated and aromatic moieties which facilitates energy absorption. When a fluorophore absorbs light energy, it transitions from the ground state singlet (S_0) to an excited singlet (S_1 or S_2) on the femtosecond timescale. Once excited, the fluorophore can take a variety of decay pathways back to the ground state S_0, which includes releasing a photon as fluorescence. Other transitions involve energy loss to the solvent including vibrational relaxation to the lowest vibrational level of the occupied singlet and internal conversion from higher singlets (e.g., S_2) to the lowest singlet (S_1). Since fluorescence lifetimes are longer (~ 10^{-8} sec) than the timescales for vibrational relaxation and internal conversion to S_1 (~ 10^{-12} sec), fluorescence decay usually happens from the lowest vibrational level of S_1. This, coupled with the tendency to decay to a higher vibrational state of S_0, causes the emitted light to be of a lower energy level (longer wavelength) than the excitation source (Lakowicz, 2006). This energy difference leads to the Stokes shift, describing the absorbance of light at shorter wavelengths and emission at longer wavelengths. Other decay pathways from the excited singlet involve non-radiative energy transfer to other molecules in solution and, in special cases, deactivation of the singlet state during isomerization of the excited fluorophore. In addition, a fluorophore can be deactivated by electron loss causing photobleaching.

The fluorescence of an excited fluorophore is determined by the balance of decay pathways back to the ground state. The fluorescent emissions from a fluorophore can be used to

track the location of individual molecules, as in microscopy, but fluorescence intensity also provides information on the environment of the fluorophores. The fluorescence yield (or fluorescence intensity) of a fluorophore is determined by the ratio of the rate of fluorescent decay to the sum of the rates of all other decay pathways from the excited singlet. This means that fluorescence intensity is sensitive to environmental factors such as temperature, viscosity, and interactions with other molecules that can prevent excitation or absorb excitation energy from the fluorophore. In certain cases energy may be transferred from an excited donor fluorophore to an acceptor molecule in the ground state, thereby exciting the acceptor through a process known as Fluorescence Resonance Energy Transfer (FRET) (Clegg, 1992). FRET is a non-radiative energy transfer through dipole-dipole coupling of donor and acceptor. The acceptor molecule need not be fluorescent as in the case of the black hole quenchers (Johansson and Cook, 2003), but the absorbance spectrum of the acceptor must overlap with the emission spectrum of the donor. To describe energy transfer, the FRET efficiency (E) is defined as the ratio of the difference between the fluorescent quantum yield of the donor with and without the acceptor to the fluorescent quantum yield of the donor alone. For a fluorescent acceptor, this can be expressed as the ratio of acceptor emissions to the sum of donor and acceptor emissions (equation 1). Thus, complete energy transfer to the acceptor results in E =1. Expressing E as a unit-less ratio contributes to the portability of FRET measurements and affords an internal control for fluctuations in excitation or variation in fluorophore concentration. However, this quantification of E demands that the fluorescence of the donor and acceptor do not vary with any process other than FRET, which necessitates careful control depending on the system.

$$E = \frac{Y_A}{Y_A + Y_D} \qquad \text{(equation 1)}$$

FRET efficiency is very sensitive to the distance separating the FRET pair (Clegg, 1992; Shrestha et al., 2015). E decreases with the inverse sixth power of the distance between donor and acceptor (R). The Forster radius (R_0) is the value of R where E=0.5 and varies for the donor-acceptor pair (equation 2). Thus, FRET can be used as a molecular ruler to determine the distance between fluorophores. R_0 is specific to the FRET pair used but generally ranges from 10-100 Å (Cy3/Cy5 R_0=56 Å). R_0 is sensitive to the refractive index of the solvent (n), the fluorescence quantum yield of the donor (Y_D), the orientation factor of the donor/acceptor dipoles (κ, κ^2 =⅔ for randomly tumbling fluorophores), and the spectral overlap integral between donor emission and acceptor absorbance ($J(\nu)$) (equation 3). Y_D and κ can be sensitive to the labeling geometry and environment of the fluorophores so the exact value of R_0 can vary depending on experimental details. Due to the ability of rapid fluorescence data collection, FRET experiments allow the changing distance between molecules to be determined with high kinetic resolution allowing the rearrangement of molecular complexes to be probed.

$$E = \frac{1}{1+\left(\frac{R}{R_0}\right)^6} \qquad \text{(equation 2)}$$

$$R_0 = \sqrt[6]{\left(8.75\times10^{-25}\right)Y_D\kappa^2 n^{-4} J\left(\nu\right)} \qquad \text{(equation 3)}$$

FRET has been a valuable tool in the study of nucleosome dynamics. Li and Widom used FRET to observe spontaneous unwrapping of DNA from the edge of the nucleosome (Li and Widom, 2004). By labeling the 5' end of the DNA with Cy3 and the histone core with Cy5 on either H2A K119C or H3 V35C, FRET was used to reveal spontaneous DNA unwrapping, unwrapping due to salt titration and the stabilization of the unwrapped state by transcription

factors (Li et al., 2004; North et al., 2012; Simon et al., 2011; Tims and Widom, 2007; Tims et al., 2011). Structures of the nucleosome solved with the Chd1 ATP-dependent chromatin remodeler show Chd1 unwrapping two turns of DNA from the nucleosome edge (Farnung et al., 2017; Nodelman et al., 2017; Sundaramoorthy et al., 2017, 2018). Thus, FRET should also lend itself to studying unwrapping by Chd1.

FRET has also been used to a monitor the activity of chromatin remodelers sliding nucleosomes. Chromatin remodelers catalyze the repositioning of nucleosomes along DNA by pulling DNA on the entry-side of the nucleosome and pushing DNA out the exit-side. Using a labeling scheme similar to the one used to monitor DNA unwrapping, nucleosome sliding can be monitored as changes in FRET as the DNA labeling site is moved relative to the histone labeling site. In bulk studies, this method has been used to characterize the linker length sensitivity of the ACF remodeling complex and its catalytic subunit, SNF2h (Hwang et al., 2014; Yang and Narlikar, 2007; Yang et al., 2006), and to investigate how remodeling activity is affected by histone mutations (Gamarra et al., 2018). Due to the complexity of the nucleosome-remodeler system, these studies did not use FRET to measure exact distances but instead used the change in FRET to characterize the apparent remodeling kinetics. In single molecule FRET (smFRET) experiments, distance is sometimes correlated with FRET by creating a calibration curve using a series of nucleosomes labeled on linker DNA incrementally farther away from the nucleosome (Blosser et al., 2009; Deindl et al., 2013). This method is more reliable in single molecule studies, which can ensure that data is collected only for nucleosomes containing both fluorophores and with only one histone label proximal to the DNA label.

Previous smFRET studies concluded that Chd1 requires sufficient linker DNA to accommodate the DBD during Chd1 unwrapping (Sundaramoorthy et al., 2017). However, these

experiments only considered unwrapping in one sequence orientation of the Widom 601, which is known to be very asymmetric in the strength of histone DNA contacts (Hall et al., 2009; Ngo et al., 2015). Here, I use FRET determine that Chd1 unwraps the nucleosome in a nucleotide- and sequence-dependent manner. I show that while the DBD contributes to unwrapping at lower Chd1 concentrations, it is not entirely necessary for unwrapping. While performing bulk FRET experiments to monitor nucleosome unwrapping and sliding, I found that processes other than FRET were affecting the fluorescence of both donor and acceptor. Labeling arrangements that allow contact between the FRET pair promoted quenching of the Cy5 acceptor. Experiments on nucleosomes containing a single Cy3 suggested the fluorescence of cyanine dyes on the histones near the entry/exit region were sensitive to DNA unwrapping. I discuss alternate fluorescence strategies to control for competing fluorescence effects while monitoring nucleosome movement.

RESULTS

DNA unwrapping by Chd1 is affected by DNA sequence and nucleotide state

Recent structures of the nucleosome-Chd1 complex reveal that Chd1 unwraps approximately two turns of DNA from the edge of the nucleosome. In these structures, the Chd1 ATPase is bound to SHL2 and the DBD is contacting DNA unwrapped from the opposite gyre (Farnung et al., 2017; Sundaramoorthy et al., 2017, 2018). These structures were all solved in the presence of the non-hydrolyzable ATP transition state mimic, ADP•BeF_3^-, leading us to question how the state of the bound nucleotide affected Chd1 induced unwrapping.

Pioneering work by Jonathan Widom used FRET to investigate spontaneous small scale unwrapping or “breathing” from the nucleosome edge, which increases accessibility of nucleosomal DNA to transcription factors. To examine unwrapping by Chd1, I followed a

similar strategy in which Cy5 maleimide was attached to histone H3(V35C) adjacent to DNA entering/exiting the nucleosome, and Cy3 was attached to the DNA end 12 bp outside the nucleosome (Li and Widom, 2004) on 12N80 and 80N12 constructs (Figure 3.1**A,B**). Using these two constructs enabled the comparison of unwrapping from either side of the Widom 601, which is asymmetric in the number of TA dinucleotides facing the histone octamer. These TA dinucleotides facilitate DNA bending around the octamer, and the side of the 601 containing more TA steps (TA-rich, left) requires more force to unwrap than the side with fewer TA steps (TA-poor, right) (Hall et al., 2009; Ngo et al., 2015). Thus, the 12N80 and 80N12 constructs probe unwrapping from the TA-rich and TA-poor sides, respectively.

To investigate how the bound nucleotide affects unwrapping by Chd1, I titrated these nucleosomes (20 nM) with Chd1 in nucleotide-free (apo), AMP-PNP and ADP•BeF_3^- nucleotide states while monitoring unwrapping as a change in FRET between the fluorophores. I monitored FRET from the nucleosomes by exciting the Cy3 donor at 510 nm by following the emission of both Cy3 at 565 nm and the Cy5 acceptor at 665 nm. In the fully wrapped state, the two fluorophores are close together, enabling FRET from Cy3 to Cy5. With unwrapping the fluorophores are move apart, reducing FRET. In ideal conditions, FRET efficiency can be calculated as a ratio of Cy5 acceptor emissions (peak=665 nm) to the difference between Cy3 donor (peak = 565 nm) and Cy5 acceptor emissions. Since it is a ratio normalized from 0 to 1, FRET efficiency internally controls for variation in nucleosome concentration or fluctuations in excitation intensity. Using FRET efficiency in this way demands that the emissions of both fluorophores are only impacted by FRET. However, emissions from the H3-Cy5 label under direct excitation at 645 nm decreased with Chd1 titration, indicating Cy5 fluorescence was responding to environmental changes independent of FRET (Figure 3.2). To determine if this

fluorescence response was due to Chd1 binding alone or nucleosome unwrapping, I titrated the nucleosomes with salt to induce unwrapping (Figure 3.3). With increasing salt, Cy5 emissions decreased under direct excitation or by excitation of Cy3 for 12N80 and 80N12 nucleosomes. This suggests that unwrapping was affecting the intrinsic fluorescence of Cy5. Therefore, instead of tracking FRET efficiency, I decided that increase in Cy3 fluorescence due to loss of FRET quenching would more appropriately report on unwrapping. While this approach lead to higher noise, the resolution was sufficient to perform my analysis. Chd1 titrations were fit using a binding isotherm to determine the concentration of at half maximum unwrapping (K_{unwrap}).

Chd1 unwraps the two sides of the Widom 601 differently depending on the state of the bound nucleotide. In AMP-PNP, Chd1 unwrapped 80N12 nucleosomes at much lower K_{unwrap} values of 13 ± 2 nM compared to 700 ± 200 nM for 12N80 nucleosomes (Figure 3.1**B**). This difference agrees with observations that the TA-poor side of the Widom 601 (observed with 80N12) unwraps more easily than the TA-rich side (observed with 12N80) (Hall et al., 2009; Ngo et al., 2015). These differences were not observed for the apo state with Chd1 unwrapping both sides at similarly high K_{unwrap} values of 800 ± 400 nM for 12N80 and 700 ± 200 nM for 80N12. The 12N80 is unwrapped at similar values in apo and AMP-PNP, in contrast with the 80N12, which Chd1 unwraps much more easily in AMP-PNP. This indicates that, in the apo state, Chd1 is either insensitive to sequence or binds and unwraps so poorly that the sequence effect is no longer observable. Surprisingly, the TA-rich side was not unwrapped more easily with AMP-PNP than apo, suggesting that the more tightly wrapped DNA presents a barrier to unwrapping that was insensitive to the AMP-PNP state. In ADP•BeF_3^- conditions, unwrapping was achieved at low Chd1 concentrations leading me to fit titrations to a stoichiometric function. The saturation point was 51±5 nM, approximately 2:1, for the 12N80, and 22±2 nM or roughly

1:1 for the 80N12, again suggesting that Chd1 unwraps the TA-poor side of the Widom 601 more easily. The lower concentrations required to unwrap the TA-poor side might also suggest that Chd1 prefers to bind the easily unwrapped side, but this would required a side-specific binding assay to confirm. These results demonstrate that unwrapping by Chd1 is affected by both DNA sequence and nucleotide state of the remodeler.

The nucleotide dependence of unwrapping is consistent with the ATPase driving unwrapping. I asked if other domains contribute to DNA unwrapping. Recent EM and crosslinking studies indicate that the chromodomains and ATPase motor of Chd1 bind to internal sites on nucleosomal DNA, ~1 and ~2 helical turns from the nucleosome dyad, respectively, whereas the Chd1 DNA-binding domain (DBD) binds to DNA unwrapping from the opposite gyre (Farnung et al., 2017; Nodelman et al., 2017; Sundaramoorthy et al., 2017, 2018). This conformation suggests that, while the ATPase and chromodomains help position the DBD on the opposite DNA gyre, the DBD is pivotal in forming interactions with the unwrapped DNA (Nodelman et al., 2017). To determine the role of the DBD, I examined nucleosome unwrapping by a Chd1 construct lacking the DBD (Chd1ΔDBD). Since the DBD contributes to Chd1 binding to the nucleosome (see Nodelman et al., 2017, Figure 3), I performed these experiments in ADP•BeF_3^- conditions, which favor tight binding. Titration of Chd1ΔDBD increased Cy3 emissions to the same degree as for titration of WT Chd1, indicating that Chd1 can induce significant unwrapping without the DBD (Figure 3.1**C**). However much more Chd1ΔDBD was required for unwrapping, resulting in K_{unwrap} values of 500±300 nM for 12N80 nucleosomes and 300 ± 200 nM for 80N12, roughly 10 and 14 times higher than for WT Chd1. Unfortunately, these data were too noisy to compare unwrapping between the two sides of the 601. Given the apparent coordination of unwrapped DNA by the DBD, the conclusion that the ATPase and

chromodomains are sufficient to induce DNA unwrapping from the nucleosome edge is unexpected. Unwrapping may in turn be mediated by contacts between the ATPase and the opposite gyre revealed by EM structures (Farnung et al., 2017; Sundaramoorthy et al., 2018; Tokuda et al., 2018). Given the sensitivity of the Chd1 to the nucleotide state and the contacts that the ATPase forms with the opposite gyre, we favor the interpretation that nucleosomal wrapping is coupled to nucleotide-dependent conformational changes of the ATPase motor.

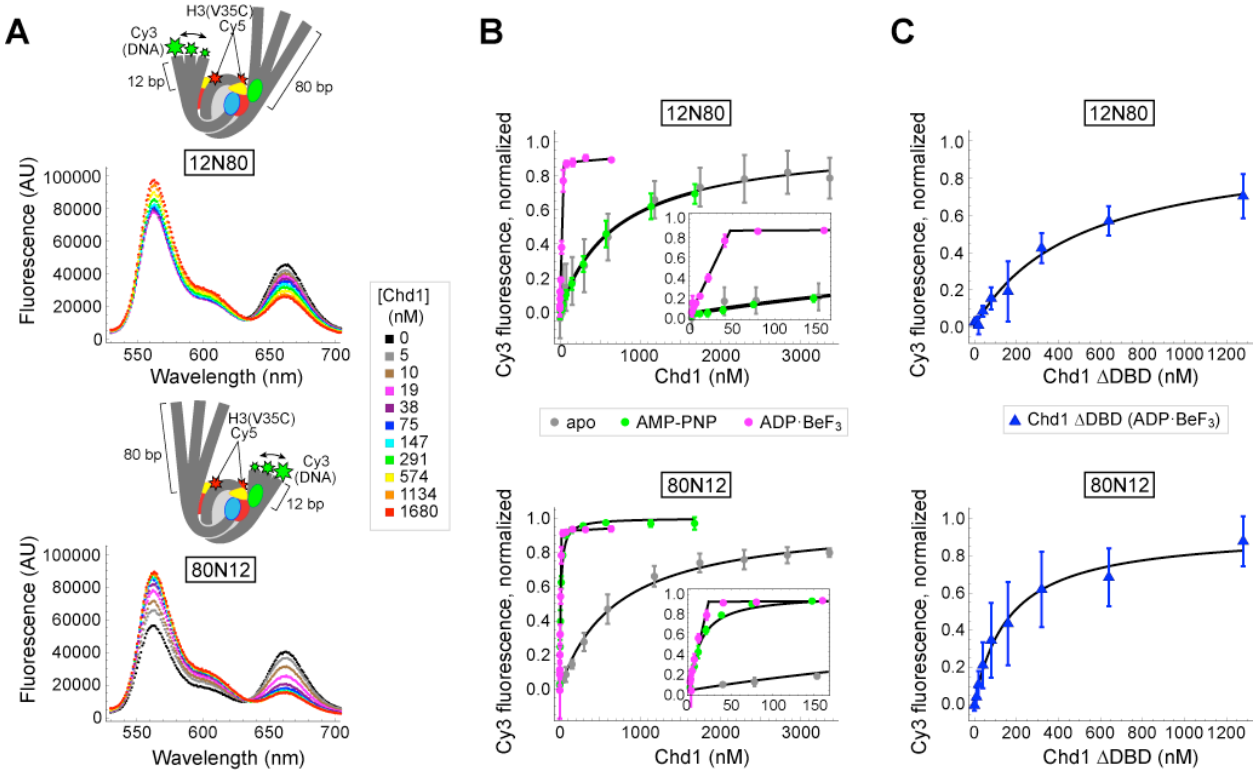

Figure 3.1: Unwrapping of DNA from the edge of the nucleosome as monitored by FRET
(**A**) Schematic illustrations show the Cy3/Cy5 FRET pair positioning on 12N80 (top) and 80N12 (bottom) nucleosomes to monitor unwrapping from the TA-rich and TA-poor sides of the Widom 601, respectively. The domains of Chd1 are shown associated with the nucleosome—chromodomains (yellow), ATPase motor (red and blue), and DNA-binding domain (green). Representative wavelength emissions scans under excitation at 510 nm reveal changes in fluorescence due to unwrapping as Chd1 is titrated on nucleosomes in the presence of 1 mM AMP-PNP.
(**B**) Cy3 peak emissions under excitation at 510 nm are plotted for 20 nM 12N80 (top) or 20 nM 80N12 (bottom) nucleosomes as Chd1 is titrated in various nucleotide conditions: apo (gray), 1 mM AMP-PNP (green), and 1 mM ADP·BeF_3^- (magenta). Insets show detail of unwrapping response at low concentrations where Chd1 unwraps at stoichiometric concentrations in ADP·BeF_3^-. Error bars represent the standard deviation from three or more replicates. Black lines show the average of individual fits to a binding isotherm
(**C**) The Chd1 DBD is not required for unwrapping DNA from nucleosomes. As in (B) but titrating Chd1ΔDBD in the presence of ADP·BeF_3^-.
(*Originally published in Tokuda et al., 2018*)

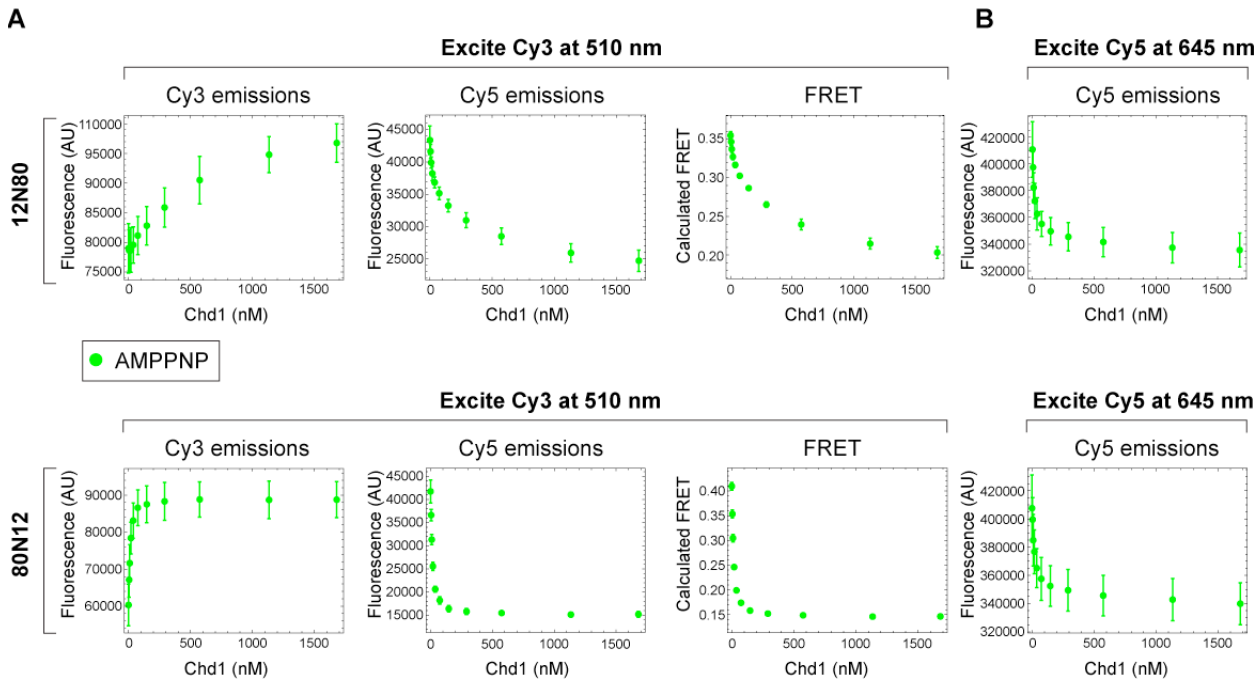

Figure 3.2: Both Cy3 and Cy5 emissions respond to the presence of Chd1
(**A**) Peak Cy3 and Cy5 emissions are shown during Cy3 excitation (510 nm) of 12N80 (top) and 80N12 (bottom) nucleosomes titrated with Chd1 in the presence of 1 mM AMP-PNP. FRET was calculated using equation 1. The two nucleosomes exhibited different signal responses, consistent with different unwrapping characteristics of the two sides of the nucleosome.
(**B**) From the same experiments as in (A), Cy5 emissions were monitored under direct excitation (645 nm), which isolates Cy5 emissions from FRET from Cy3. Emissions decrease with addition of Chd1 indicating that the Cy5 labeling position is sensitive to Chd1 binding or unwrapping independent of FRET. The two nucleosomes exhibited very similar responses due to the presence of the H3 V35C-Cy5 histone label on both sides of the nucleosome. Plotted points represent the mean ± standard deviation for three independent titrations.
(*Originally published in Tokuda et al., 2018*)

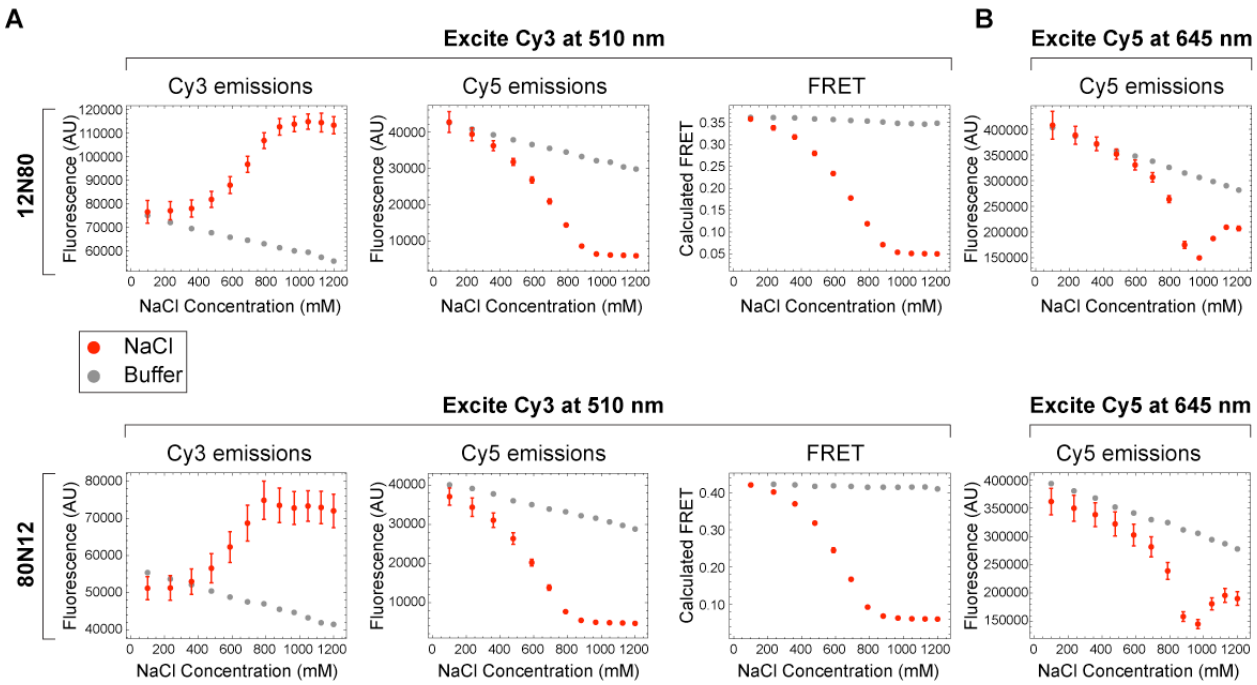

Figure 3.3: Cy5 emissions are sensitive to salt titration-induced DNA unwrapping
(A) To determine if the H3 V35C-Cy5 label is sensitive to unwrapping, 12N80 (top) and 80N12 (bottom) nucleosomes were titrated with NaCl to promote salt-induce nucleosome unwrapping. Peak Cy3 and Cy5 emissions are shown during Cy3 excitation. FRET efficiency was calculated using equation 1. To account for reductions in fluorescence due to dilution, experiments were repeated with buffer (gray), which shows a linear decrease, as expected. Note that the buffer titration did not cause a significant drop in FRET, since FRET is a ratio of fluorescence of two dyes, both of which are affected by dilution. With salt titration (red), signals responded similarly to the Chd1 titrations in Figure 3.2. Salt titration error bars represent standard deviation of three independent experiments. Buffer titrations were performed twice with a representative shown here.
(**B**) From the same experiments as in (A), Cy5 emissions were monitored under direct excitation (645 nm), which isolates Cy5 emissions from FRET from Cy3. Cy5 emissions decrease with salt titration suggesting unwrapping of DNA is sufficient to affect fluorescence of the H3 V35C-Cy5 label, independent of Chd1 binding.
(*Originally published in Tokuda et al., 2018*)

Closely placed FRET pairs diminish acceptor emission

To study the activity and regulation of Chd1 I sought to monitor the kinetics of nucleosome sliding using FRET. Chd1 slides mononucleosomes away from DNA ends towards more centered positions on the DNA. Similar to the approach used in unwrapping experiments, this movement can be tracked by labeling the DNA and histones at the edge of the nucleosome with a FRET pair (Blosser et al., 2009; Yang and Narlikar, 2007; Yang et al., 2006). Initially in close proximity, the dyes exhibit high FRET efficiency that decreases as they are separated during nucleosome sliding. One complication from this labeling scheme arises from the two histone-labeling sites, proximal and distal to the exit-DNA fluorophore, which can convolute the FRET response and increases noise. To avoid this problem, I took advantage of a propensity for hexasomes reconstituted on the Widom 601 to retain the sole H2A/H2B dimer on the TA-rich side of the Widom 601 (Levendosky et al., 2016). To generate FRET nucleosomes, I purified hexasomes positioned on the end of DNA fragments containing the Widom 601 flanked by 0 and 80 bp of linker DNA on either side (0N80). The histone core was labeled with the Cy3 donor on H2A T120C and the 5' end of the 0 bp linker was labeled with the Cy5 acceptor. I added unlabeled H2A/H2B dimer to these hexasomes to form nucleosomes containing the FRET pair only in the proximal arrangement.

I assembled reactions with Chd1 and ATP in a fluorometer to monitor nucleosome sliding. I followed sliding reactions by exciting Cy3 fluorescence at 510 nm and monitoring Cy3 and Cy5 peak emissions in consecutive experiments at 565 and 665 nm, respectively (Figure 3.4**A**). As the dyes move apart during remodeling, Cy3 and Cy5 emissions are expected change in an anti-correlated manner with Cy3 increasing as energy transfer to Cy5 decreases. Indeed, Cy3 emissions followed an exponential increase during sliding, consistent with a decrease in

quenching by FRET. Unexpectedly, Cy5 emissions increased slightly before decreasing, suggesting a process other than FRET was contributing to the Cy5 emissions change.

To establish how the distance between dyes was contributing to FRET in this system, I generated a series of FRET nucleosomes with increasing linker length on the shorter, exit-side DNA that carries Cy5 (i.e., 0, 3, 7, 9, 12, 14 and 19 bp. See Figure 3.5**A**). As expected, the Cy3 starting emissions increased for constructs with longer linker DNA (Figure 3.4**A**). Strangely, Cy5 starting emissions were not systematically lower with longer linker length; instead, Cy5 emissions for the 3 bp nucleosomes were higher than the 0 bp construct, even though the fluorophores were further apart. Though the close proximity of the dyes in the 0 bp nucleosomes would be expected to produce high FRET transfer and Cy5 emissions, it was instead leading to the quenching of Cy5 emissions. This suggests that the unexpected Cy5 kinetic traces of the 0 bp nucleosomes were due to a process other than FRET arising from the close proximity of the dyes and not to a side effect from the remodeling process. In kinetic traces of the 3 bp and 12 bp constructs, Cy5 emissions were roughly anti-correlated with Cy3 emissions, and the inverted Cy5 traces roughly overlap with Cy3 (Figure 3.4**A,B**). So increasing the initial distance between the fluorophores was enough to establish the anti-correlated signal response, as expected from a purely FRET-based change in intensities.

Next, I compared how the Cy3/Cy5 distance was affecting Cy5 emissions with and without the influence FRET. I collected emission scans of nucleosomes before and after remodeling by exciting Cy3 (510 nm) to induce FRET, or by directly exciting Cy5 (645 nm) to bypass FRET. As expected from the kinetic traces, the Cy3 emissions during Cy3 excitation increased systematically with longer exit DNA, whereas Cy5 emissions due to FRET were not correlated with linker length (Figure 3.5**C**). Instead the Cy5 emissions were low for the 0 bp

nucleosomes, highest for the 3 bp nucleosomes and decreased with longer linker length. I would expect that Cy5 emissions under direct excitation should be independent of the Cy3/Cy5 distance and remain unchanged with remodeling. Though this was true for nucleosomes with linker lengths longer than 3 bp, Cy5 emissions from the 0 bp nucleosomes were much lower before remodeling (Figure 3.5**B**). With an additional 3 bp, Cy5 emissions before remodeling were much higher than for 0 bp nucleosomes and only just below the intensity reached after remodeling. For constructs with exit DNA 7 bp or longer, the Cy5 emissions were identical before and after remodeling. These observations strongly suggest that the close proximity of Cy3/Cy5 in the 0 bp nucleosomes is quenching Cy5 emissions.

To bolster this hypothesis and help account for unforeseen effects of remodeling or from the addition of ATP, I examined a nucleosome construct initially positioned away from the DNA end that Chd1 slides back towards the end position. This nucleosome construct is missing 10 bp of DNA from one end of the Widom 601 and only has 10 bp of DNA flanking the other side ([-10]N10). This nucleosome is essentially shifted 10 bp off the end of a DNA fragment the size of the footprint of the histone octamer. After remodeling by Chd1, this construct becomes centered on the DNA, forming an end positioned nucleosome with no flanking DNA on either side. This construct contained Cy3 on the -10 DNA end and Cy5 on H2A T120C, reversing the labeling positions in this construct supports that the label positions were not responsible for the Cy5 quenching at the end position. Cy5 emissions from (-10)N10 nucleosomes were higher before remodeling and decreased after repositioning to the DNA ends, indicating that Cy5 was quenched when the Cy3/Cy5 were in close proximity regardless of remodeling (Figure 3.5**B**).

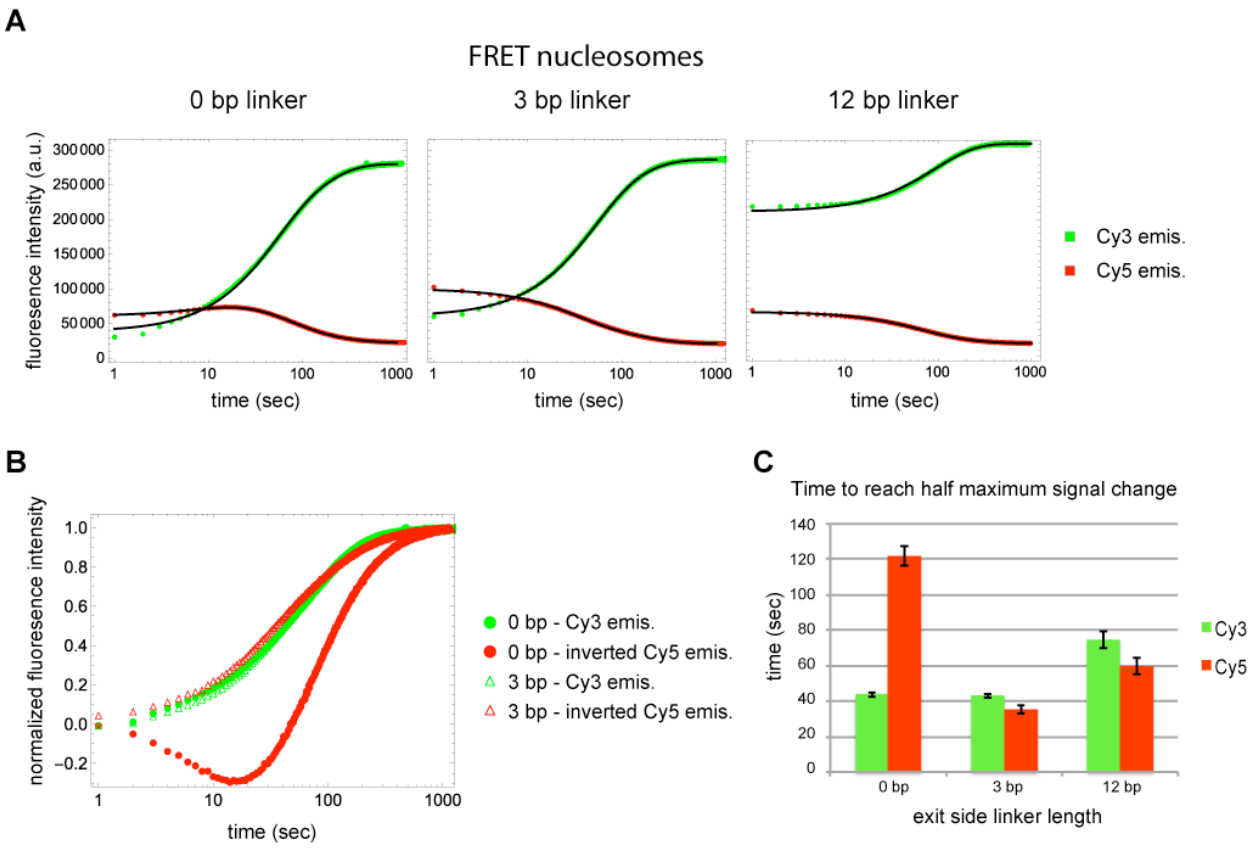

Figure 3.4: Sliding of FRET-labeled nucleosomes with the FRET pair in close proximity results in non-monotonic signal response

(**A**) Peak emission traces of Cy3 (565 nm, green) and Cy5 (565 nm, red) under Cy3 excitation (510 nm) during sliding of 10 nM nucleosome by 50 nM Chd1 with 25 µM ATP. Results are shown for experiments using nucleosomes with Cy5 positioned at the end of DNA 0, 3 and 12 bp from the edge of the nucleosome.

(**B**) The traces from 0 bp and 3 bp nucleosomes in (A) are overlaid with the Cy5 traces inverted to highlight the differences in the signal response. For the 3 bp nucleosome, Cy3 and Cy5 exhibit very similar signal changes, as expected for a change in FRET efficiency during displacement of the fluorophores.

(**C**) To compare the different signal response, the time to reach half maximum signal change is charted. The Cy3 and Cy5 signal responses are similar for nucleosomes other than the 0 bp nucleosome. Shown is the mean ± standard deviation of three independent experiments.

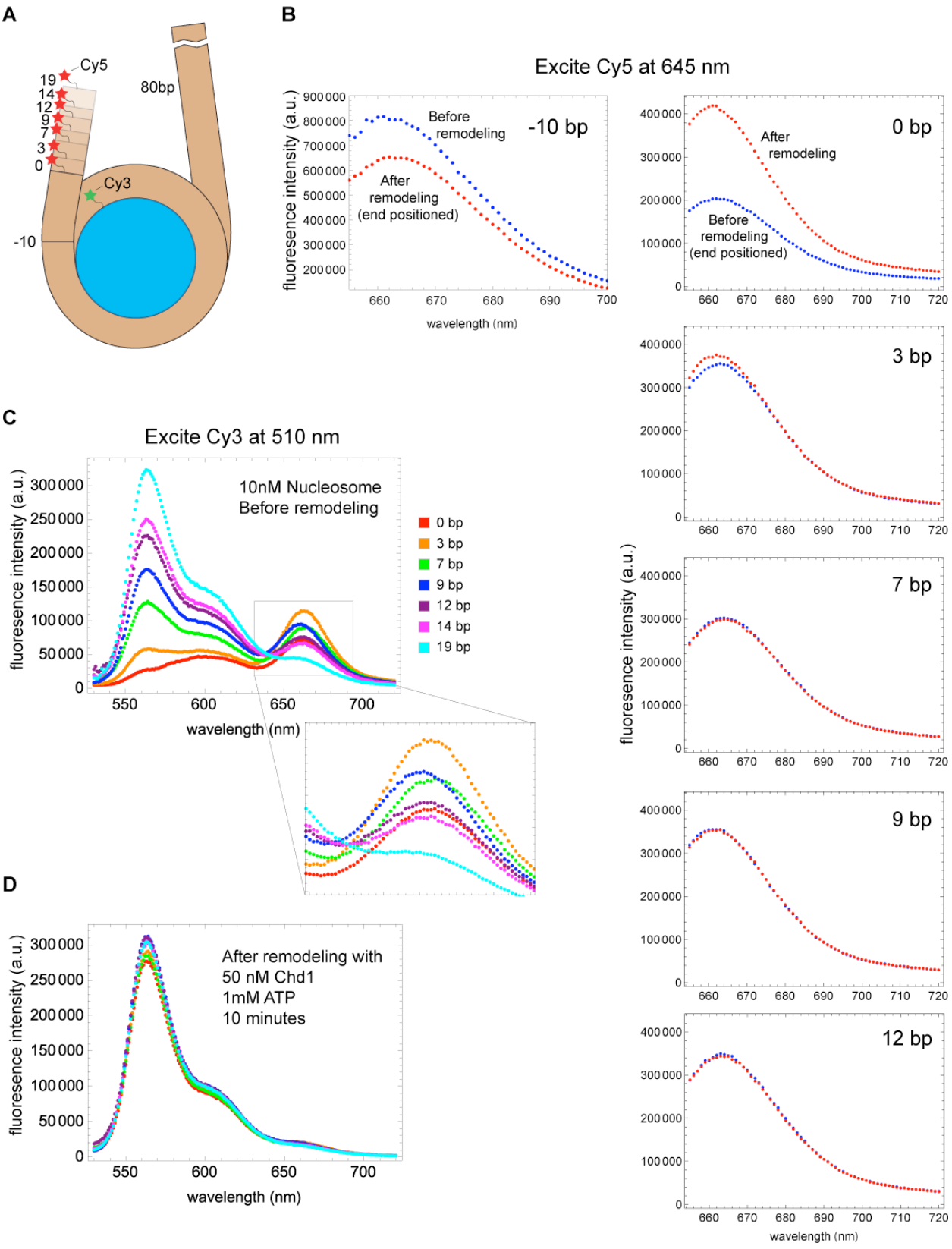

Figure 3.5: Cy5 emissions are not systematically dependent on FRET pair proximity
(*Figure legend continued on the next page*)

(Figure 3.5 *legend continued from previous page*)
(**A**) This cartoon schematic illustrates the different linker lengths used. Cy5 is positioned at the end of short DNA linkers and Cy3 is conjugated to H2A T120C on the histone core. On the other side of the nucleosome, 80 bp of DNA is available to accept repositioned nucleosomes. The -10 DNA labeling position is also shown for the (-10)N10 nucleosome, but here the labels are reversed with Cy5 on the histones and Cy3 on the DNA.
(**B**) Cy5 emissions spectra under direct excitation (645 nm) are shown for nucleosomes (made from 10 nM hexasome + 12 nM dimer) with various linker lengths (0, 3, 6, 9 and 12)N80 and for the (-10)N10 nucleosomes. Emissions are shown before (blue) and after (red) remodeling 10 nM nucleosomes with 50 nM Chd1 and 1mM ATP.
(**C**) Emission spectra under excitation of Cy3 (510 nm) for nucleosomes from (B) with various linker lengths (0, 3, 6, 9, 12, 14 and 19)N80 prior to remodeling. Cy3 emissions peak at 565 nm and Cy5 at 665 nm. Inset shows the details of Cy5 emissions, with 0 bp nucleosome emissions lower than for 3 bp.
(**D**) As in (C) but after remodeling with 50 nM Chd1 and 1mM ATP. Results are representative of two or more independent experiments.

Static quenching of contacting fluorophores reduces FRET acceptor emissions at short range

The close range quenching of the FRET acceptor detailed above suggested a process called static quenching. Static quenching results from intermolecular contact of two fluorophores forming a ground state, non-fluorescent complex (Johansson, 2006; Johansson and Cook, 2003; Johansson et al., 2002). This quenching contact is driven by hydrophobic stacking interactions and requires the two fluorophores be within contact range. Though the distance between the labeling sites on the 0 bp FRET nucleosomes is ~25 Å, the linkers created by the labeling chemistry are long enough to permit the dyes to contact. The degree of static quenching in ensemble would be determined by the overlap of the spheres created by the free tumbling of fluorophores centered at the labeling sites. Importantly, no quenching is possible once the labels are out of contact range. The requirement for contact to produce quenching results in much shorter distance sensitivity for static quenching than for FRET. In agreement with this idea, static

quenching was limited to approximately the first 3 bp shifted, with no detectable change before and after remodeling for linkers of 7 bp or longer (Figure 3.5**B**). In contrast, FRET was still detectable at the longest linker investigated (19 bp or ~65 Å).

The short distance sensitivity led me to consider using static quenching to detect the initial movement of nucleosomes. After Chd1 shifts nucleosomes, it maintains a dynamic equilibrium of nucleosomes around the center of the DNA. However, this allows for some back and forth movement that can bring a subpopulation of nucleosomes within 10-20 bp of the end position. Nucleosomes within this range contribute to the FRET signal and complicate the observed kinetics by convoluting the initial remodeling away from DNA ends with back-and-forth movement. Alternatively, static quenching is unaffected by nucleosomes moving back to positions as short as 7 bp from the DNA end, which Chd1 does not do.

The hypothesis that fluorophores within contact range are being statically quenched predicts that both Cy5 and Cy3 would be quenched. By directly exciting Cy5, I was able to identify static quenching independent from FRET. In the context of a FRET nucleosome, this same approach is impossible for Cy3, since direct excitation of Cy3 leads FRET quenching by Cy5. Since, static quenching should also occur between two of the same fluorophore, I made 0 bp nucleosomes as before but with Cy3 on both labeling sites. Under direct excitation, Cy3 emissions increased exponentially during remodeling by Chd1 (Figure 3.7,). Since there is no FRET to affect the Cy3 fluorescence intensity, static quenching is the favored model. The signal to noise for these traces was acceptable, and this technique proved useful in comparing Chd1 remodeling of histone mutations and alternate DNA sequences (used in Figure 2.14, Figure 2.16 and Figure 2.19**)**. I dubbed this technique Static Quenching Of Fluorescence (SQOF).

DNA and histone labeling positions are both affected by changes in PIFE from Chd1 binding/remodeling/unwrapping

While I was encouraged by the utility of SQOF as a method to track nucleosome sliding, I was also wary of fluorescence artifacts that can distort my observations. With this in mind I decided to investigate how the environments of the individual Cy3 dyes might be affecting the fluorescence observe by SQOF.

Cy3 is often used as a reporter of protein binding. The binding of two molecules where one is labeled with Cy3 near the binding site produces an increase in Cy3 emission. This phenomenon, known as Protein Induced Fluorescence Enhancement (PIFE), is the result of *cis-trans* isomerization about central alkene chain in cyanine dyes (Hwang and Myong, 2014; Sanborn et al., 2007; Stennett et al., 2015; Sundstroem and Gillbro, 1982). While PIFE is observed in many cyanine dyes, it is more pronounced in Cy3. In the ground state, Cy3 occupies the stable trans state, but upon photo-excitation, it can isomerize between the *cis* and *trans* states. Twisting of the double bond during isomerization leads to non-radiative deactivation of the excited state that competes with fluorescence (Stennett et al., 2015). When isomerization is inhibited by low temperature or high viscosity (e.g., protein binding, molecular crowding), Cy3 fluorescence increases. PIFE has been used to study protein binding and movement of nucleic acid translocases (Hwang et al., 2011). The distance sensitivity of PIFE to protein binding is estimated to be between 0 and 3 nm (Hwang and Myong, 2014). Cy3 PIFE has specifically been used to measure binding of remodelers to the nucleosome by labeling the H4 tail near the ATPase binding site at SHL 2 (Leonard and Narlikar, 2015) and also by labeling DNA at the entry/exit region where the DBD binds (Racki et al., 2009). Since the entry/exit region is labeled in my FRET and SQOF experiments, I anticipated that part of the changes in fluorescence

intensity could also arise from PIFE. To investigate whether PIFE was affecting my SQOF experiments, I generated single Cy3 labeled nucleosomes containing Cy3 on either the 5' end of the 0 bp linker DNA (0N80 DNA-Cy3) or H2A T120C (0N80 H2A-Cy3). For each construct, I observed Cy3 emissions under direct excitation during Chd1 binding or remodeling in the presence of ADP•BeF_3^- or ATP, respectively. For both labeling sites, Cy3 emissions were unaffected by Chd1 binding with ADP•BeF_3^- (Figure 3.6**A**, magenta and purple traces). During ATP-dependent remodeling, emissions of H2A-Cy3 increased while DNA-Cy3 decreased (Figure 3.6**A**, green and orange traces). The opposing signal change of these constructs indicated these sites were uniquely affected by remodeling. The drop in DNA-Cy3 emissions is consistent with a loss of PIFE, suggesting that Cy3 isomerization was more restricted before remodeling and then moved more freely after remodeling. This agrees with previous observations that Cy3 isomerization is restricted when positioned at the 5' end of DNA (Harvey et al., 2009; Lee et al., 2014; Sanborn et al., 2007). Crowding from the H2A C-terminal and H3 N-terminal histone tails may also contribute to this effect. The increase in H2A-Cy3 emissions suggests that Cy3 movement became more constrained with remodeling. It was unclear whether the increase in H2A-Cy3 emissions was due to the new position of the nucleosomes on the DNA after remodeling or an active remodeling process.

A major difference between 0N80 nucleosomes before and after remodeling is the presence of flanking DNA near the H2A labeling site. The presence of flanking DNA next to the H2A labeling site could restrict Cy3 isomerization, which would lead to higher initial fluorescence. Unwrapping of DNA near the H2A-Cy3 would be expected to liberate Cy3 to isomerize more freely, decreasing fluorescence emissions. To investigate this scenario, I generated centered, 40N40 H2A-Cy3 nucleosomes to simulate a nucleosome after remodeling.

Initial Cy3 emissions from this construct were higher than for 0N80 H2A-Cy3, which agrees with the idea that flanking DNA restricts Cy3 isomerization (Figure 3.6**B**, cyan and brown traces). Instead of increasing as for the 0N80, 40N40 H2A-Cy3 emissions decreased with ATP-dependent remodeling (Figure 3.6**B**, cyan trace). This decrease in fluorescence is consistent with repeated unwrapping of DNA by Chd1 during active remodeling. Interestingly, though there is some variation in the raw fluorescence signals due to the extreme sensitivity to nucleosome concentration, the 40N40 and 0N80 appear to converge toward similar fluorescence intensity with ATP remodeling, presumably because they both establish a dynamic equilibrium of centered nucleosomes. In contrast with the 0N80, emissions from the 40N40 H2A-Cy3 decreased due to Chd1 binding in the presence of ADP•BeF_3^- (Figure 3.6**B**, brown trace), suggesting that the 40 bp of DNA flanking the H2A-Cy3 site facilitates Chd1 binding and unwrapping on that side, which in turn changes the local environment and fluorescence of Cy3 (Nodelman et al., 2017). The H2A-Cy3 emissions from the 40N40 demonstrated a larger decrease with ADP•BeF_3^- than ATP. I attribute this to more dynamic unwrapping by Chd1 during active ATP hydrolysis, as opposed to Chd1 binding with ADP•BeF_3^-, which would progressively trap more nucleosomes in the unwrapped state. During ATP-dependent remodeling, the increasing emissions from the 0N80 H2A-Cy3 briefly overshoot the equilibrium value before settling back down to equilibrium (Figure 3.6**A and B**, green traces). This overshoot can be explained by interplay between DNA sliding off the exit side and the unwrapping of exit-side DNA. Initial remodeling by Chd1 slides DNA off the exit-side near the H2A-Cy3 site, increasing fluorescence. Subsequent unwrapping facilitated by the newly available exit DNA leads to decreased Cy3 fluorescence with the equilibrium emissions established by steady unwrapping/rewrapping dynamics.

The decrease in emissions from the H2A label due to DNA unwrapping helps explain the decrease in FRET independent H2A-Cy5 emissions from my unwrapping investigation (Figure 3.2 and Figure 3.3). Like Cy3, Cy5 can also isomerize about its central alkene linkage inducing PIFE. Thus the Cy5 signal may have been responding to unwrapping. Since there are two copies of histone H3, this construct contained Cy5 on both sides of the nucleosome. This explains why, under direct excitation, the Cy5 signal response was so similar for both the 80N12 and 12N80 while the Cy3 FRET signal was different. The Cy5 signal was essentially averaging the unwrapping from both sides.

These results indicate that PIFE contributes to the fluorescence signal at both histone and DNA labeling positions, and the effect is dependent on nucleosome characteristics that change during Chd1 binding and remodeling. To estimate how significantly PIFE affects FRET measurements, I compared the amplitude of raw Cy3 emissions before and after remodeling as monitored by PIFE and FRET (Figure 3.6**C**). The amplitude of PIFE from H2A-Cy3 (~ 40 k) and DNA-Cy3 (~ -30 k) was dwarfed by the amplitude of FRET quenching (~200 k for the 3bp nucleosome). In the context of SQOF, the opposing PIFE amplitudes would come close to canceling out, but the presence of multiple competing processes and the overshoot in H2A-Cy3 emissions (Figure 3.6**B**, green) increase noise at best and introduce systematic error at worst. Due to the use of two fluorophores in SQOF, I cannot directly compare SQOF amplitudes to those of PIFE and FRET. However, since the 0 bp FRET construct is quenched by SQOF and the 3 bp is not, I can compare the amplitudes of Cy3 emissions from these constructs as an indirect estimation of the magnitude of SQOF quenching in the 0 bp construct. This indicates that the amplitude of SQOF quenching for one fluorophore is around 50 k, which is close to the amplitudes observed from PIFE experiments. This means that the SQOF traces would be

significantly affected by PIFE. Since PIFE and SQOF both report on rearrangements concomitant with nucleosome sliding, I feel that SQOF measurements are still informative. However, a labeling scheme that avoids the influence of PIFE may reduce noise and simplify data interpretation.

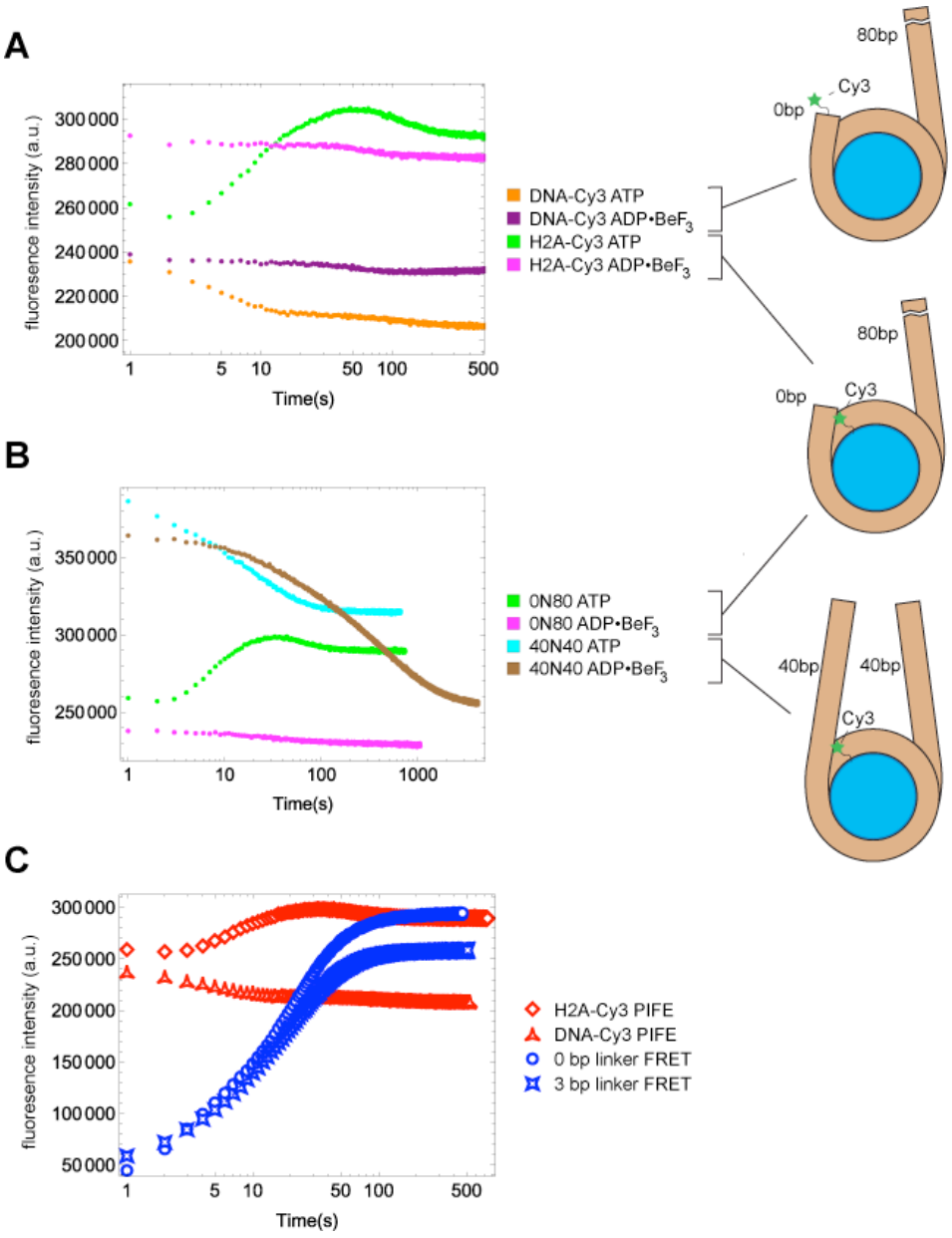

Figure 3.6: Histone and DNA labeling sites respond differently to remodeling
(**A**) Cartoons illustrate 0N80 nucleosomes containing single Cy3 labels either on the end of 0 bp linker DNA (above) or on H2A T120C (below). Nucleosomes were generated from 10 nM hexasomes incubated with 12 nM H2A/H2B dimer to ensure the presence of only one histone label on the histone labeled constructs. Chd1 (50 nM) was added in the presence of 1 mM ATP to promote nucleosome sliding or 1mM ADP•BeF_3^- to promote binding without sliding. Remodeling results in decreased florescence from the DNA label (orange) and increased florescence from the histone label (green). Binding did not significantly alter fluorescence (purple and magenta). Traces are representative of two or more replicates.
(**B**) As in (A) but comparing fluorescence from Cy3 histone labels on 0N80 and 40N40 (lower cartoon) nucleosomes. results are similar to (A) for the 0N80 nucleosomes, but 40N40 signals decrease with binding (brown) and remodeling (cyan).
(**C**) Raw Cy3 (565 nm) fluorescence amplitude is compared for remodeling reactions observed by FRET or PIFE.

Alternate strategies to avoid fluorescence artifacts

PIFE has the potential to interfere with the interpretation of kinetics experiments intended to monitor nucleosome sliding. To exclude PIFE from remodeling assays, I used Cy3B, which does not isomerize or PIFE (Cooper et al., 2004; Hwang and Myong, 2014). The lack of Cy3B isomerization in free solution results in longer fluorescence lifetime and greater quantum yield than Cy3. The absorbance (558 nm) and emission (572 nm) maxima of Cy3B are only slightly red shifted relative to Cy3 (Cooper et al., 2004). I made 0N80 nucleosomes containing Cy3B on H2A T120C and the non-fluorescent quencher, Dabcyl, on the 5' end of the 0 bp flanking DNA. The Cy3B-Dabcyl pair was chosen because the primary quenching method was static quenching (94%) with FRET (69%) contributing much less to the overall quenching (Johansson, 2006; Marras et al., 2002). Thus the Cy3B-Dabcyl nucleosomes use a mixture of SQOF and FRET. Comparing Cy3-Cy3 and Cy3B-Dabcyl remodeling in identical reactions reveals some important distinctions (Figure 3.7). In these reactions, Cy3-Cy3 SQOF exhibits faster kinetics than Cy3B-Dabcyl (Figure 3.7**B**). This difference may be due to the shorter distance sensitivity of SQOF. The SQOF signal change is complete once every nucleosome has moved at least 4-7 bp from the end, whereas by FRET, nucleosomes that are between 7 and 19 bp from the end can still be quenched, slowing the signal response. However, non-uniform remodeling kinetics could also contribute to the difference between Cy3-Cy3 and Cy3B-Dabcyl kinetics. Chd1 may move away from the DNA end faster than for subsequent steps. In addition, Cy3B-Dabcyl would detect back-and-forth movement past the range of SQOF but within the range of FRET. This slower sliding and back-and-forth movement farther from the DNA end would cause slower observed kinetics relative to Cy3-Cy3 SQOF. Another consequence of the long range quenching of FRET

is more complete initial quenching at the end position. This causes a three-fold higher signal change in Cy3B-Dabcyl (Figure 3.7**A**).

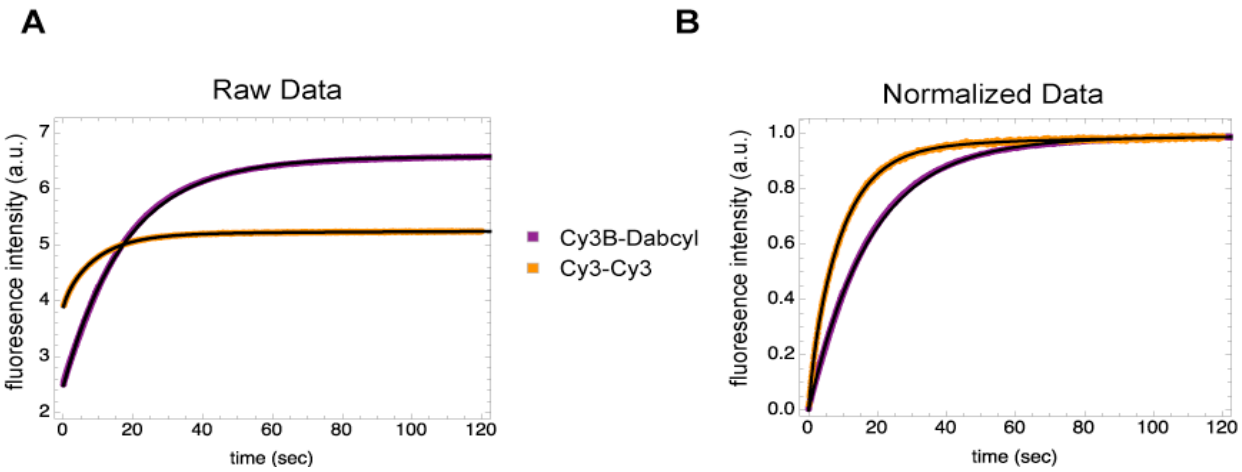

Figure 3.7: Differing contributions of fluorescence responses affect kinetic observations
Stopped flow fluorometer traces of remodeling reactions monitored by Cy3-Cy3 SQOF (orange) and Cy3B-Dabcyl (purple), which is influenced by both SQOF and FRET. Nucleosomes were generated from 10 nM hexasomes incubated with 12 nM H2A/H2B dimer to ensued only one histone label. Saturating amounts of Chd1 (400 nM) were used with 25 µM ATP. Black lines represent exponential fits to the data.
(**A**) Traces of raw fluorescence intensity highlight the larger amplitude of the Cy3B-Dabcyl reaction
(**B**) Traces of normalized fluorescence highlight the faster observable remodeling on Cy3-Cy3 experiments. Cy3B-SQOF fit to double exponentials (listed in order of decreasing contributing to amplitude: k1=0.060±0.004 sec^{-1}, k2=0.0056±0.0007 sec^{-1}) and Cy3-Cy3 fit to triple exponentials (k1=0.12±0.02 sec^{-1}, k2=0.9±0.2 sec^{-1}, k2=0.014±0.005 sec^{-1}).

DISCUSSION

Here, I used fluorescence changes to study how Chd1 affects nucleosome structure and positioning. I used FRET to investigate unwrapping of the nucleosome by Chd1. In agreement with studies revealing stronger DNA histone contacts on the TA-rich side of the Widom 601 (Hall et al., 2009; Ngo et al., 2015), I observe that Chd1 unwraps the TA-poor side of the nucleosome at lower concentrations than the TA-rich side in both AMP-PNP and ADP•BeF_3^-. Unwrapping in ADP•BeF_3^- was much more efficient than in AMP-PNP, occurring at nearly stoichiometric levels. This may be due to tighter overall binding in ADP•BeF_3^-. The nucleotide dependence of Chd1 on unwrapping suggests that particular conformations of the ATPase motor influence DNA unwrapping. Given the extensive contacts between the DBD and the unwrapped DNA in cryo-EM structures, I expected that the nucleotide-dependent changes in the ATPase were being conveyed through the DBD. However, a DBD truncation mutant (Chd1ΔDBD) was able to promote unwrapping, albeit at high concentrations of Chd1. The K_{unwrap} values of Chd1ΔDBD titrations were 10-14 times higher than WT Chd1, which may reflect poor binding when Chd1 is missing the DBD. Nonetheless, the clear FRET changes with Chd1ΔDBD indicate that the ATPase alone has a means of unwrapping DNA, yet is more effective in cooperation with the DBD. In EM structures, a basic loop extending from lobe 1 of the ATPase (residues 476-481) contacts the unwrapped DNA on the opposite gyre (Sundaramoorthy et al., 2018). Based on my results, we propose that this interaction may help stabilize unwrapped DNA even in the absence of the DBD (Tokuda et al., 2018).

A previous smFRET investigation concluded that a 6 bp linker was insufficient for unwrapping by Chd1 (Sundaramoorthy et al., 2017). These experiments measured FRET between two labeling sites, one on the DNA near the dyad and the other at entry/exit region.

Histograms of single molecules FRET revealed Chd1 unwrapping nucleosomes primarily from the TA-poor side of the nucleosome flanked by a 47 bp linker in both AMP-PNP and ADP•BeF_3^- conditions. No unwrapping was observed from the TA-rich side, which was flanked by only 6 bp, making it difficult to determine if unwrapping was limited by the stronger histone contacts on the TA-rich side–as my data suggest–or by an insufficient binding site for the DBD. Though I never directly tested unwrapping with linker DNA smaller than 12 bp, my unwrapping data indicate that Chd1 can promote unwrapping in the absence of the DBD, which dismisses the need for linker. However at low concentrations of Chd1, the linker may be necessary for Chd1 binding.

It is unclear whether DNA unwrapping by Chd1 is a necessary part of nucleosome sliding or relates to another role for Chd1 other than nucleosome sliding. Recent smFRET studies of nucleosome sliding by Chd1 identified down spikes in FRET consistent with DNA unwrapping (Kirk et al., 2018). A subpopulation of these down spikes occurred in conjunction with translocation, implying a connection between translocation and unwrapping. Transient unwrapping may help coordinate remodelers active on opposing SHL2 sites by signaling which remodeler is currently initiating sliding. Or, unwrapping may serve as a checkpoint to ensure that the nucleosome is properly wrapped before sliding. Alternatively, unwrapping may have a purpose other than for nucleosome sliding. In addition to sliding nucleosomes, Chd1 can assemble nucleosomes from histones deposited on DNA (Lusser et al., 2005). Unwrapping by Chd1 may be necessary for nucleosome assembly and its observation during sliding merely coincidental. However, though ISWI remodelers also slide and assemble nucleosomes, there is currently no evidence they unwrap DNA, adding to distinctions between Chd1 and ISWI remodelers. Chd1 cannot assemble nucleosomes with the linker histone H1, which promotes a

wrapped state, but ISWI has no such hindrances (Lusser et al., 2005). Chd1 is incapable of sliding nucleosomes contain the linker histones H1 or H5 which promote a wrapped state, while ISWI is not as negatively affected (Maier et al., 2008). These differences suggest that unwrapping is not intrinsically necessary for nucleosome assembly or sliding. Other functions for unwrapping could include exposing nucleosome-occluded sites to transcription factors or establishing a conformation of the nucleosome that is more permissive to transcription.

Our FRET studies of nucleosome unwrapping revealed fluorescence effects that complicated data interpretation. During Chd1- or salt-induced unwrapping, the emissions from H3 V35C-Cy5 decreased under direct excitation (Figure 3.3). This observation is consistent with decreased emissions from single Cy3 nucleosomes labeled at the nearby H2A T120C site in conditions that would promote unwrapping (Figure 3.6). In both cases, unwrapping increases space for the fluorophore to isomerize, which saps energy from fluorescence emission. This is equivalent to a loss of PIFE that boosts H2A-Cy3 fluorescence in the wrapped nucleosome. This observation makes it tempting to use PIFE to monitor unwrapping by Chd1, but protein binding could still complicate the signal. Instead, a better strategy may be to monitor unwrapping using a FRET assay that avoids PIFE altogether. Since FRET efficiency is a unitless ratio dependent on donor and acceptor fluorescence, it is internally controlled for fluctuations in fluorescence or inconsistencies in nucleosome concentration making it a sensitive and repeatable assay (Clegg, 1992). Replacing the histone label with Cy3B, which does not PIFE, and labeling the DNA with Cy5 should allow FRET efficiency to be calculated without the complications of Cy3 PIFE. Of course, controls would need to be done to make sure that PIFE from the DNA label was not complicating the FRET efficiency.

Static quenching can impact FRET experiments in arrangements where donor and acceptor can come into contact. Contact between certain pairs of fluorophores can form non-fluorescent complexes, effectively removing the fluorescence signal of both fluorophores from the experiment (Johansson et al., 2002; Marras et al., 2002). While the acceptor emissions are expected to increase when a FRET pair is in close proximity in a FRET system, static quenching makes acceptor emissions appear low when the fluorophores are close together. On the nucleosome, static quenching was strongest when the DNA was labeled within the 3 bp of the nucleosome edge in conjunction with the H2A T120C histone-labeling site. The short distance sensitivity of this interaction permits observation of just the initial nucleosome movement away from the DNA end without the influence from back and forth movements farther along the DNA. I sought to use this to my advantage by making Cy3-Cy3 SQOF nucleosomes to monitor nucleosome sliding. While this labeling scheme did produce a fluorescence increase with sliding, I discovered that PIFE from each of the labeling sites also affected Cy3 emissions. Future experimentation with dyes that do not isomerization and PIFE could produce a candidate dye better suited to SQOF experiments. In addition to the short distance sensitivity, another advantage of SQOF is that emissions from only one fluorophore needs to be tracked. This allows for the use of high pass filters or large slit widths in monochromators, which increases signal strength and allows lower nucleosome concentrations to be used.

One consequence of using FRET (or SQOF) labels at the nucleosome edge to monitor nucleosome sliding is that the fluorescence responses from unwrapping and sliding are indistinguishable. The fluorescence response due to sliding can be eliminated by using non-hydrolyzable ATP analogs, thereby isolating the unwrapping signal, but separating the sliding signal from unwrapping is more challenging. While native gel sliding and SQOF produce similar

results (discussed in **Chapter 4**), which indicates that SQOF is primarily reporting on sliding, unwrapping complicated the interpretation of sliding in some cases (Qiu et al., 2017). To avoid this problem, I proposed moving the FRET labels from the nucleosome edge to internal positions that would not be sensitive to DNA unwrapping from the nucleosome edge. I explore the advantages and challenges of this approach in **Chapter 5**.

Here, I have analyzed how movements of the nucleosome in response to Chd1 affect the excitation and decay pathways of fluorescent labels on the nucleosome. Diverse labeling methods take advantage of FRET, SQOF and PIFE to observe nucleosome unwrapping, sliding and binding.

Chapter 4: Requirement for the Entry-Side H2A Acidic Patch Dominates Over SNF2h Linker Length Sensing

ABSTRACT

The nucleosome acidic patches are distinctive epitopes on each face of the nucleosome used by chromatin factors for recognition. Mutations in the acidic patch reduce nucleosome sliding by ATP-dependent chromatin remodelers, but it was not clear which of the two acidic patches remodelers required. By combining H2A/H2B dimers and hexasomes with and without acidic patch mutations, I generated nucleosomes with mutations on the entry-side, exit-side or both acidic patches. Chd1 was mildly impaired by mutations in either acidic patch with an additive effect when both acidic patches mutated. However, SNF2h was heavily reliant on the presence of the entry-side acidic patch and remodeled asymmetric nucleosomes unidirectionally off DNA ends. While SNF2h activity is dramatically reduced on nucleosomes with mutations in both acidic patches, these nucleosomes are still centered. These results indicate that while SNF2h does not require the acidic patch for linker length sensing, the acidic patch is so important for SNF2h activity that asymmetric disruption of the acidic patch dominates the linker length response of SNF2h.

INTRODUCTION

Eukaryotic cells organize DNA into chromatin as a means for modulating DNA accessibility to transcription factors that drive gene expression. ATP-dependent chromatin remodelers (remodelers) alter the chromatin landscape by sliding nucleosomes on the DNA, but many details of how remodelers recognize and respond to nucleosomal epitopes are still unknown.

Remodelers share a conserved ATPase motor domain capable of DNA translocation and are differentiated by a compliment of accessory domains that regulate their activity in response to nucleosomal epitopes. Decoding how these epitopes influence remodeling is crucial for understanding the organization of chromatin. Members of the ISWI and CHD remodeler families require the H4 N-terminal tail and linker DNA adjacent to the nucleosome for robust activity (Corona et al., 2001; Hauk et al., 2010; Hwang et al., 2014; Stockdale et al., 2006; Yang et al., 2006; Zofall et al., 2004). Recently, the nucleosome acidic patch has been shown to be another epitope influencing remodeler activity. However, families of remodelers exhibit a wide range of depressed activity when the acidic patch is mutated (Dann et al., 2017; Gamarra et al., 2018; Levendosky et al., 2016). Though this variation is expected to result from differences in regulatory modules between remodelers, little is known about where the acidic patch falls in the hierarchy of epitope importance.

The acidic patch consists of eight acidic residues clustered on H2A and H2B that participate in chromatin condensation (Kalashnikova et al., 2013; Luger et al., 1997). Basic residues on the H4 N-terminal tail (H4-tail) form electrostatic interactions with the acidic patch of nearby nucleosomes, and removal of the H4 tail or acetylation of H4 K16 promote chromatin unfolding (Dorigo et al., 2003; Shogren-Knaak et al., 2006). Importantly, the acidic patch is a

distinctive feature of the nucleosome used by many chromatin factors for nucleosome recognition and binding (Kalashnikova et al., 2013; Luger et al., 1997; McGinty and Tan, 2015). The structures of several chromatin factors have been solved interacting with the acidic patch through an arginine inserted into the acidic pocket formed by H2A E61, D90, and E92 (Barbera et al., 2006; Makde et al., 2010; McGinty et al., 2014; Morgan et al., 2016). Certain factors can occlude the interaction between the H4-tail and acidic patch and decompress chromatin, while others promote the interaction to form fibers between nucleosomes to condense chromatin further (Kalashnikova et al., 2013). Given its distinctive structure and broad use as a recognition epitope, it follows that remodelers would also use the acidic patch for nucleosome recognition. However, direct interaction between remodelers and the acidic patch have not been well resolved in available structures (Farnung et al., 2017; Liu et al., 2017; Sundaramoorthy et al., 2017, 2018). This absence may be due to the dynamic nature of the remodeling process preventing the capture of the specific conformations in which acidic patch sensing takes place. Indeed, rearrangements of the SNF2h remodeler only bring it within the vicinity of the acid patch in certain states of the bound nucleotide (Leonard and Narlikar, 2015).

Members of the ISWI and CHD families of remodelers reposition nucleosomes in response to the asymmetric distribution of essential nucleosomal features. These remodelers slide nucleosomes away from DNA ends or short linkers, evenly spacing nucleosomes *in vivo* and centering mononucleosomes on DNA *in vitro* (Gkikopoulos et al., 2011; McKnight et al., 2011; Stockdale et al., 2006; Yang et al., 2006). The catalytic domains of both Chd1 and SNF2h act at superhelical position 2 (SHL ±2), two turns of DNA on either side of the nucleosome dyad (Saha et al., 2005; Schwanbeck et al., 2004; Zofall et al., 2006). Due to the symmetry of the nucleosome, remodelers can act from either SHL 2 position to slide the nucleosome in opposite

directions (Leonard and Narlikar, 2015; Nodelman et al., 2017; Racki et al., 2009). To center nucleosomes, the remodeler positioned on the DNA gyre adjacent to the longer linker DNA, pulls DNA on the entry-side, pumping it around the histone core and off the exit side. There are conflicting theories about whether the remodeler is stimulated by entry-side DNA or inhibited by exit-side DNA, and ISWI and CHD remodelers may differ in this regard (Leonard and Narlikar, 2015; Nodelman et al., 2017; Yang et al., 2006). Remodelers on each SHL 2 are distinctly positioned to sense and respond to the linker DNA or histones on opposite sides of the nucleosome differently.

Due to the ease of manipulating linker DNA length, our understanding of how remodelers respond to asymmetric nucleosomes largely comes from linker length asymmetry. However, little is known about how asymmetry in the histone core may bias remodeler activity and sliding directionality.

I previously used a method for introducing asymmetry into H2A and H2B with control over how histone asymmetry relates to linker DNA asymmetry (Levendosky et al., 2016). I found that hexasomes (nucleosomes missing one H2A/H2B dimer) assembled on the Widom 601 were predominantly oriented with the missing H2A/H2B dimer on the TA-poor side. By combining mutant and WT H2A/H2B dimers and hexasomes, I could make nucleosomes with a histone mutation on only the entry or exit side. With this control I can begin to probe how remodelers respond to asymmetric histone mutations.

Recent work revealed mutations in the nucleosome acidic patch (here referred to as APM, consisting of four amino acid changes on H2A: E61A/E64A/D90A/E92A, Figure 4.1**A**) dramatically reduce nucleosome centering by SNF2h by ~200-fold (Gamarra et al., 2018). Disruption of either of the autoinhibitory elements, AutoN or NegC, partially rescues mutation of

the acidic patch (Gamarra et al., 2018). The striking reduction of SNF2h remodeling of APM nucleosomes contrasts with my previous work in which I showed Chd1 suffered only a two-fold reduction in remodeling with an identical mutation (Levendosky et al., 2016). I reasoned that three factors could account for this discrepancy. First, in my previous study (Levendosky et al., 2016), I measured nucleosome sliding rates by fluorescence changes coupled to exit DNA movement, yet I did not take into account the possibility of DNA unwrapping. It is now understood that Chd1 is capable of unwrapping two turns of DNA from the nucleosome edge (Farnung et al., 2017; Nodelman et al., 2017; Sundaramoorthy et al., 2017, 2018; Tokuda et al., 2018), meaning that unwrapping and sliding effects may be convoluted in this assay. Thus, unwrapping could make sliding appear deceptively fast in this assay. Second, Chd1 and SNF2h may have different dependences on the acidic patch. Remodelers exhibit a range of diminished activity to mutations in the acidic patch (Dann et al., 2017). The ACF complex, containing SNF2h and the regulatory component Acf1, slides APM nucleosomes only ~10-fold slower—a 20-fold increase over SNF2h alone (Gamarra et al., 2018). Chd1 functions as a monomer and contains all required regulatory elements, which like ACF, might explain a more moderate sensitivity to disruption of the acidic patch. Third, I only examined the effects of APM incorporated into the entry-side dimer, unlike other studies that mutated both acidic patches (Levendosky et al., 2016). At the time, my objective was to find an epitope on H2A/H2B that could explain the drastic reduction in hexasome sliding by Chd1 when the entry-side H2A/H2B dimer was missing. If Chd1 were sensitive to the exit side acidic patch, I would have not detected that in my previous approach.

Here I investigated the influence of mutations in the entry- and exit-side acidic patches on nucleosome sliding by Chd1 and Snf2h remodelers. I confirmed modest reductions in Chd1

activity with entry- or exit-side APM, and cumulative reductions with APM on both H2A/H2B dimers. In contrast, Snf2h showed a strong requirement for the entry side but not exit side acidic patch. With asymmetrically placed acidic patch mutations, Snf2h moved nucleosomes unidirectionally away from the mutated dimer, shifting the octamer partially or completely off the DNA. This implies that the requirement for the acidic patch dominates over the requirement for entry-side linker DNA. This strong reliance on the entry-side acid patch suggests that Snf2h and Chd1 differ in how their regulatory elements are coupled to nucleosome epitopes.

RESULTS

Chd1 is sensitive to mutations in the acidic patch on each side of the nucleosome

To determine if experimental setup or APM placement are responsible for the different degrees of dependence of SNF2h and Chd1 on the acidic patch, I performed native gel sliding assays with Chd1 on nucleosomes containing the APM on the entry, exit or both H2A/H2B dimers. End positioned nucleosomes (with linker DNA extending from on only one side) migrate faster through native gels than centered nucleosomes (Eberharter et al., 2004). By quenching with EDTA at successive time points to block ATP hydrolysis, the reaction progress is monitored as centered nucleosome bands migrating higher in the gel. Since Chd1 is competed off the nucleosome with competitor DNA before loading the gels, unwrapping by Chd1 should not affect the results.

I analyzed the effects of asymmetric APM placement on remodeling by Chd1. By adding H2A/H2B dimer to hexasomes, I made nucleosomes containing a single APM on the entry or exit side, a double APM on both H2A/H2B dimers or WT nucleosomes (Levendosky et al., 2016). This produced nucleosomes with all four possible combinations of WT and APM dimer

placement (Figure 4.1**B**). To control for DNA sequence effects that can bias sliding (Winger and Bowman, 2017), I generated end positioned nucleosomes with 80 bp of linker DNA in both orientations of the 601 (0N80 and 80N0).

Native gel sliding confirmed the trends observed in my previous fluorescence experiments. This suggests that nucleosome unwrapping during active remodeling does not significantly influence bulk fluorescence. This may be explained by the use of the ATP transition state mimic, ADP•BeF_3^-, in structures solved with Chd1 unwrapping DNA, trapping the enzyme in what is expected to be a short lived state that might not significantly contribute to bulk fluorescence (Farnung et al., 2017; Nodelman et al., 2017; Sundaramoorthy et al., 2017, 2018). Additionally, these structures suggest that Chd1 requires some exit DNA to favor binding and unwrapping, meaning that before unwrapping can influence the fluorescence signal, some translocation must first occur. Thus the initial signal would be reporting on translocation by Chd1 rather than unwrapping. In agreement with previous observations, Chd1 shifted WT nucleosomes more rapidly towards the TA-poor side of the 601 (Winger and Bowman, 2017), resulting in faster centering for the 0N80 nucleosomes (Figure 4.2, 0N80 WT/WT and 80N0 WT/WT**)**. Chd1 shifted nucleosomes containing the APM on the entry-side H2A/H2B dimer ~two-fold slower than WT, irrespective of sequence orientation (Figure 4.2, 0N80 WT/APM and 80N0 APM/WT). Even more than the entry-side, Chd1 was also sensitive to APM on the exit-side, remodeling those nucleosomes three-fold slower than WT (Figure 4.2, 0N80 APM/WT and 80N0 WT/APM). The decrease in remodeling was consistent between both sequence orientations with regards to placement of the APM on the entry/exit side of the nucleosome (Figure 4.2**D**). This indicates the remodeler experiences each acidic patch distinctly. With both acidic patches mutated, the remodeling was further decreased to ~10 fold slower than WT (Figure 4.2**,** 0N80

and 80N0 APM/APM). The additive effect of APM implies that either a single remodeler can sense both acidic patches, or two remodelers on opposite sides of the nucleosome can communicate, possibly using the acidic patch. Though the effect of mutating both acidic patches is much more substantial, and similar to that observed for ACF (Gamarra et al., 2018), Chd1 remains ~20-fold less sensitive to APM than SNF2h.

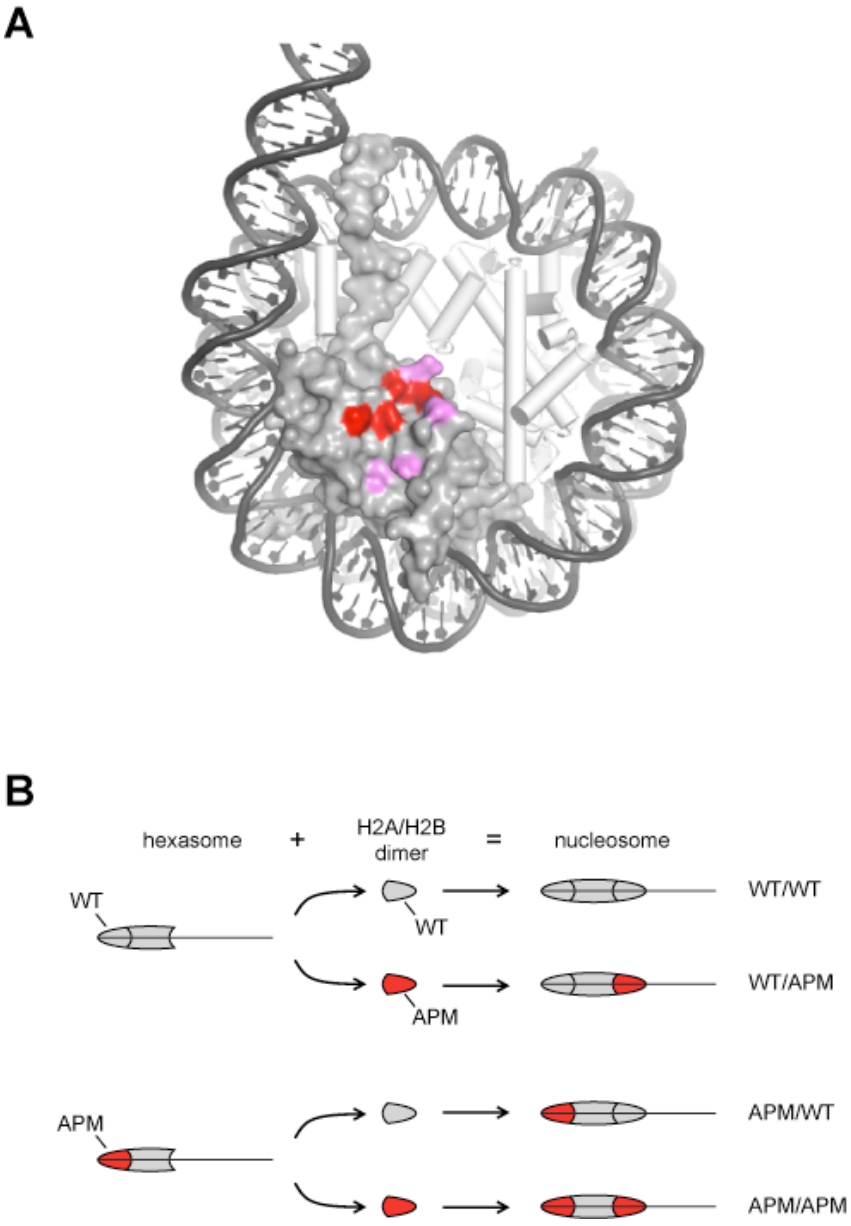

Figure 4.1: Design of APM nucleosomes
(**A**) The location of the acidic patch on H2A/H2B (gray surface) is highlighted in pink. The residues mutated in the APM quadruple mutation (H2A: E61A/E64A/D90A/E92A) are shown in red. Adapted from pdb:1KX5 crystal structure (Davey, et al. 2002)
(**B**) Method for the design of nucleosomes containing oriented APM H2A/H2B dimers. Hexasomes are generated containing either WT (gray) or APM (red) H2A/H2B dimers. WT or APM H2A/H2B dimers are combined with these to create all four possible combinations of H2A/H2B dimer epitopes.

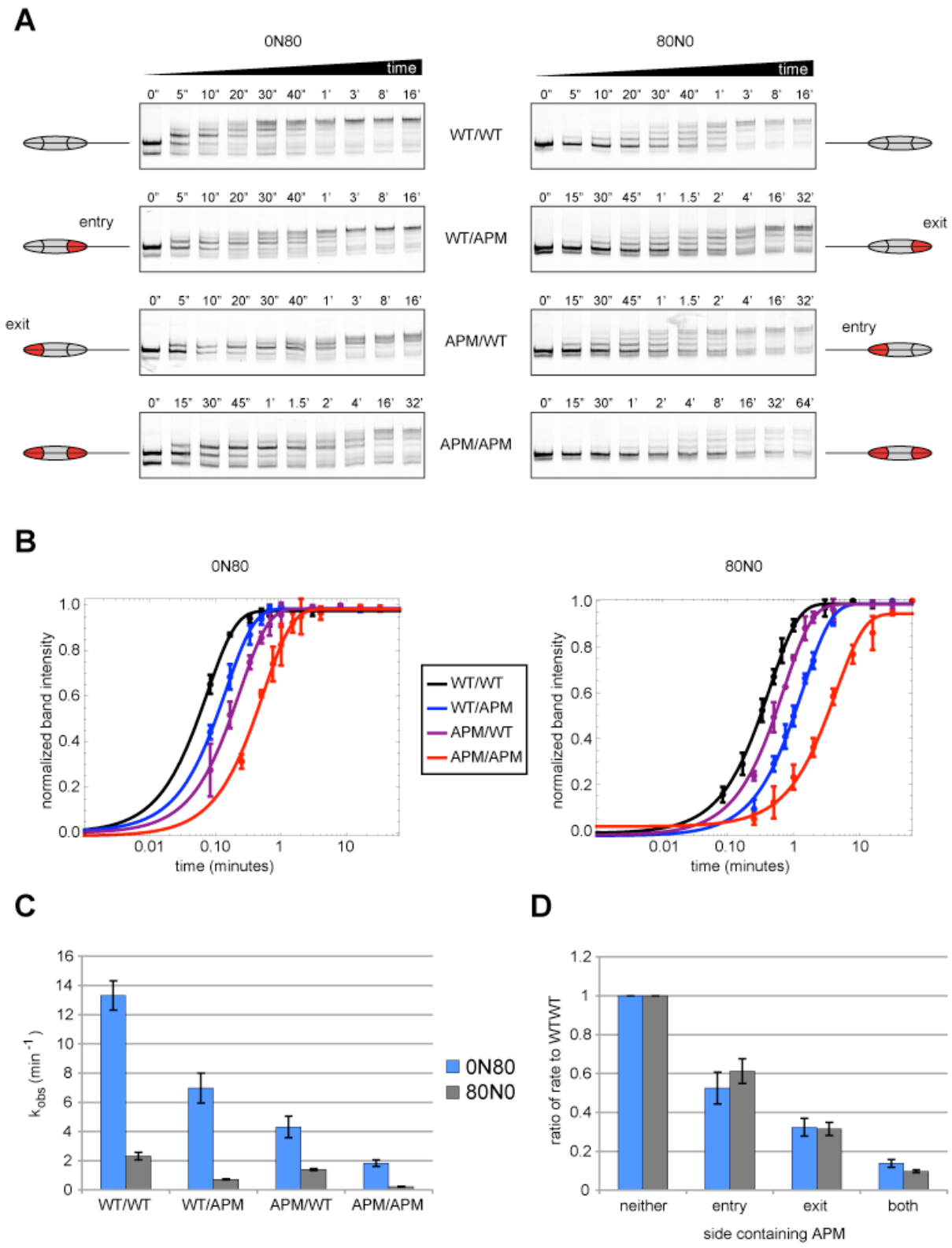

Figure 4.2: Chd1 slides nucleosomes with mutated acidic patches slower than WT
(*Figure legend continued on the next page*)

(Figure 4.2 *legend continued from the previous page*)
(**A**) Native gels show Chd1 remodeling nucleosomes with all four arrangements of APM and WT H2A/H2B dimer. The location of the APM with regard to the canonical entry or exit side is indicated above the cartoons of the asymmetric nucleosomes. The nucleosome cartoons are aligned with the end positioned nucleosome with residual hexasome running just below in the gel. Nucleosomes shifted toward the center by Chd1 run higher in the gel. Reactions contained 40 nM hexasome, 60 nM H2A/H2B dimer, 200 nM Chd1, and 100 μM ATP. Depending on the rate of reaction, three different time series were used (indicated above each gel). Results are representative of three independent replicates.
(**B**) Averaged parameters of single exponential fits plotted over mean normalized band intensity of shifted nucleosomes in (B) demonstrate a cumulative defect due to APM and a larger effect from mutation of the exit-side acidic patch. Error bars show standard deviation of three replicates.
(**C**) Mean observed rates ± standard deviation from fits obtained in (C).
(**D**) Bar chart depicting the ratio of sliding rates relative to WT nucleosome highlights that the position of the APM relative to the direction of sliding affects remodeling more than any sequence effects.

SNF2h requires the acidic patch on the entry-side dimer for productive sliding

Since Chd1 was sensitive to both acidic patches, though with a slightly greater impact from the exit side, I was curious if SNF2h followed the same pattern. As previously reported, Snf2h slid nucleosomes containing APM on both H2A/H2B dimers much slower than WT, but this could be due to sensitivity to the entry or exit acidic patches, or possibly an additive effect from both.

As described above for Chd1, all combinations of APM/ WT nucleosomes were subjected to native gel sliding by SNF2h to determine its specificity for one or both acidic patches (Figure 4.3). In agreement with previous results (Gamarra et al., 2018), SNF2h shifted nucleosomes with both APMs much slower than WT, but still tended to center the symmetric nucleosomes (Figure 4.3, 0N80 and 80N0 APM/APM). As observed with Chd1, Snf2h was sensitive to the 601 sequence orientation, sliding both WT/WT and APM/AMP nucleosomes more readily in the 0N80 orientation with the TA-poor side of the 601 on the entry-side. In light of the conserved similarity between Chd1 and SNF2h ATPase domains, this sequence effect

suggests that the DNA sequence may affect the action of the ATPase motor. Interestingly, with asymmetrically placed APMs, Snf2h showed different behaviors depending on whether the APM was on the entry or exit side dimer. When the APM was on the exit-side, nucleosomes initially moved toward the center (up the gel) and then back to the end position (down the gel) (Figure 4.3, 0N80 APM/WT and 80N0 WT/APM). Since nucleosomes positioned on either end of the DNA are indistinguishable by this assay, I could not determine whether the nucleosomes were shifted to the center and back to the original position or to the center and then on to the opposite end. After moving up the gel, the return of nucleosomes to the lower, end position coincided with the emergence of free DNA in the lanes (Figure 4.3, asterisks). This is consistent with nucleosomes sliding unidirectionally off the opposite end of the DNA. So, when the APM is on the exit-side, SNF2h pulls DNA on the long end and pushes DNA off the short end. But even after reaching the center of the DNA where the flanking DNA is the same length, SNF2h maintains its original direction and slides the nucleosomes off the other end. When the APM is on the entry-side, SNF2h failed to move nucleosomes toward the center from their original positions (Figure 4.3, 0N80 WT/APM and 80N0 APM/WT). In fact, the emergence of hexasome (gel band just below original nucleosome position) and free DNA (Figure 4.3, hexagons) implies that SNF2h slid these nucleosomes backwards, directly off the adjacent DNA end. This implies that the remodeler bound to the same DNA gyre as the APM is inactive and the remodeler on the other gyre dictates the direction of sliding.

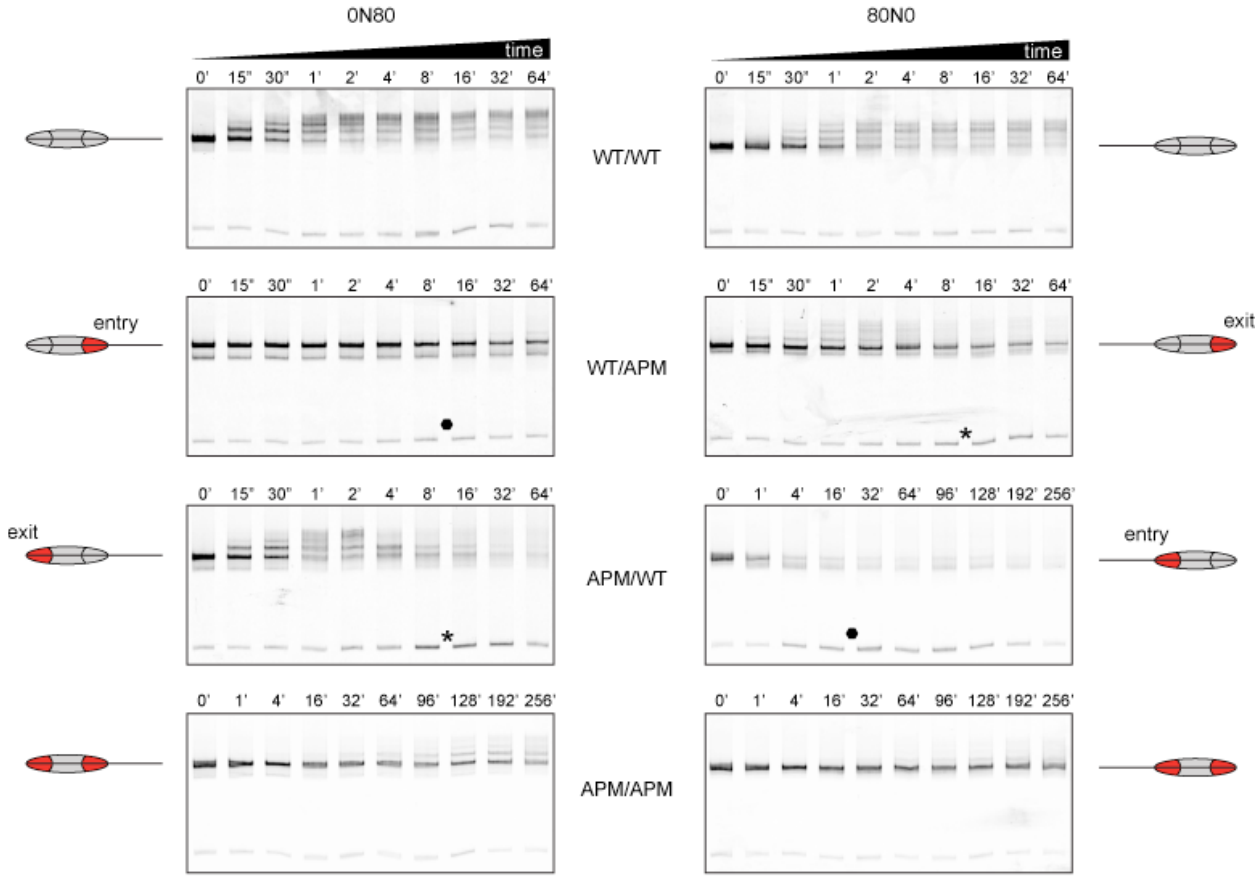

Figure 4.3: SNF2h requires the entry-side acidic patch for nucleosome centering
Native gels showing SNF2h remodeling nucleosomes with all four arrangements of WT and APM H2A/H2B dimers. Cartoons on either side highlight the position of the APM relative to the canonical DNA entry and exit sides. The increase in free DNA when SNF2h slides off DNA ends is shown as asterisks with APM on the exit-side (0N80 APM/WT and 80N0 WT/APM) and as hexagons with APM on the entry-side (0N80 WT/APM and 80N0 APM/WT). Remodeling reactions contained 40 nM hexasome, 80 nM H2A/H2B dimer, 1 µM SNF2h, and 2 mM ATP. Two different time courses were used to follow the reactions (indicated above the gels). Results are representative of two or more independent replicates.

SNF2h unidirectionally slides nucleosomes with asymmetrically mutated acidic patches off DNA ends

To verify the apparent unidirectional movement of nucleosomes containing asymmetrically mutated AP, I tracked nucleosome sliding by SNF2h using histone mapping. This method labels a single cysteine histone mutant with the photo-activatable crosslinker 4-azidophencyl bromide (APB). Here I use H2B S53C, which forms crosslinks to only one DNA strand, 54-55 bp in the 5' direction from the nucleosome dyad. After remodeling with SNF2h and ATP, UV exposure promotes APB crosslinking to DNA. Subsequent alkaline treatment cleaves DNA into fragments that are run on a denaturing gel alongside a Sanger sequencing ladder, allowing the position of the octamer to be determined. Since both DNA strands are labeled (FAM and Cy5), histone mapping allows nucleosome positions to be determined even with extreme shifts of DNA past the histone core, where the DNA end can be pulled up to 50 bp from the original edge of the nucleosome up to the SHL2 region where the motor acts (Patel et al., 2013; Zofall et al., 2006).

Histone mapping shows that asymmetric mutation of the acidic patches strongly biases the direction of sliding by SNF2h. As expected from the native gel sliding experiments, when both acidic patches are mutated simultaneously, SNF2h positioned nucleosomes toward the center (Figure 4.4). In contrast, for the 0N80 nucleosome containing the APM on only the "0" side H2A/H2B dimer, SNF2h shifted nucleosomes along the entire length of the DNA. In fact, the cross-links show that the histone octamer was shifted further than the available 80 bp in the linker, indicating that the DNA end was pulled onto the histone core by up to 58 bp past the canonical nucleosome edge (Figure 4.4**A**, 84, 94, and 138 bp products). As previously pointed out for other remodelers that show similar abilities (Patel et al., 2013; Zofall et al., 2006), such

an extreme shift would bring the DNA end just past SHL2 where SNF2h is active, indicating the remodeler moved off the end of the DNA. This position would leave the leading H2A/H2B dimer exposed and might lead to dimer loss or dissociation of the octamer from the DNA, which is in fact what was observed in the native gel sliding assays (Figure 4.3). A similar effect was observed for 80N0 nucleosomes with the APM only on the 80-bp side dimer. In that case, SNF2h appeared to only act on the side of the histone octamer containing the wild type acidic patch, on the zero side. In this case, the 80N0 APM/WT nucleosome was shifted toward the zero side, resulting in the histone core being shifted off the DNA end by 51 bp (Figure 4.4).

Together, these results indicate SNF2h requires the acidic patch on the entry-side of the nucleosome for robust nucleosome sliding. The entry-side is contiguous with the SHL2 site where the active remodeling takes place. As shown before, mutations in both acidic patches slow SNF2h remodeling by 200-fold (Gamarra et al., 2018). Here I show that mutation of one acidic patch strongly biases remodeling in favor of drawing DNA onto the side with the WT acidic patch, resulting in unidirectional movement. Surprisingly, the directional bias imposed by the asymmetric acidic patch mutation outweighs the requirement for linker DNA on the entry side, causing SNF2h to slide off DNA ends.

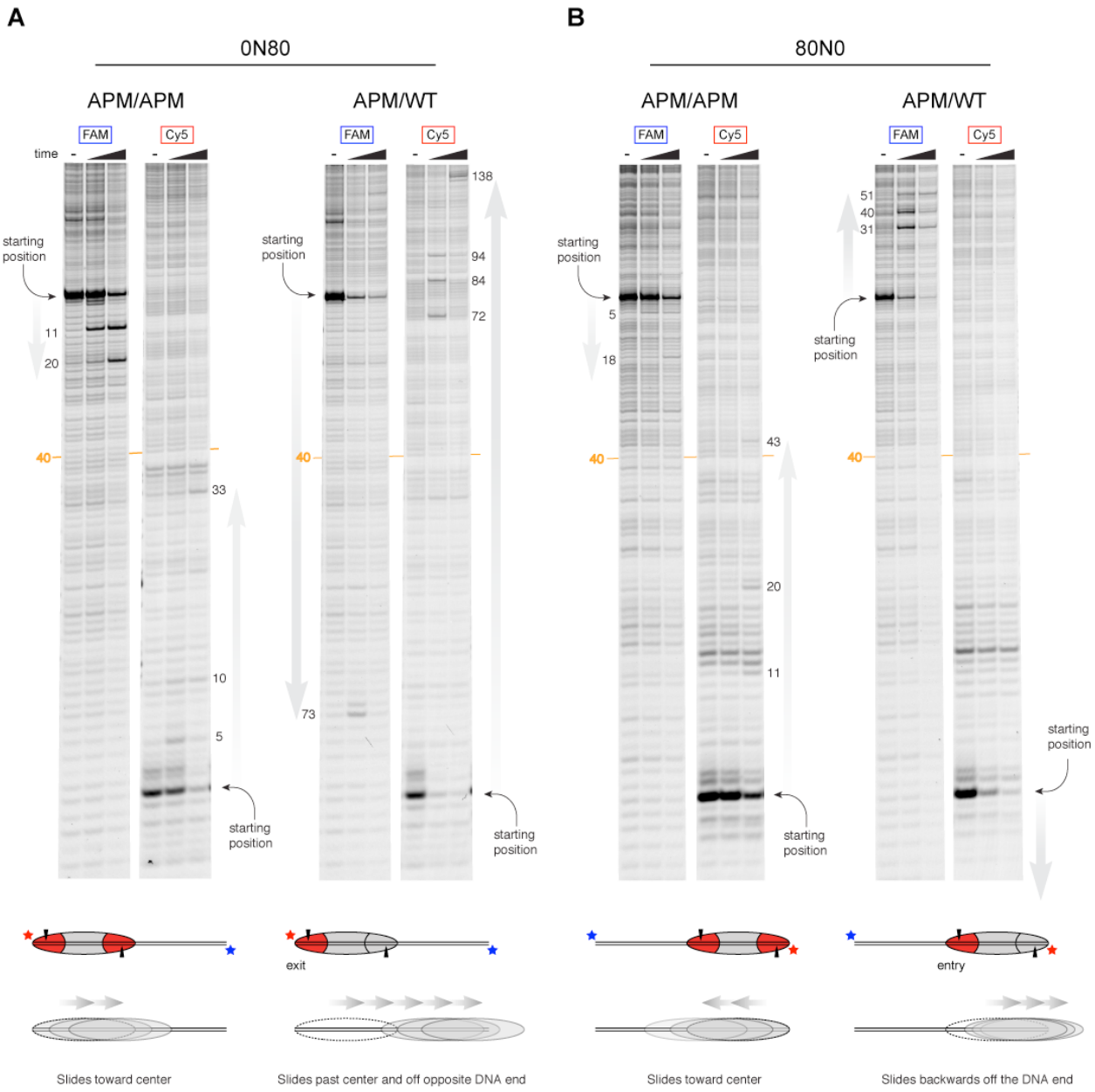

Figure 4.4: SNF2h slides nucleosomes with asymmetric APM off DNA ends
Denaturing gels of histone mapping experiments compare SNF2h remodeling of 0N80 (**A**) and 80N0 (**B**) nucleosomes with APM on one or both H2A/H2B dimers. For each nucleosome, gel scans of the FAM and Cy5 labeled strands are aligned to the position of a centered nucleosome (orange line). Gray arrows indicate the direction of sliding alongside the distance shifted (nt) of major bands. Time points used are 0', 4', 64'. Reaction conditions are 100 nM hexasome, 200 nM H2A/H2B dimer, 1 µM SNF2h, and 2 mM ATP. These results are representative of two independent experiments. Cartoon schematics represent the position of APM (red) and WT (gray) H2A/H2B dimers with the canonical entry/exit locations indicated. The location of the FAM (blue stars) and Cy5 (red stars) are shown with the histone crosslinking position (black triangles). Underneath, an interpretation of the gel data shows the nucleosomes sliding away from the end position (dotted oval) toward the center for APM/APM nucleosomes and off DNA ends for the APM/WT nucleosomes.

DISCUSION

In this work I demonstrate fundamental differences in how Chd1 and SNF2h respond to APM. Consistent with previous fluorescence assays, Chd1 shifted nucleosomes with the APM on the entry-side two-fold slower than WT nucleosomes by native sliding assay (Figure 4.2). Mutation of the exit-side acidic patch lead to a three-fold decrease and mutation of both acidic patches further slowed Chd1 remodeling to ten-fold slower than WT. This may indicate that one remodeler can sense both acidic patches. In recent EM structures of the Chd1-nucleosome complex, the DBD is bound to exit DNA, suggesting that regions of Chd1 could also reach the exit-side acidic patch. Alternatively, two-remodelers bound at each SHL 2 could use the acidic patch to help coordinate movement.

Though dramatically slower when both acidic patches were mutated, SNF2h was primarily affected by the entry-side acidic patch. The impairment of SNF2h remodeling APM is underscored on asymmetric nucleosomes containing one WT acidic patch and one APM (Figure 4.3). While Chd1 preserved centering activity on these nucleosomes, SNF2h slid unidirectionally off the DNA ends, suggesting the requirement for the acidic patch superseded linker length sensitivity (Figure 4.4). Taken together, these data suggest that Chd1 and SNF2h rely on the acidic patch to different degrees likely owing to their unique compliments of regulatory modules.

ISWI contains two regulatory modules thought to participate in acidic patch recognition. These modules, AutoN and NegC, are located just before and after the ATPase motor, respectively (Clapier and Cairns, 2012). AutoN restricts non-specific ATPase activity by occluding the closure of the two lobes of the catalytic core around the ATP to stimulate hydrolysis (Clapier and Cairns, 2012; Yan et al., 2016). The H4-tail competes with AutoN binding on lobe two of the ATPase and stabilizes an active conformation of the remodeler. NegC

cooperates with the HAND-SANT-SLIDE (HSS) DNA binding domain to couple linker length sensing to nucleosome remodeling (Clapier and Cairns, 2012; Hwang et al., 2014). Mutations in either AutoN or NegC slightly increase basal remodeling activity on WT nucleosomes, but provide a significant rescue of activity on APM nucleosomes (Gamarra et al., 2018). This suggests a model in which the acidic patch acts as an alternate binding site for AutoN and NegC away from their inhibitory contacts to allow SNF2h to commence translocation (Gamarra et al., 2018). In this model, the HSS binds to linker DNA thereby drawing NegC toward the acidic patch where it is sequestered away from the ATPase (Gamarra et al., 2018). Mutation of NegC was observed to diminish linker length sensitivity in SNF2h (Hwang et al., 2014) and reduces the proportion of centered nucleosomes (Gamarra et al., 2018; Leonard and Narlikar, 2015). On nucleosomes with asymmetric APM, I observed a dramatic imbalance in remodeling, with the direction of remodeling dictated by the remodeler bound to the DNA gyre containing the intact acidic patch, regardless of the presence of linker DNA or the DNA sequence. This implies that although the HSS and NegC cooperate to sense and relay linker length information to the ATPase in WT nucleosomes, the acidic patch is essential for releasing NegC inhibition and the HSS alone is incapable of removing the autoinhibition imposed by NegC.

I propose that the major factor removing inhibition of the ATPase is the acidic patch, and the HSS binding to DNA has a relatively minor influence. This model suggests that on WT nucleosomes, NegC establishes an equilibrium between association near the acidic patch and inhibiting the ATPase. By binding linker DNA, the HSS can subtly shift this equilibrium away from inhibiting the ATPase, thus favoring activity of the remodeler with linker DNA on its entry-side and promoting nucleosome centering. On nucleosomes with mutations in both acidic patches, the ability of the HSS to shift NegC away from the ATPase is so weak that sliding is

drastically diminished, but the delicate influence of the HSS still promotes the eventual centering of nucleosomes. So, as long as the acidic patches are balanced, SNF2h can center nucleosomes. With APM on only one side, that balance is heavily skewed to favor remodeling from the side with the intact acidic patch. The ATPase on the side with the APM is generally inhibited by NegC, while on the other side, the intact acidic patch can draw NegC away from the ATPase, permitting activity. This imbalance is so severe that the influence of the HSS binding to linker DNA is insignificant, and SNF2h slides these asymmetric nucleosomes unidirectionally. This implies that asymmetric APM effectively overwhelms the linker length sensing capabilities of SNF2h.

This sliding off DNA ends supports an antagonistic model of centering for ISWI and CHD remodelers. This model postulates that remodelers are positioned on either SHL 2 with the action of one opposing that of the other, whether taking turns in a synchronous fashion or actively fighting against the activity of the other (Leonard and Narlikar, 2015; Racki et al., 2009). Members of both the ISWI and CHD remodeler families have been observed with two remodelers bound, one at each SHL 2 position on a single nucleosome (Nodelman et al., 2017; Racki et al., 2009; Sundaramoorthy et al., 2018). Alternately, a single remodeler can sample both SHL 2 sites through alternate binding and release of the DBD and ATPase domains to swing from one side to the other (Qiu et al., 2017). The utility of this arrangement for nucleosome centering/spacing is evident if the presence or absence of linker DNA provides an advantage to remodeling from one side over the other (Leonard and Narlikar, 2015; Yang et al., 2006). Once centered, the nucleosome is in a dynamic equilibrium with the action of the opposing remodelers balanced. Making one SHL 2 position more or less advantageous for the bound remodeler can disrupt that balance. I previously demonstrated this concept by generating hexasomes on the

Widom 601 with linker DNA oriented with respect to the missing dimer. Chd1 remodeled these hexasomes in a unidirectional fashion away from the side missing the dimer (Levendosky et al., 2016). This shows Chd1 requires the dimer on the same DNA gyre bound by the ATPase for full activity, and removing one H2A/H2B dimer imbalances the centering equilibrium. Similarly, for full activity, SNF2h requires the acidic patch on the H2A/H2B dimer wrapped by the same DNA gyre where the remodeler is active. If one acidic patch is mutated, the remodeler on the opposite gyre then directs sliding, regardless of linker DNA. With remodeling on one side of the nucleosome much more favorable than the other, instead of centering, nucleosomes are slid unidirectionally off the DNA end.

Why then is Chd1 so different than SNF2h in response to acidic patch mutation? Since SNF2h is often in complex with other regulatory subunits, it may be tuned for different responses to nucleosomal epitopes than Chd1, which often functions as a monomer. In complex with Acf1, SNF2h is less sensitive to APM, suggesting that Acf1 offers an alternate route to release inhibition from AutoN and NegC. Indeed, Acf1 communicates linker length sensing to SNF2h by sequestering the H4 tail when linker DNA is unavailable, favoring inhibition by AutoN (Fyodorov and Kadonaga, 2002; Hwang et al., 2014). The H4-tail binding site on Acf1 may also provide an alternate binding site for AutoN, shifting the equilibrium of AutoN away from the ATPase even when the acidic patch is not available. This would explain the more subdued reliance of ACF on the acidic patch. This scenario ensures that the ACF complex is complete before remodeling nucleosomes with an occluded acidic patch. I expect that Chd1 might also have alternate means of relief of autoinhibition to soften the response to disruptions in nucleosomal epitopes. This predicts the existence of mutations in Chd1 that would produce more severe reductions in activity on APM nucleosomes.

SNF2h demonstrated a strong reliance on the entry-side acidic patch, whereas the moderate deficit in Chd1 remodeling was only slightly more pronounced for the exit-side APM. This implies that while bound at one SHL2 site, Chd1 can probe both acidic patches. This result is consistent with structures showing the DBD of Chd1 bound to exit DNA, within reach of the exit-side acidic patch (Farnung et al., 2017; Sundaramoorthy et al., 2018). However, these structures do not reveal any well-ordered interactions between Chd1 and the acidic patch. Therefore, how the presence or absence of the acidic patch affects Chd1 remodeling is unclear.

The unidirectional response of SNF2h on nucleosomes with one disrupted acidic patch may have direct consequences for chromatin organization. The acidic patch is recognized by a number of chromatin factors including: the latency-associated nuclear antigen (LANA), which tethers the genome of Kaposi's sarcoma-associated herpesvirus to the host chromosome (Barbera et al., 2006); Interlukin-33, a chromatin-associated cytokine (Roussel et al., 2008); regulator of chromatin condensation 1 (RCC1), which localizes the RanGTP gradient around chromatin (Makde et al., 2010); the bromo-associated homology domain of silent information regulator 3 (Sir3), which maintains silenced genomic regions in yeast (Armache et al., 2011); the centromeric protein, CENP-C (Kato et al., 2013); the ubiquitylation module of Polycomb repressive complex 1 (McGinty et al., 2014), and the SAGA deubiquitinating module (Morgan et al., 2016). These diverse factors bind in an overlapping fashion, occluding other factors or remodelers from accessing the acidic patch (Kalashnikova et al., 2013). Binding of the LANA peptide in the acidic patch disrupts SNF2h activity to a similar degree as APM, indicating that occlusion of the acidic patch is as significant as mutation (Gamarra et al., 2018). Since all remodelers explored thus far exhibit reduced activity when the acidic patch is disrupted, the presence of chromatin factors could be used as a means to regulate remodeler activity

(Kalashnikova et al., 2013). Binding of the H4-tail to the acidic patch of adjacent nucleosomes would quiet remodeler activity, possibly stabilizing tightly packed chromatin. Given the unidirectional remodeling observed for SNF2h on asymmetric APM nucleosomes, the possibility of occluding only one acidic patch would add yet another dimension to remodeler regulation. Organized occlusion of the acidic patch could prompt the packing or loosening of nucleosome arrays.

Chapter 5: The Nucleosome Absorbs Additional DNA During Remodeling

ABSTRACT

The manner of DNA propagation around the histone core during chromatin remodeling is a matter debate. Using a 3-color single molecule FRET approach, we present direct evidence that DNA moves onto the nucleosome before DNA is pushed off. The lag between the movement of entry and exit DNA shortens with increasing ATP, suggesting an ATP binding event is required to drive DNA towards the exit side. The discontinuous movement indicates that DNA is absorbed by the nucleosome during remodeling. I use a site-specific crosslinking assay with nucleosomes containing ssDNA gaps to limit DNA movement by the Chd1 ATPase to determine that less than 5 bp are buffered on the nucleosome. I discuss how these observations fit into current theories of DNA propagation.

INTRODUCTION

ATP-dependent chromatin remodelers (remodelers) translocate on nucleosomal DNA at an internal SHL 2 site to catalyze the movement of DNA around the histone core to reposition nucleosomes. How DNA movement is propagated around the histone core to result in stability positioned nucleosome is not understood. Knowledge of DNA propagation is fundamental to understanding how remodelers reposition nucleosomes.

Two prominent theories to explain the movement of DNA around the nucleosome are the loop/bulge propagation model (Schiessel et al., 2001) and the twist-diffusion model (van Holde

and Yager, 2003, 1985). In the loop/bulge propagation model, the remodeler disrupts histone DNA contacts where DNA enters the nucleosome, creating a large loop of DNA away from the histone core. This loop then propagates around the nucleosome moving DNA off the exit side. In the twist-diffusion model, the DNA moves around the nucleosome in a segmented corkscrewing motion without fully breaking histone contacts. The remodeler distorts the DNA at SHL 2, directing the movement of one bp towards the dyad. This distortion diffuses throughout the nucleosome, resulting in movement of a single base pair, as shown for ISWI remodelers (Deindl et al., 2013). Evidence exists to support either model.

There is also controversy over the order of DNA movement at the entry and exit side. The Chd1 chromatin remodeler has been shown to form a small, ~1 bp bulge at SHL2 by pulling DNA on the entry-side. Coupled to ATP hydrolysis, the bulge is pushed towards the dyad, suggesting an entry-then-exit mechanism (Winger et al., 2018). In contrast, previous single molecule FRET (smFRET) studies indicated that ISWI remodelers shift DNA off the exit-side before pulling DNA onto the entry-side (Deindl et al., 2013). Meanwhile, other smFRET studies using Chd1 detected no difference in movement between the two sides (Kirk et al., 2018). These smFRET studies did not measure the entry/exit difference directly, but instead measured and compared the time between ATP addition and movement on entry and exit separately. Since remodeling activity has been demonstrated to be sequence dependent (Winger and Bowman, 2017)(see also **Chapter 4**), the sequence context could distort these conclusions.

To investigate these possibilities, we collaborated with smFRET experts Anton Sebantsev and Sebastian Deindl at the University of Uppsala. We cooperated in the conception and design of the 3 color smFRET labeling scheme employed in this work. With DNA prepared by our collaborators, I generated all hexasome and nucleosome constructs. Our collaborators collected

and analyzed extensive smFRET data while I performed native gel sliding and site specific crosslinking assays. At the time of writing this dissertation, many of the data and ideas presented in this chapter have been submitted for publication and are currently under review (Sebantsev et al., 2019, *submitted*).

Here, we provide direct evidence that DNA is pulled onto the nucleosome before exiting from the other side, indicating that the nucleosome absorbs at least one bp during remodeling. The lag times between the movement of entry and exit DNA are well fit by single exponential decay and decrease with higher ATP concentrations, indicating that a single ATP binding event is required for exit-side movement. I use biochemical methods to narrow the estimated DNA buffered by the nucleosome. I used ssDNA gaps to restrict the movement of Chd1 at SHL 2 and observed movement at multiple DNA positions around the nucleosome. I observe that 5 bp of movement by the ATPase is sufficient to move DNA at the exit-side, setting an upper limit on the DNA buffering capacity of the nucleosome. Finally, I discuss how these observations fit into current views of DNA propagation during remodeling. Narrowing down among these possible scenarios of DNA translocation will help focus future models, leading to a better understanding of chromatin remodelers and DNA propagation around the nucleosome.

RESULTS

Design of three color smFRET nucleosomes to measure sequence of DNA translocation

We sought to directly compare the movement of DNA at the nucleosome entry and exit within the same molecule. With our collaborators, we developed a 3 color smFRET scheme to simultaneously observe entry and exit movement within the same nucleosome (Sebantsev et al., 2019, *submitted*). This approach entails labeling the nucleosomes with different dyes on DNA at

the entry-side, exit-side and a central histone site. By rapidly alternating excitation of the dyes, the movement of the entry and exit DNA relative to the histone label can be simultaneously measured as FRET between pairs of fluorophores. One obstacle to this scheme is presented by the two-fold symmetry of the nucleosome, which results in two histone labeling sites, one on either histone copy, each with a distinct position relative to the DNA labels. In two-color smFRET studies, this problem is often circumvented by under-labeling the histone site to create three populations of nucleosomes containing the histone label proximal or distal to the DNA label, or both, and then excluding all but the proximally labeled nucleosomes from analysis (Deindl et al., 2013). In 3-color smFRET experiments, we wished to avoid the complication of distinguishing between the populations of differently labeled nucleosomes presented by this solution, which would severely limit the number of correctly labeled molecules. Therefore, we used a method of generating nucleosomes by combining unlabeled hexasomes oriented to the DNA sequence with H2A/H2B dimer bearing a single fluorophore (Levendosky et al., 2016) (see also Figure 4.1).

Chd1 unwrapping DNA from the nucleosome edge poses another challenge to this FRET scheme (Farnung et al., 2017; Nodelman et al., 2017; Sundaramoorthy et al., 2017, 2018; Tokuda et al., 2018) (see also **Chapter 3**). To measure DNA sliding relative to the histone core, a common FRET scheme labels the histones near the entry/exit region and the linker DNA 3-4 bp outside the nucleosome. However, when using this approach, the FRET signals from unwrapping and DNA sliding are indistinguishable. To avoid the influence of unwrapping in our experiments, we moved the DNA FRET labels to more interior nucleosome positions, beyond the two turns of DNA (~ 20 bp) unwrapped by Chd1 (Farnung et al., 2017; Sundaramoorthy et al., 2018). We also repositioned the histone label from the entry/exit region to a site near SHL 4

to ensure the movement of the DNA labels during sliding would more closely follow a straight line between the histone and DNA labels.

Chd1 binding to these nucleosomes with and without ATPγS, which should promote unwrapping, did not change the FRET measured at the entry or exit sides. This indicates that our interior labeling scheme was unaffected by unwrapping. In contrast, ATP-dependent remodeling by Chd1 did produce FRET changes consistent with DNA sliding. Interestingly, the entry-side DNA consistently moved onto the nucleosome before the exit side moved off (Figure 5.1**A**). The duration of this lag between entry and exit-side movement (t_{lag}) decreased with higher ATP concentrations, showing that ATP binding is required to couple entry and exit movement (Figure 5.1**B,C**). Since the nucleosomal DNA sequence affects sliding by Chd1, we reversed the sequence orientation (Winger and Bowman, 2017). Though the reversed DNA sequence resulted in longer t_{lag} between entry- and exit-side movement, the order of movement remained consistent (Figure 5.1**D**). The histograms of t_{lag} fit well to single exponential decay, indicating that a single ATP dependent event was coupling entry and exit side movement. These results strongly support the model that the entry-side DNA is pulled onto the nucleosome with one ATP driven event before the exit-side DNA is pushed off with a second round of ATP hydrolysis. This model implies that during the lag the nucleosome absorbs or buffers at least one additional bp of DNA between the ATPase and the exit DNA. Since this 3-color smFRET method is not calibrated for distance, we cannot use FRET efficiency to determine how much DNA the nucleosome is buffering, leading us to explore other methods.

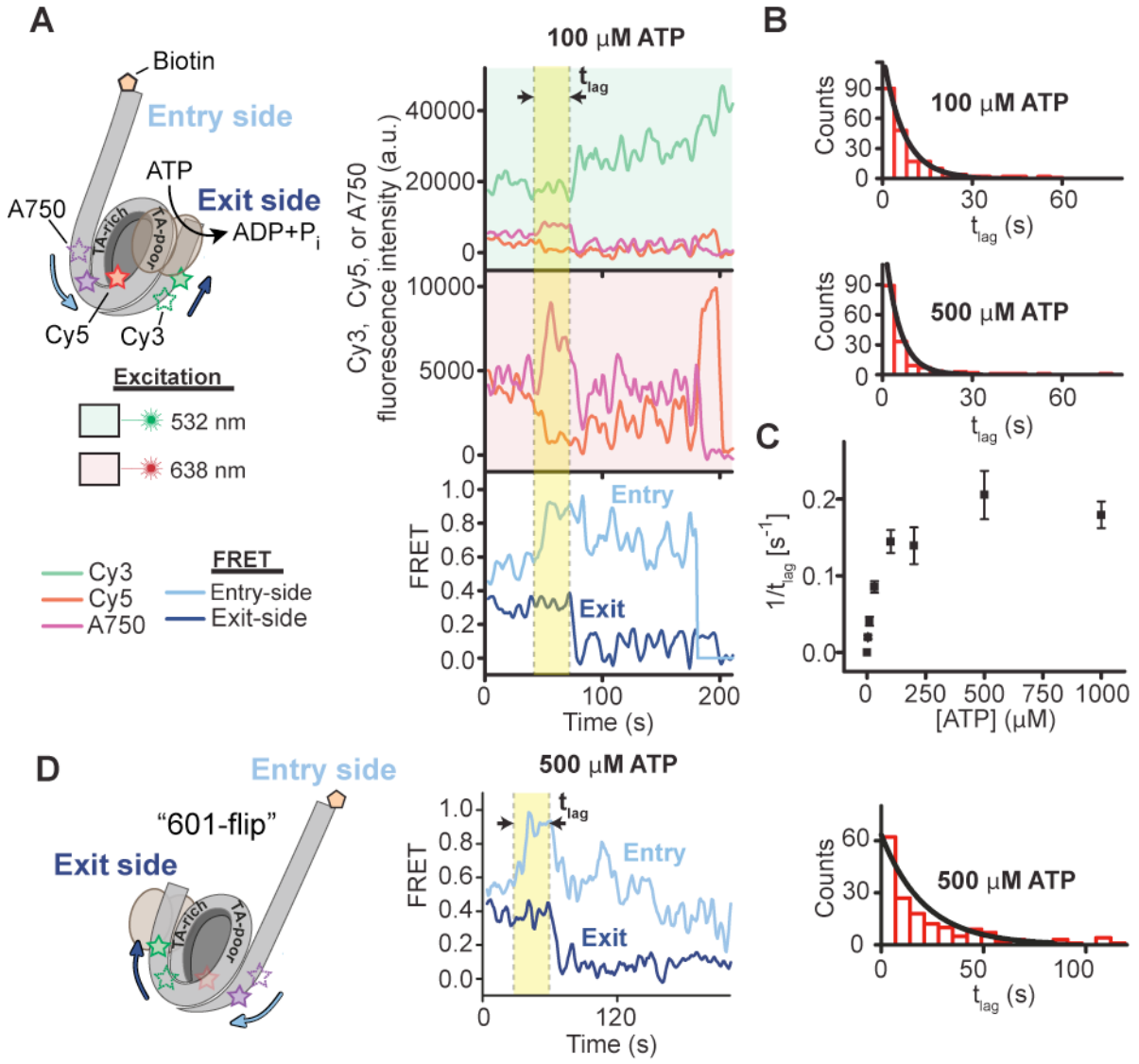

Figure 5.1: An ATP-dependent lag separates entry and exit-DNA movement during Chd1 nucleosome remodeling

(**A**) Cartoon representation of 3-color smFRET scheme with A750 labeling DNA interior to the entry-side, Cy3 labeling DNA interior to the exit-side and Cy5 labeling the histone core at H2B K120C. Open and closed stars show the location of DNA labels before and after nucleosome sliding, respectively. Nucleosomes are tethered to the surface of total internal reflectance (TIRF) microscope slide via biotin located at the end of 84 bp linker DNA. Fluorescence traces of nucleosome sliding with 300 nM Chd1 and 100 µM ATP show emissions from Cy3 (green line), Cy5 (orange line) and A750 (magenta line) as a result of alternating excitation at 532 nm (green background) and 638 nm (pink background) to monitor FRET at the exit and entry sides, respectively. FRET traces indicate entry side (light blue) movement prior to exit side (dark blue). Time between movements (t_{lag}) highlighted in yellow. (**B**) Representative histograms of t_{lag} resulting from remodeling reactions with 100 and 500 µM ATP are shown with single exponential fits (black line). (N=185-220 events)
(*Figure legend continued on next page*)

(Figure 5.1 *legend continued from previous page*)
(**C**) Plot of mean ±SEM of $1/t_{lag}$ with increasing ATP. (N= 40-340 events)
(**D**) Cartoon representation of nucleosome with flipped 601 sequence. Representative smFRET traces and histogram of t_{lag} are shown as in (A) and (B). (N= 190 events)
Data collected and analyzed by Anton Sebantsev and Sebastian Deindl

The nucleosome absorbs less than 5 bp of DNA during remodeling

To determine how much DNA the nucleosome could absorb during remodeling, I used ssDNA gaps to limit the range of movement of the ATPase. It has been demonstrated that 2 bp ssDNA gaps at SHL 2 arrest the action of the remodeler ATPase (McKnight et al., 2011; Saha et al., 2005; Schwanbeck et al., 2004; Zofall et al., 2006). When the gaps made away from the dyad are drawn towards SHL 2 during remodeling, the sliding process stalls once the gaps reach 21-22 bp from the nucleosome dyad. By making nucleosomes containing gaps a specific distance (*m*) from this stalling point, I can see how translocation of a specific number of bp by the ATPase translates to movement elsewhere on the nucleosome. In order to limit movement of the ATPase, I made nucleosomes positioned on the Widom 601 containing 2 bp ssDNA gaps at *m*= 5 and *m*= 8 bp (Figure 5.2**A**). As expected, movement of these gapped nucleosomes by native gel sliding was restricted. Native gel sliding reports on remodeling as Chd1 shifts end positioned nucleosomes towards the middle of the DNA, typically producing 4 super-shifted bands in ungapped nucleosomes. Chd1 was only able to reposition gapped nucleosomes to the first super-shifted position (Figure 5.2**B**). Interestingly, Chd1 could move *m*= 8 nucleosomes to this position faster than *m*= 5 nucleosomes, which also retained more starting material than the *m*= 8 by the last time-point (64 minutes). The different patterns of movement for these two nucleosomes

suggest that the amount of translocation by the ATPase at SHL 2 affects the probability of nucleosomes reaching the first super-shifted position.

To simultaneously monitor DNA movement at multiple places on these gapped nucleosomes, I used site-specific histone crosslinking to compliment our smFRET results. This method gives the position of the DNA sequence relative to the histone core by cleaving DNA adjacent to a single cysteine histone site using a photoactivatable crosslinker (Kassabov and Bartholomew, 2004; Kassabov et al., 2002; Levendosky et al., 2016; Nodelman et al., 2016). While this technique usually uses only one histone position, I made nucleosomes with multiple sites to concurrently monitor DNA near the entry/exit region with H2B (S53C) and at the dyad with H3 (M120C) (Figure 5.2**C**). I assembled reactions containing these nucleosomes, Chd1 and ATP, and tracked progress by allowing remodeling reactions to proceed for increasing durations before inducing crosslinking by UV exposure. Importantly, I crosslinked the reactions during active remodeling, without chemical quenching or removal of the remodeler. This increased the likelihood of observing short-lived states that relax to other positions after remodeling ceases.

For both m= 5 and m= 8 nucleosomes, DNA movement was divided into fast, gap-limited shifts and slower, 601-phased shifts. On m= 5 nucleosomes, DNA at the entry-side, dyad and exit-side rapidly moved 3-4 nt from the initial position within 7 seconds of ATP addition (Figure 5.3 orange plots and arrows). Movement at all these sites indicates that a 4 bp translocation by the ATPase is sufficient to propagate DNA around the nucleosome. The fast DNA shifts were larger for m= 8 nucleosomes, with shifts of 9, 7 and 4 nt at the entry, dyad and exit, respectively. The fast, 4 nt shift on the exit side indicates the nucleosome is not buffering more than 4 bp of DNA during remodeling.

The slow DNA shifts are likely caused by the intrinsic curvature of the Widom 601 that facilitates bending around the histone core. This curvature leads to an energy landscape with stable nucleosome positions in phase with the 10-11 bp periodicity of the DNA duplex where the curvature cooperates with DNA wrapping the histones. In the unstable intermediate positions (~ 5 bp), the DNA curvature is "inside out" with respect to bending around the histone core, and nucleosomes eventually settle into the phased positions. In the native gel sliding experiments, Chd1 was competed off of the nucleosome with competitor DNA, which means only the phased positions were observed in the gel. In contrast, histones crosslinking was performed on active remodeling reactions with Chd1 still on the nucleosome, allowing observation of the intermediate positions, which are unlikely to be stable on their own. In crosslinking assays, these slow shifts resulted in 11 bp movement of DNA at the entry-side and dyad for both the *m*= 5 and *m*= 8 nucleosomes. On the exit-side, however, there were no crosslinks beyond the fast 4 nt shift. This absence may be due to a previously observed sequence bias that interferes with crosslinking at some positions on this side of the Widom 601 (Levendosky et al., 2016). The decrease in the 4 nt crosslink at longer time-points suggests that the slow 601-phased shift still occurred, though the product was not visible. Consistent with observations from native gel sliding, the slow shifts of *m*= 8 nucleosomes occurred earlier and produced larger peaks than for *m*= 5 nucleosomes. This suggests that the positions apparent in the native gel sliding were due to the 11 bp 601-phased shift and not the fast 4 bp shift. In addition, the more robust movement of the *m*= 8 nucleosomes indicates the extra 3 bp of movement is sufficient to move the nucleosome past an energy barrier preventing the *m*= 5 nucleosomes from stability repositioning to the Widom 601 phasing.

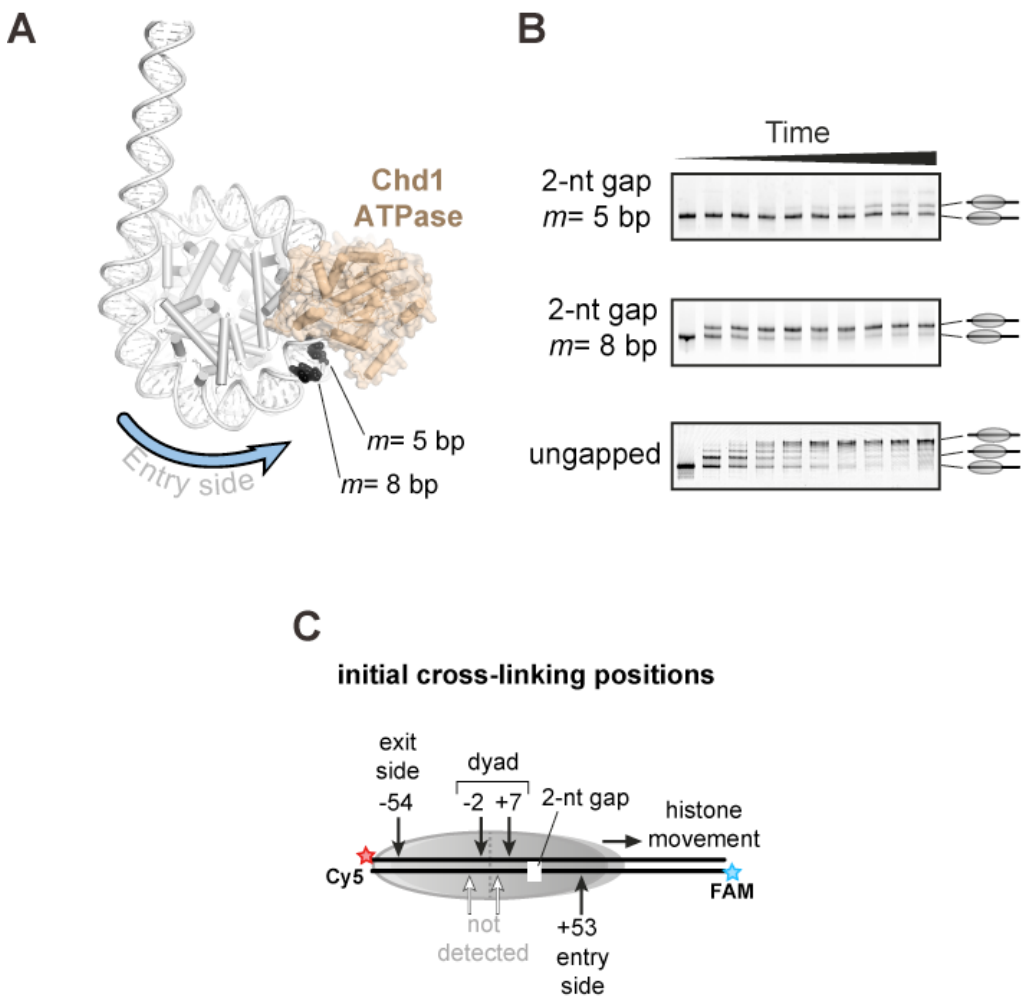

Figure 5.2: DNA gaps limits the range of DNA movement by remodelers
(**A**) The locations of 2 nt ssDNA gaps are shown (black spheres) relative to the site of the Chd1 ATPase (beige) (Farnung et al., 2017). As entry DNA is drawn onto the nucleosome, the gaps reach the active site of the remodeler and stall sliding.
(**B**) Native gel sliding assays containing 150 nM nucleosome with 200 nM Chd1 and 1 mM ATP for gapped nucleosomes and 100 µM ATP for ungapped nucleosomes. Movment is restricted by the gaps. Representative of two and three independent experiments for the gapped and ungapped nucleosomes, respectively. Gel lanes contain reaction time points at 0", 15", 30", 1', 2', 4', 8', 16', 32' and 64'.
(**C**) Locations of the site specific crosslinking sites used to monitor movement at the entry, dyad and exit-side of the nucleosome in Figure 5.3. The ssDNA gaps obscure the detection of dyad crosslinking sites on the bottom strand (FAM label).

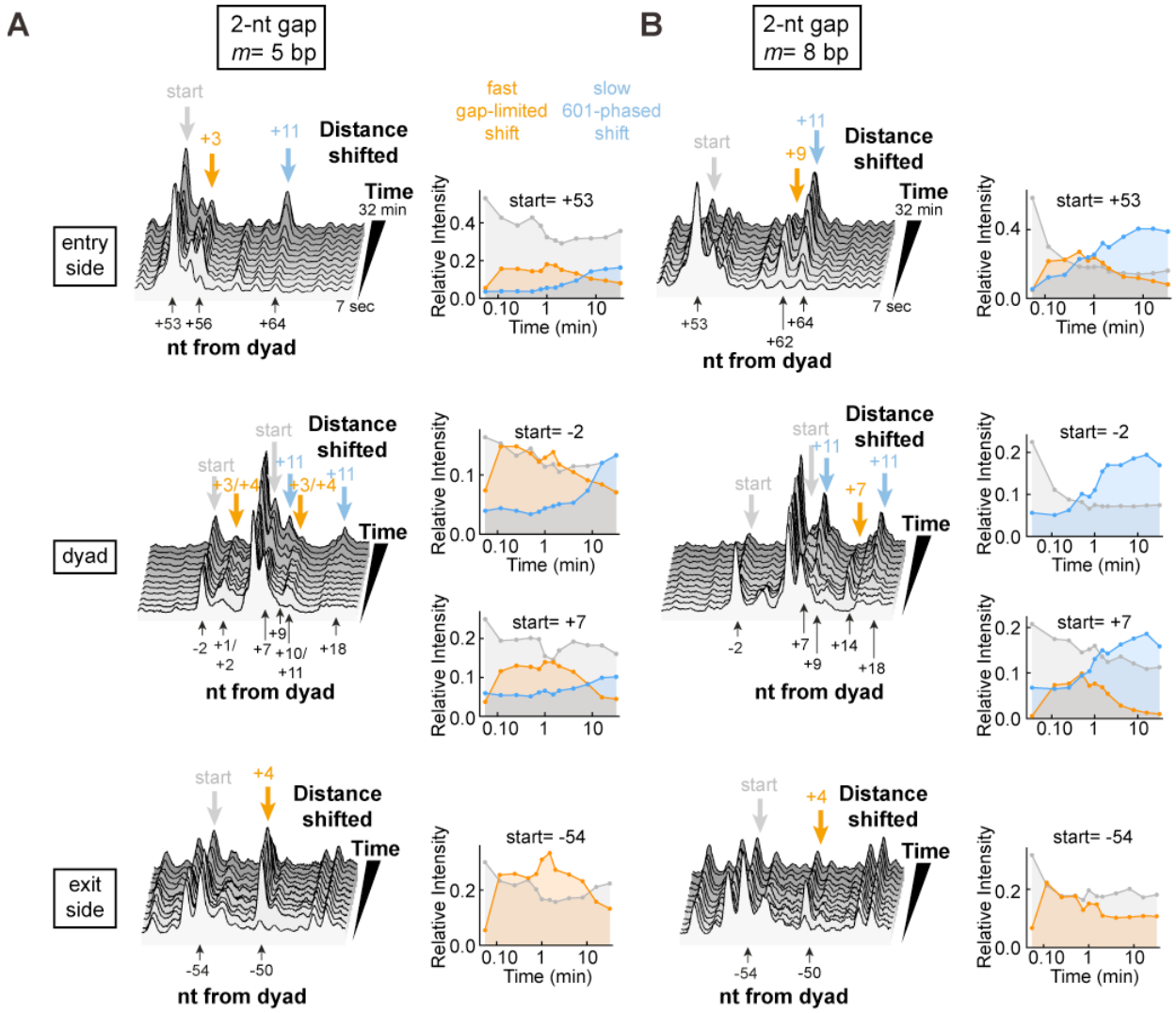

Figure 5.3: The nucleosome absorbs less than 5 bp during remodeling
Each series of gel scans shows the shift in crosslinking patterns during site specific crosslinking experiments. Remodeling reactions with *m*= 5 (**A**) or *m*= 8 (**B**) nucleosomes (150 nM) and 200 nM Chd1 with 1 mM ATP simultaneously reveal DNA movement at the nucleosome entry-side (top), dyad (middle) and exit-side (bottom). Arrows highlight the emergence of fast, gap-limited shifts (orange) and slow, 601-phased shifts (blue). The intensity of the bands are plotted to the right of each time course of gel scans. Reaction time points were collected at 0", 7", 15", 30", 45", 60", 90", 2', 4', 8', 16' and 32'.

DISCUSSION

Here we demonstrate an upper limit to DNA buffering on the nucleosome. In 3 color smFRET experiments, a lag between movement of entry and exit DNA indicates the nucleosome transiently absorbs 1 bp or more during remodeling (Sebantsev et al., 2018 *submitted*). Using nucleosomes with gaps placed to limit translocation of the ATPase to 5 bp, I observed rapid DNA movement of 3-4 bp at the entry, dyad and exit regions. Together, these observations suggest that 1-4 bp of DNA are absorbed on the nucleosome between the entry side SHL 2 and the exit DNA.

The observation that small lengths of DNA are absorbed by the nucleosome favors the twist-diffusion model over the loop/bulge model of DNA propagation. The loop/bulge model implies a more significant disruption of histone contacts with many bp of DNA looping away from the octamer. The loop then travels like a wave around the nucleosome without twisting about the helical axis. Since the strong histone contacts are comprised of arginines protruding into the DNA minor groove, the size of the loop must be close to the 10 bp periodicity of the DNA. Otherwise the minor groove on one side of the loop would be out of alignment with the arginine contacts. Thus, the smaller, 1-4 bp buffering capacity observed is insufficient to stabilize a loop without twisting of the DNA. In agreement, single molecule studies have identified 1-2 bp step sizes during remodeling (Deindl et al., 2013).

These results are more consistent with the twist diffusion model, which predicts the formation of twist defects that can diffuse around the nucleosome (van Holde and Yager, 2003, 1985). Twist defects are areas where the DNA is either over- or under-twisted relative to canonical nucleosomal DNA. For instance, an under-twist between two histone contacts on the nucleosome would compress an extra bp of DNA in that region. Molecular dynamics simulations

suggest that twist defects can spontaneously diffuse around the nucleosome in a corkscrewing motion to reposition DNA (Brandani et al., 2018) and this diffusion can be directed by remodelers (Brandani and Takada, 2018). In agreement, recent studies from our lab suggest that Chd1 induces a twist defect at SHL 2, compressing an additional bp between the histone contacts at SHLs 1.5 and 2.5 while drawing DNA onto the entry side (Winger et al., 2018). In a post-ATP-hydrolysis state, Chd1 directs the compressed DNA towards the dyad. Structures of the nucleosome reveal stretching of DNA at SHLs 2 and 5 in certain sequence contexts (Luger et al., 1997; Ong et al., 2007). This suggests that remodelers could use the intrinsic tendency of DNA at SHL 2 to adopt twist defects to catalyze DNA movement. Thus, remodelers may be acting as "Brownian ratchets" to promote twist defects and channel their diffusion in a unidirectional manner.

In principle these twist defects could store an extra bp of DNA between each histone contact, which would amount to 9 bp stored between SHL 2 and the DNA exit region. The 1-4 bp buffering capacity we observed suggests this amount is much lower, and twist defects may be limited to SHL 2 and SHL 5. Further experiments that use gaps closer to SHL 2 to restrict motion of the ATPase to only 2-3 bp could refine the estimate of the buffering capacity of the nucleosome during remodeling.

In addition to fast, gap-limited movements directed by the remodeler, I observed slower shifts towards positions in-phase with the periodicity of the Widom 601. This periodicity, arising from the curvature of the Widom 601, results in stable nucleosome positions in multiples of the 10-11 bp phasing of the DNA. Intermediate positions, out of phase by about 5 bp, would be unstable due to the curvature of the Widom 601 resisting bending around the octamer. These intermediate positions eventually settle into either of the adjacent energy wells in-phase with the

Widom 601. After the *m*= 5 nucleosomes were rapidly shifted by 3-4 bp, those nucleosomes were sitting on an unstable peak in the energy landscape where they could either relax back to the initial position or move forward into the next energy well visible as an 11 bp shift. For the *m*= 8 nucleosomes, Chd1 could move these just past the unstable energy peak, which made them more likely to settle forward into 11bp shifted position. Indeed, the *m*= 8 nucleosomes populated the 11 bp shifted position faster and more extensively than the *m*= 5 nucleosomes. Since the *m*= 5 nucleosomes actually moved past the gaps, the 601-phased shifts appear to be independent of the remodeler. These observations illustrate how the activity of Chd1 and sequence-dependent characteristics of the nucleosome both contribute to the ultimate nucleosome positioning. These results place valuable constraints on current models of chromatin remodeling.

Chapter 6: Methods and References

METHODS

Protein production and modifications

Expression and purification of proteins used in this dissertation were carried out as previously described for a truncated form of *Saccharomyces cerevisiae* Chd1 (residues 118-1274) (Hauk et al., 2010; Patel et al., 2011), *Xenopus laevis* histones (Luger et al., 1999), the ubiquitin variant G76C (Long et al., 2014), and human SNF2h was purified analogously to Chd1. The ubiquitin sequence used in this work was identical to human and *X. laevis*, which is 96% identical to *S. cerevisiae* ubiquitin.

Conjugation of H2B and ubiquitin (H2B-Ub) was carried out essentially as described (Long et al., 2014) to produce a nonhydrolyzable H2B-Ub mimic. A cysteine was introduced in place of the C-terminal lysine of *X. laevis* H2B (annotated as K117 in crystal structures using *X. laevis* histones, and equivalent to K120 in mammalian and full length *X. laevis* H2B). Based on the concentration of reduced cysteines using Ellman's reagent, H2B (K117C) and His-tagged Ubiquitin (G76C) were combined at a 2:1 ratio at a protein concentration of ~ 10 mg/mL in denaturing conditions. TCEP (5 mM C_f) was added and incubated for 30 minutes. Crosslinking of the two proteins was carried out by adding 100 mM 1,3 dichloroacetone to a final amount equal to half the total moles of reduced cysteines, and then quenching with 2-mercaptoethanol after 45 minutes. Un-crosslinked histones were removed using nickel affinity purification under denaturing conditions. The amount of crosslinked H2B-Ub was estimated from SDS-PAGE and refolded at a 1:1 ratio with *X. laevis* H2A. The H2A/H2B-Ub dimer was purified by size exclusion chromatography as described for unmodified H2A/H2B (Dyer et al., 2004). For

fluorescently tagged histones, H2A(T120C) was labeled with maleimide derivatives of Cy3 or Cy3B prior to refolding as previously described (Shahian and Narlikar, 2012).

Production of hexasomes and nucleosomes

Xenopus laevis histones were refolded in equimolar ratios to obtain dimers (H2A/H2B), tetramers $(H3/H4)_2$, and octamers $(H3/H4/H2A/H2B)_2$ and purified by size exclusion chromatography as previously described (Dyer et al., 2004). Nucleosomes were generated by combining either the histone octamer or H2A/H2B dimer and H3/H4 tetramer (2:1 ratio) with DNA containing the Widom 601 or Widom 603 sequence (Lowary and Widom, 1998). To favor hexasome formation, dimer and tetramer were combined in 1.2 : 1 ratio. Reconstitution by salt dialysis was performed as described (Luger et al., 1999). Nucleosomes and hexasomes were purified to ≥95% homogeneity by separating different nucleosomal species and free DNA over a 7% native acrylamide column (60:1 acrylamide:bisacrylamide) using a BioRad Prep Cell (Model 491) or MiniPrep Cell apparatus.

Addition of H2A/H2B dimer to hexasome was carried out separately for each reaction. H2A/H2B dimer (stored in 10 mM Tris-HCl (pH 7.8), 2 M NaCl, 1 mM EDTA, 5 mM 2-mercaptoethanol) was diluted roughly 10-30 fold to 6 μM in reaction buffer. Dimer dilutions were performed just prior to experiments. Hexasome was added to the reaction buffer first, followed by dimer in the indicated molar ratio. Dimer addition was allowed to proceed at room temperature for 2-3 minutes before additional reaction components were introduced; time courses of dimer addition indicated that incorporation of the dimer into hexasomes was complete within 30 s (data not shown). A similar pre-incubation step was carried out for nucleosome-containing reactions.

Native gel sliding

Nucleosome sliding reactions were carried out as previously described with some minor adjustments (Eberharter et al., 2004; Patel et al., 2011). Briefly, fluorescently labeled nucleosome (or hexasome) and Chd1 were diluted and combined in slide buffer (20 mM HEPES (pH 7.8), 100 mM KCl, 5 mM $MgCl_2$, 0.1 mg/mL BSA, 1 mM DTT, 5% sucrose (w/v)) at room temperature. Reactions were started with the addition of ATP and at each time point, 1 µL of the reaction was added into into 24 µL of fresh quench buffer (20 mM HEPES (pH 7.8), 100 mM KCl, 0.1 mg/mL BSA, 1 mM DTT, 5% sucrose (w/v), 5 mM EDTA, 125 ng/µL salmon sperm DNA (Invitrogen) in Chapter 2, but using 25 mM EDTA and 1µg/µl salmon sperm DNA in Chapter 4 and Chapter 5) and placed on ice. Reactions in Chapter 2 contained 150 nM nucleosome, 50 nM Chd1 and 2.5 mM ATP, and . To visualize reaction products, 2.5 µL of the quenched time point samples were separated using 7% native polyacrylamide gels (60:1 acrylamide to bis-acrylamide) that were electrophoresed (125 V) for 2 hours at 4˚C. Reaction products were observed by their fluorescent labels using a Typhoon 9410 variable mode imager (GE Healthcare).

Histone mapping (site specific crosslinking) and Chd1 cross-linking

Histone mapping and Chd1 cross-linking experiments were conducted as previously described (Kassabov and Bartholomew, 2004; Nodelman et al., 2017). For each, single cysteine residues on either the nucleosome (H2B-S53C) or Chd1 (N459C or V721C) were labeled with 200-400 µM 4-azidophenacyl bromide (APB) at room temperature and in the dark for 2-3 hr and then quenched with DTT. For histone mapping, APB-labeled nucleosomes were incubated with Chd1 in slide buffer (20 mM Tris-HCl (pH 7.8), 50 mM KCl, 5mM $MgCl_2$, 5% sucrose (w/v), 0.1 mg/mL BSA, 1 mM DTT). Sliding reactions were initiated with the addition of ATP. In

Chapter 2, reactions contained 150 nM nucleosome, 50 nM Chd1 and 2 mM ATP. In Chapter 4, reactions contained 100 nM hexasome, 200 nM H2A/H2B dimer, 1 μM SNF2h, and 2 mM ATP. In Chapter 5, reactions contained 150 nM nucleosome, 200 nM Chd1 and 1mM ATP.

In Chapter 2 and Chapter 4, at each time-point, 50 μL of the reaction was added to 100 μL of quench buffer (20 mM Tris-HCl (pH 7.8), 50 mM KCl, 5% sucrose (w/v), 0.1 mg/mL BSA, 5 mM DTT, 5 mM EDTA, 150 ng/μL salmon sperm DNA) and placed on ice. In Chapter 5, samples were not quenched with EDTA and competitor and instead were UV irradiated at the indicated time. For Chd1 cross-linking in Chapter 2, 300 nM APB-labeled Chd1 was incubated with 150 nM Cy3-40-601-40-FAM template DNA, nucleosomes, or hexasomes and 2 mM ADP BeF_3 (generated in each reaction by adding 2 mM ADP, 15 mM NaF, 3 mM $BeCl_2$, and 6 mM $MgCl_2$) in slide buffer without additional $MgCl_2$. Incubations were carried out for 30 minutes in the dark at room temperature.

For both histone mapping and Chd1 crosslinking experiments, APB was crosslinked to the DNA by irradiating at 302 nm for 15 sec using a UV Transilluminator (VWR). Samples were denatured with 0.1% SDS and heating to 70°C, and then subjected to phenol chloroform extraction and EtOH precipitation to remove uncrosslinked material. The crosslinked DNA was resuspended and cleaved with NaOH. The fragmented DNA was EtOH precipitated again, resuspended with formamide loading buffer, and separated on an 8 M urea, 8% polyacrylamide (19:1 acrylamide:bis-acrylamide) sequencing gel. The samples were run for 1.25 hours (1.75 hours for Chd1 crosslinking) at 65 W alongside a sequencing ladder of the nucleosomal DNA to allow precise identification of cross-link locations. Gels were imaged on a Typhoon 9410 variable mode imager (GE Healthcare) and analyzed using ImageJ (http:// imagej.nih.gov/ij/).

Exonuclease III digestion

ExoIII digestion was carried out on nucleosomes and hexasomes with fluorescently labeled DNA. Samples containing nucleosome (100 nM), hexasome alone (100 nM), or hexasome (100mM) preincubated for 2-3 minutes with 2 fold molar excess H2A/H2B dimer were incubated at room temperature for 10 minutes in reaction buffer consisting of 20 mM HEPES (pH 7.6), 50 mM KCl, 10 mM $MgCl_2$, 5% sucrose (w/v), 0.1 mg/mL BSA, and 1 mM DTT. For each sample condition, four 10 µL digestion reactions were made containing 0, 10, 40, and 160 units of ExoIII (New England Biolabs). After digesting for 5 minutes at room temperature, reactions were quenched by the addition of 40 µL of quench buffer (20 mM HEPES (pH 7.6), 50 mM KCl, 20 mM EDTA, 1.2% SDS) and placed on ice. DNA was isolated from the digestion reactions by adding an equal volume of phenol:chloroform:isoamyl alcohol (25:24:1), vortexing, centrifuging for 2 minutes, and removing the top (aqueous) layer to a new tube. To completely remove phenol, this step was repeated using chloroform:isoamyl alcohol (24:1). DNA was precipitated by adding 1.5 µL of 10 mg/mL glycogen, 5 µL of 3 M sodium acetate and 250 µL 100% EtOH and then chilled at -80° C for > 20 minutes followed by centrifugation (21,130 rcf) for 30 minutes at 4° C. After a 70% EtOH wash and air drying of the pellet, samples were resuspended in 8 µL of formamide loading buffer and separated on urea sequencing gels as described for histone mapping.

Single molecule FRET

Biotinylated and dye-labeled nucleosomes and hexasomes (alone or pre-incubated with an approximately twofold molar excess of unlabeled H2A/H2B dimer) were surface-immobilized on poly(ethylene glycol)-coated quartz microscope slides via a biotin-streptavidin linkage, as previously described (Blosser et al., 2009; Deindl et al., 2013). Immobilized samples were excited with a 532 nm Nd:YAG laser (CrystaLaser), and fluorescence emissions from Cy3 and

Cy5 were detected using a prism-type TIRF microscope, filtered with a 550 nm long-pass filter (Chroma Technology), spectrally separated by a 635 nm dichroic mirror (Chroma Technology), and imaged onto the two halves of an Andor iXon Ultra 897 (512 × 512) CCD camera. The imaging buffer contained 12 mM HEPES, 40 mM Tris-HCl (pH 7.5), 60 mM KCl, 3 mM $MgCl_2$, 0.32 mM EDTA, 10% glycerol, an oxygen scavenging system (800 μg ml^{-1} glucose oxidase, 40 μg ml^{-1} catalase, 10% glucose) to reduce photobleaching, 2 mM Trolox (Sigma-Aldrich) to suppress photoblinking of the dyes (Rasnik et al., 2006), and 0.1 mg/ml BSA (Promega). Remodeling was induced by infusing the sample chamber with the imaging buffer containing 300 nM Chd1 remodeling enzyme and ATP using a syringe pump (Harvard Apparatus).

Fluorescence Experiments

Static quenching of fluorescence (SQOF) experiments were carried out using Cy3-Cy3 or Cy3B-Dabcyl pairs. Reactions were monitored for 0-601-80 nucleosomes or hexasomes, with exit-side H2A T120C labeled with Cy3 or Cy3B and the zero-end of DNA labeled with Cy3 or Dabcyl (IDT).

FRET unwrapping experiments were conducted on 12N80 and 80N12 nucleosomes with Cy3 on the end of the 12 bp linker and Cy3 labeling the histone core at H3 V35C.

FRET sliding experiments were performed on 10 nM hexasome + 12 nM dimer with Cy5 on the end of short linker DNA (varying lengths) on the TA-rich side of the 601. The histones were labeled with Cy3 on H2A T120C.

PIFE experiments were performed using 10 nM hexasomes + 12 nM dimer containing a single Cy3 on either the histones at H2A T120C on the TA-rich side of the 601 or at the end of 0 bp DNA on the TA-rich side of the 601.

In Chapter 2, sliding reactions were conducted with 10 nM nucleosome or 10 nM hexasome with 12 nM dimer (unless otherwise noted), 25, 400, or 600 μM Chd1, and 25 μM ATP (except for Figure 2.12 in which 1 mM ATP was used). In other chapters, reaction conditions are specified in figure legends. All reactions were performed in sliding buffer (100 mM KCl, 20 mM HEPES (pH 7.5), 5 mM $MgCl_2$, 100 μM EDTA, 5% sucrose w/v, 1 mM DTT, 0.2% Nonidet P-40, and 0.1 mg/mL BSA) at 25 °C.

Sliding reactions were monitored by either fluorometer or stopped-flow. Fluorometer experiments were conducted on a Fluorolog-3 fluorometer (Horiba) using a 2 mL reaction volume with a stir bar in the cuvette. First, 10 nM nucleosome or hexasome followed by H2A/H2B dimer was added to the cuvette and allowed to equilibrate for 2-3 minutes. Next, Chd1 was added, and after another brief equilibration, the sliding reaction was initiated with 25 μM ATP. Cy3 (or Cy3B) was excited at 510 nm and fluorescence was monitored at 565 nm using a 4 nm slit width and 1 second integration time. Stopped flow experiments were conducted on an SX20 stopped-flow (Applied Photophysics Limited) with nucleosome (or hexasome and dimer) and Chd1 in one syringe and ATP in the other. Cy3 (or Cy3B) was excited at 510 nm and emissions were monitored above 570 nm with a long-pass filter. Fluorescence signal was integrated over 0.01 seconds for the first ten seconds of the reaction and then 0.1 seconds for the remainder of the trace. Each progress curve is the average of 3-6 technical replicates. Progress curves were fit in Mathematica (Wolfram) using a single, double, or triple exponential function of the form:

$$y_{obs} = a_1\left(1 - e^{-k_1 x}\right) + a_2\left(1 - e^{-k_2 x}\right) + a_3\left(1 - e^{-k_3 x}\right) + c$$

Where k_1, k_2 and k_3 are observed rates, a_1, a_2 and a_3 are corresponding amplitudes, and c is a constant.

REFERENCES

Arimura, Y., Tachiwana, H., Oda, T., Sato, M., and Kurumizaka, H. (2012). Structural analysis of the hexasome, lacking one histone H2A/H2B dimer from the conventional nucleosome. Biochemistry *51*, 3302–3309.

Armache, K., Garlick, J.D., Canzio, D., Narlikar, G.J., and Kingston, R.E. (2011). Structural basis of silencing: Sir3 BAH domain in complex with a nucleosome at 3.0 Å resolution. Science *334*, 977–982.

Bagchi, A., Papazoglu, C., Wu, Y., Capurso, D., Brodt, M., Francis, D., Bredel, M., Vogel, H., and Mills, A.A. (2007). CHD5 Is a Tumor Suppressor at Human 1p36. Cell *128*, 459–475.

Bannister, A.J., and Kouzarides, T. (2011). Regulation of chromatin by histone modifications. Cell Res. *21*, 381–395.

Bao, Y., Konesky, K., Park, Y.-J., Rosu, S., Dyer, P.N., Rangasamy, D., Tremethick, D.J., Laybourn, P.J., and Luger, K. (2004). Nucleosomes containing the histone variant H2A.Bbd organize only 118 base pairs of DNA. EMBO J. *23*, 3314–3324.

Barbera, A.J., Chodaparambil, J. V, Kelley-Clarke, B., Joukov, V., Walter, J.C., Luger, K., and Kaye, K.M. (2006). The nucleosomal surface as a docking station for Kaposi's sarcoma herpesvirus LANA. Science *311*, 856–861.

Bloomfield, V.A. (1996). DNA condensation. Curr. Opin. Struct. Biol. *6*, 334–341.

Blosser, T.R., Yang, J.G., Stone, M.D., Narlikar, G.J., and Zhuang, X. (2009). Dynamics of nucleosome remodelling by individual ACF complexes. Nature *462*, 1022–1027.

Bohm, V., Hieb, A.R., Andrews, A.J., Gansen, A., Rocker, A., Toth, K., Luger, K., and Langowski, J. (2011). Nucleosome accessibility governed by the dimer/tetramer interface. Nucleic Acids Res. *39*, 3093–3102.

Böhm, V., Hieb, A., Andrews, A., Gansen, A., Rocker, A., Tóth, K., Luger, K., and Langowski, J. (2011). Nucleosome Dynamics Studied by Single Molecule FRET. Biophys. J. *100*, 68a.

Bondarenko, V.A., Steele, L.M., Újvári, A., Gaykalova, D.A., Kulaeva, O.I., Polikanov, Y.S., Luse, D.S., and Studitsky, V.M. (2006). Nucleosomes Can Form a Polar Barrier to Transcript Elongation by RNA Polymerase II. Mol. Cell *24*, 469–479.

Bowman, G.D., and Poirier, M.G. (2015). Post-Translational Modifications of Histones That Influence Nucleosome Dynamics. Chem. Rev. *115*, 2274–2295.

Brahma, S., Udugama, M.I., Kim, J., Hada, A., Bhardwaj, S.K., Hailu, S.G., Lee, T.H., and Bartholomew, B. (2017). INO80 exchanges H2A.Z for H2A by translocating on DNA proximal to histone dimers. Nat. Commun. *8*.

Brandani, G.B., and Takada, S. (2018). Chromatin remodelers couple inchworm motion with twist-defect formation to slide nucleosomal DNA. PLoS Comput. Biol. *14*, e1006512.

Brandani, G.B., Niina, T., Tan, C., and Takada, S. (2018). DNA sliding in nucleosomes via twist defect propagation revealed by molecular simulations. Nucleic Acids Res. *46*, 2788–2801.

Brinkers, S., Dietrich, H.R.C., De Groote, F.H., Young, I.T., and Rieger, B. (2009). The persistence length of double stranded DNA determined using dark field tethered particle motion. J. Chem. Phys. *130*, 0–9.

Cheung, V., Chua, G., Batada, N.N., Landry, C.R., Michnick, S.W., Hughes, T.R., and Winston, F. (2008). Chromatin- and transcription-related factors repress transcription from within coding regions throughout the Saccharomyces cerevisiae genome. PLoS Biol. *6*, 2550–2562.

Chua, E.Y.D., Vasudevan, D., Davey, G.E., Wu, B., and Davey, C.A. (2012). The mechanics behind DNA sequence-dependent properties of the nucleosome. Nucleic Acids Res. *40*, 6338–6352.

Clapier, C.R., and Cairns, B.R. (2009). The Biology of Chromatin Remodeling Complexes. Annu. Rev. Biochem. *78*, 273–304.

Clapier, C.R., and Cairns, B.R. (2012). Regulation of ISWI involves inhibitory modules antagonized by nucleosomal epitopes. Nature *492*, 280–284.

Clegg, R.M. (1992). Fluorescence Resonance Energy Transfer and Nucleic Acids. Methods Enzymol. *211*, 353–388.

Cooper, M., Ebner, A., Briggs, M., Burrows, M., Gardner, N., Richardson, R., and West, R. (2004). Cy3B: Improving the Performance of Cyanine Dyes. J. Fluoresc. *14*, 1–6.

Corona, D.F. V, Becker, P.B., Clapier, C.R., La, G., and Butenandt-institut, A. (2001). Critical Role for the Histone H4 N Terminus in Nucleosome Remodeling by ISWI. Mol. Cell. Biol. *21*, 875–883.

Cui, F., and Zhurkin, V.B. (2010). Structure-based analysis of DNA sequence patterns guiding nucleosome positioning in vitro. J. Biomol. Struct. Dyn. *27*, 821–841.

Dann, G.P., Liszczak, G.P., Bagert, J.D., Müller, M.M., Nguyen, U.T.T., Wojcik, F., Brown, Z.Z., Bos, J., Panchenko, T., Pihl, R., et al. (2017). ISWI chromatin remodellers sense nucleosome modifications to determine substrate preference. Nature *548*, 607–611.

Davey, C.A., Sargent, D.F., Luger, K., Maeder, A.W., and Richmond, T.J. (2002). Solvent Mediated Interactions in the Structure of the Nucleosome Core Particle at 1.9Å Resolution. J. Mol. Biol. *319*, 1097–1113.

Dechassa, M.L., Sabri, A., Pondugula, S., Kassabov, S.R., Chatterjee, N., Kladde, M.P., and Bartholomew, B. (2010). SWI/SNF Has Intrinsic Nucleosome Disassembly Activity that Is Dependent on Adjacent Nucleosomes. Mol. Cell *38*, 590–602.

Deindl, S., Hwang, W.L., Hota, S.K., Blosser, T.R., Prasad, P., Bartholomew, B., and Zhuang, X. (2013). ISWI Remodelers Slide Nucleosomes with Coordinated Multi-Base-Pair Entry Steps and Single-Base-Pair Exit Steps. Cell *152*, 442–452.

Delmas, V., Stokes, D.G., and Perry, R.P. (1993). A mammalian DNA-binding protein that contains a chromodomain and an SNF2/SWI2-linke helicase domain. Proc. Natl. Acad. Sci. *90*, 2414–2418.

Dorigo, B., Schalch, T., Bystricky, K., and Richmond, T.J. (2003). Chromatin Fiber Folding: Requirement for the Histone H4 N-terminal Tail. J. Mol. Biol. *327*, 85–96.

Dorigo, B., Schalch, T., Kulangara, A., Duda, S., Schroeder, R.R., and Richmond, T.J. (2004). Nucleosome arrays reveal the two-start organization of the chromatin fiber. Science (80-.). *306*, 1571–1573.

Dyer, P.N., Edayathumangalam, R.S., White, C.L., Bao, Y., Chakravarthy, S., Muthurajan, U.M., and Luger, K. (2004). Reconstitution of Nucleosome Core Particles from Recombinant Histones and DNA. Methods Enzymol. *375*, 23–44.

Eberharter, A., Längst, G., and Becker, P.B. (2004). A nucleosome sliding assay for chromatin remodeling factors. Methods Enzymol. *377*, 344–353.

Eltsov, M., MacLellan, K.M., Maeshima, K., Frangakis, A.S., and Dubochet, J. (2008). Analysis of cryo-electron microscopy images does not support the existence of 30-nm chromatin fibers in mitotic chromosomes in situ. Proc. Natl. Acad. Sci. *105*, 19732–19737.

Farnung, L., Vos, S.M., Wigge, C., and Cramer, P. (2017). Nucleosome–Chd1 structure and implications for chromatin remodelling. Nature *154*, 490.

Ferreira, H., Flaus, A., and Owen-Hughes, T. (2007). Histone Modifications Influence the Action of Snf2 Family Remodelling Enzymes by Different Mechanisms. *374*, 563–579.

Flaus, A., Martin, D.M.A., Barton, G.J., and Owen-Hughes, T. (2006). Identification of multiple distinct Snf2 subfamilies with conserved structural motifs. Nucleic Acids Res. *34*, 2887–2905.

Fleming, A.B., Kao, C.-F., Hillyer, C., Pikaart, M., and Osley, M.A. (2008). H2B ubiquitylation plays a role in nucleosome dynamics during transcription elongation. Mol. Cell *31*, 57–66.

Fyodorov, D. V., and Kadonaga, J.T. (2002). Binding of Acf1 to DNA Involves a WAC Motif and Is Important for ACF-Mediated Chromatin Assembly. Mol. Cell. Biol. *22*, 6344–6353.

Gall, J.G. (1966). Chromosome fibers studied by a spreading technique. Chromosoma *20*, 221–233.

Gamarra, N., Johnson, S.L., Trnka, M.J., Burlingame, A.L., and Narlikar, G.J. (2018). The nucleosomal acidic patch relieves auto-inhibition by the ISWI remodeler SNF2h. Elife *7*, 1–24.

Gao, X., Tate, P., Hu, P., Tjian, R., Skarnes, W.C., and Wang, Z. (2008). ES cell pluripotency and germ-layer formation require the SWI/SNF chromatin remodeling component BAF250a. Proc. Natl. Acad. Sci. U. S. A. *105*, 6656–6661.

Gerhold, C.B., and Gasser, S.M. (2014). INO80 and SWR complexes: Relating structure to function in chromatin remodeling. Trends Cell Biol. *24*, 619–631.

Gkikopoulos, T., Havas, K.M., Dewar, H., and Owen-Hughes, T. (2009). SWI/SNF and Asf1p cooperate to displace histones during induction of the saccharomyces cerevisiae HO promoter. Mol. Cell. Biol. *29*, 4057–4066.

Gkikopoulos, T., Schofield, P., Singh, V., Pinskaya, M., Mellor, J., Smolle, M., Workman, J.L., Barton, G.J., and Owen-Hughes, T. (2011). A Role for Snf2-Related Nucleosome-Spacing Enzymes in Genome-Wide Nucleosome Organization. Science (80-.). *333*, 1758–1760.

Gordon, F., Luger, K., and Hansen, J.C. (2005). The core histone N-terminal tail domains function independently and additively during salt-dependent oligomerization of nucleosomal arrays. J. Biol. Chem. *280*, 33701–33706.

Grigoryev, S.A., and Woodcock, C.L. (2012). Chromatin organization - The 30nm fiber. Exp. Cell Res. *318*, 1448–1455.

Grigoryev, S.A., Arya, G., Correll, S., Woodcock, C.L., and Schlick, T. (2009). Evidence for heteromorphic chromatin fibers from analysis of nucleosome interactions. Proc. Natl. Acad. Sci. *106*, 13317–13322.

Hall, M.A., Shundrovsky, A., Bai, L., Fulbright, R.M., Lis, J.T., and Wang, M.D. (2009). High-resolution dynamic mapping of histone-DNA interactions in a nucleosome. Nat. Struct. Mol. Biol. *16*, 124–129.

Hansen, J.C. (2002). Conformational Dynamics of the Chromatin Fiber in Solution: Determinants, Mechanisms, and Functions. Annu. Rev. Biophys. Biomol. Struct. *31*, 361–392.

Hansen, J.C., van Holde, K.E., and Lohr, D. (1991). The mechanism of nucleosome assembly onto oligomers of the sea urchin 5 S DNA positioning sequence. J. Biol. Chem. *266*, 4276–4282.

Hansen, J.C., Connolly, M., McDonald, C.J., Pan, A., Pryamkova, A., Ray, K., Seidel, E., Tamura, S., Rogge, R., and Maeshima, K. (2018). The 10-nm chromatin fiber and its relationship to interphase chromosome organization. Biochem. Soc. Trans. *46*, 67–76.

Harvey, B.J., Perez, C., and Levitus, M. (2009). DNA sequence-dependent enhancement of Cy3 fluorescence. Photochem. Photobiol. Sci. *8*, 1105–1110.

Hauk, G., McKnight, J.N., Nodelman, I.M., and Bowman, G.D. (2010). The Chromodomains of the Chd1 Chromatin Remodeler Regulate DNA Access to the ATPase Motor. Mol. Cell *39*, 711–723.

van Holde, K., and Yager, T. (2003). Models for chromatin remodeling: a critical comparison. Biochem. Cell Biol. *81*, 169–172.

van Holde, K.E., and Yager, T.D. (1985). Structure and Function of the Genetic Apparatus ©. In Structure and Function of the Genetic Apparatus, C. Nicolini et al., ed. (New York: Plenum Press), pp. 35–53.

Hong, J., Feng, H., Wang, F., Ranjan, A., Chen, J., Jiang, J., Ghirlando, R., Xiao, T.S., Wu, C., and Bai, Y. (2014). The Catalytic Subunit of the SWR1 Remodeler Is a Histone Chaperone for the H2A.Z-H2B Dimer. Mol. Cell *53*, 498–505.

Hsieh, F.-K., Kulaeva, O.I., Patel, S., Dyer, P.N., Luger, K., Reinberg, D., and Studitsky, V.M. (2013). Histone chaperone FACT action during transcription through chromatin by RNA polymerase II. Proc. Natl. Acad. Sci. *110*, 7654–7659.

Huang, S., Gulzar, Z.G., Salari, K., Lapointe, J., Brooks, J.D., and Pollack, J.R. (2011). Recurrent deletion of CHD1 in prostate cancer with relevance to cell invasiveness. Oncogene *31*, 4164–4170.

Huynh, V.A.T., Robinson, P.J.J., and Rhodes, D. (2005). A method for the in vitro reconstitution of a defined "30 nm" chromatin fibre containing stoichiometric amounts of the linker histone. J. Mol. Biol. *345*, 957–968.

Hwang, H., and Myong, S. (2014). Protein induced fluorescence enhancement (PIFE) for probing protein-nucleic acid interactions. Chem. Soc. Rev. *43*, 1221–1229.

Hwang, H., Kim, H., and Myong, S. (2011). Protein induced fluorescence enhancement as a single molecule assay with short distance sensitivity. Proc. Natl. Acad. Sci. U. S. A. *108*, 7414–7418.

Hwang, W.L., Deindl, S., Harada, B.T., and Zhuang, X. (2014). Histone H4 tail mediates allosteric regulation of nucleosome remodelling by linker DNA. Nature 1–18.

Johansson, M.K. (2006). Choosing Reporter–Quencher Pairs for Efficient Quenching Through Formation of Intramolecular Dimers. Methods Mol. Biol. *335*, 17–29.

Johansson, M.K., and Cook, R.M. (2003). Intramolecular dimers: a new design strategy for fluorescence-quenched probes. Chemistry *9*, 3466–3471.

Johansson, M.K., Fidder, H., Dick, D., and Cook, R.M. (2002). Intramolecular Dimers: A New Strategy to Fluorescence Quenching in Dual-Labeled Oligonucleotide Probes. J. Am. Chem. Soc. *124*, 6950–6956.

Kalashnikova, A.A., Porter-Goff, M.E., Muthurajan, U.M., Luger, K., and Hansen, J.C. (2013). The role of the nucleosome acidic patch in modulating higher order chromatin structure. J. R. Soc. Interface *10*, 20121022.

Kang, J.-G., Hamiche, A., and Wu, C. (2002). GAL4 directs nucleosome sliding induced by NURF. EMBO J. *21*, 1406–1413.

Kassabov, S.R., and Bartholomew, B. (2004). Site-Directed Histone-DNA Contact Mapping for Analysis of Nucleosome Dynamics. Methods Enzymol. *375*, 1–18.

Kassabov, S.R., Henry, N.M., Zofall, M., Tsukiyama, T., and Bartholomew, B. (2002). High-Resolution Mapping of Changes in Histone-DNA Contacts of Nucleosomes Remodeled by ISW2. Mol. Cell. Biol. *22*, 7524–7534.

Kato, H., Kato, H., Jiang, J., Jiang, J., Zhou, B.-R., Zhou, B.-R., Rozendaal, M., Rozendaal, M., Feng, H., Feng, H., et al. (2013). A conserved mechanism for centromeric nucleosome recognition by centromere protein CENP-C. Science (80-.). *340*, 1110–1113.

Kelley, D.E., Stokes, D.G., and Perry, R.P. (1999). CHD1 interacts with SSRP1 and depends on both its chromodomain and its ATPase/helicase-like domain for proper association with chromatin. Chromosoma *108*, 10–25.

Kemble, D.J., McCullough, L.L., Whitby, F.G., Formosa, T., and Hill, C.P. (2015). FACT Disrupts Nucleosome Structure by Binding H2A-H2B with Conserved Peptide Motifs. Mol. Cell *60*, 294–306.

Kireeva, M.L., Walter, W., Tchernajenko, V., Bondarenko, V., Kashlev, M., and Studitsky, V.M. (2002). Nucleosome Remodeling Induced by RNA Polymerase II: Loss of the H2A/H2B Dimer during Transcription. Mol. Cell *9*, 541–552.

Kireeva, M.L., Hancock, B., Cremona, G.H., Walter, W., Studitsky, V.M., and Kashlev, M. (2005). Nature of the nucleosomal barrier to RNA polymerase II. Mol. Cell *18*, 97–108.

Kirk, J., Lee, J.Y., Lee, Y., Shin, S., Lee, E., Song, J.-J., and Hohng, S. (2018). Yeast Chd1p remodels nucleosomes with unique DNA unwrapping and translocation dynamics. bioRxiv.

Krietenstein, N., Wal, M., Watanabe, S., Park, B., Peterson, C.L., Pugh, B.F., and Korber, P. (2016). Genomic Nucleosome Organization Reconstituted with Pure Proteins. Cell *167*, 709–721.e12.

Krogan, N.J., Kim, M., Ahn, S.H., Zhong, G., Kobor, M.S., Cagney, G., Emili, A., Shilatifard, A., Buratowski, S., and Greenblatt, J.F. (2002). RNA polymerase II elongation factors of Saccharomyces cerevisiae: a targeted proteomics approach. Mol. Cell. Biol. *22*, 6979–6992.

Kubik, S., O'Duibhir, E., Jonge, W. de, Mattarocci, S., Albert, B., Falcone, J.-L., Bruzzone, M.J., Holstege, F.C.P., and Shore, D. (2018). Sequence-Directed Action of RSC Remodeler and Pioneer Factors Posisitons + 1 Nucleosome to Facilitate Transcription. bioRxiv.

Kulaeva, O.I., Gaykalova, D.A., Pestov, N.A., Golovastov, V. V, Vassylyev, D.G., Artsimovitch, I., and Studitsky, V.M. (2009). Mechanism of chromatin remodeling and recovery during passage of RNA polymerase II. Nat. Struct. Mol. Biol. *16*, 1272–1278.

Kuryan, B.G., Kim, J., Tran, N.N.H., Lombardo, S.R., Venkatesh, S., Workman, J.L., and Carey, M. (2012). Histone density is maintained during transcription mediated by the chromatin remodeler RSC and histone chaperone NAP1 in vitro. Proc. Natl. Acad. Sci. 1931–1936.

Lakowicz, J.R. (2006). Principles of Fluorescence Spectroscopy (Singapore: Springer).

Lechner, C.C., Agashe, N.D., and Fierz, B. (2016). Traceless Synthesis of Asymmetrically Modified Bivalent Nucleosomes. Angew. Chem. Int. Ed. Engl. *55*, 2903–2906.

Lee, J.-S., Garrett, A.S., Yen, K., Takahashi, Y.-H., Hu, D., Jackson, J., Seidel, C., Pugh, B.F., and Shilatifard, A. (2012). Codependency of H2B monoubiquitination and nucleosome reassembly on Chd1. Genes Dev. *26*, 914–919.

Lee, W., von Hippel, P.H., and Marcus, A.H. (2014). Internally labeled Cy3/Cy5 DNA constructs show greatly enhanced photo-stability in single-molecule FRET experiments. Nucleic Acids Res. *42*, 5967–5977.

Leonard, J.D., and Narlikar, G.J. (2015). A Nucleotide-Driven Switch Regulates Flanking DNA Length Sensing by a Dimeric Chromatin Remodeler. Mol. Cell 1–37.

Levendosky, R.F., Sabantsev, A., Deindl, S., and Bowman, G.D. (2016). The Chd1 chromatin remodeler shifts hexasomes unidirectionally. Elife *5*.

Li, G., and Widom, J. (2004). Nucleosomes facilitate their own invasion. Nat. Struct. Mol. Biol. *11*, 763–769.

Li, G., Levitus, M., Bustamante, C., and Widom, J. (2004). Rapid spontaneous accessibility of nucleosomal DNA. Nat. Struct. Mol. Biol. *12*, 46–53.

Li, M., Hada, A., Sen, P., Olufemi, L., Hall, M.A., Smith, B.Y., Forth, S., McKnight, J.N., Patel, A., Bowman, G.D., et al. (2015). Dynamic regulation of transcription factors by nucleosome remodeling. Elife 1–16.

Li, M., Liu, X., Xia, X., Chen, Z., and Li, X. (2017). Complex of Snf2-Nucleosome complex with Snf2 bound to SHL2 of the nucleosome .

Lin, J.J., Lehmann, L.W., Bonora, G., Sridharan, R., Vashisht, A.A., Tran, N., Plath, K., Wohlschlegel, J.A., and Carey, M. (2011). Mediator coordinates PIC assembly with recruitment of CHD1. Genes Dev. *25*, 2198–2209.

Liokatis, S., Klingberg, R., Tan, S., and Schwarzer, D. (2016). Differentially Isotope-Labeled Nucleosomes To Study Asymmetric Histone Modification Crosstalk by Time-Resolved NMR Spectroscopy. Angew. Chemie - Int. Ed. *55*, 8262–8265.

Liu, W., Lindberg, J., Sui, G., Luo, J., Egevad, L., Li, T., Xie, C., Wan, M., Kim, S.T., Wang, Z., et al. (2012). Identification of novel CHD1-associated collaborative alterations of genomic structure and functional assessment of CHD1 in prostate cancer. Oncogene *31*, 3939–3948.

Liu, X., Li, M., Xia, X., Li, X., and Chen, Z. (2017). Mechanism of chromatin remodelling revealed by the Snf2-nucleosome structure. Nature *544*, 440–445.

Long, L., Furgason, M., and Yao, T. (2014). Generation of nonhydrolyzable ubiquitin–histone mimics. Methods *70*, 134–138.

Lorch, Y., and Kornberg, R.D. (2015). Chromatin-remodeling and the initiation of transcription. Q. Rev. Biophys. *48*, 465–470.

Lorch, Y., Maier-Davis, B., and Kornberg, R.D. (2018). Histone Acetylation Inhibits RSC and Stabilizes the +1 Nucleosome. Mol. Cell *0*.

Lowary, P.T., and Widom, J. (1997). Nucleosome packaging and nucleosome positioning of genomic DNA. Proc. Natl. Acad. Sci. *94*, 1183–1188.

Lowary, P.T., and Widom, J. (1998). New DNA sequence rules for high affinity binding to histone octamer and sequence-directed nucleosome positioning. J. Mol. Biol. *276*, 19–42.

Luger, K., Mäder, A.W., Richmond, R.K., Sargent, D.F., and Richmond, T.J. (1997). Crystal structure of the nucleosome core particle at 2.8 A resolution. Nature *389*, 251–260.

Luger, K., Rechsteiner, T.J., and Richmond, T.J. (1999). Expression and Purification of Recombinant Histones and Nucleosome Reconstitution BT - Chromatin Protocols. In Chromatin Protocols, (New Jersey: Humana Press), pp. 1–16.

Lusser, A., Urwin, D.L., and Kadonaga, J.T. (2005). Distinct activities of CHD1 and ACF in ATP-dependent chromatin assembly. Nat. Struct. Mol. Biol. *12*, 160–166.

Maeshima, K., Hihara, S., and Eltsov, M. (2010). Chromatin structure: Does the 30-nm fibre exist in vivo? Curr. Opin. Cell Biol. *22*, 291–297.

Maeshima, K., Rogge, R., Tamura, S., Joti, Y., Hikima, T., Szerlong, H., Krause, C., Herman, J., Seidel, E., DeLuca, J., et al. (2016). Nucleosomal arrays self-assemble into supramolecular globular structures lacking 30-nm fibers. EMBO J. *35*, 1115–1132.

Maier, V.K., Chioda, M., Rhodes, D., and Becker, P.B. (2008). ACF catalyses chromatosome movements in chromatin fibres. EMBO J. *27*, 817–826.

Makde, R.D., England, J.R., Yennawar, H.P., and Tan, S. (2010). Structure of RCC1 chromatin factor bound to the nucleosome core particle. Nature *467*, 562–566.

Marfella, C.G.A., and Imbalzano, A.N. (2007). The Chd family of chromatin remodelers. Mutat Res *618*, 30–40.

Margueron, R., Justin, N., Ohno, K., Sharpe, M.L., Son, J., Drury, W.J., Voigt, P., Martin, S.R., Taylor, W.R., De Marco, V., et al. (2009). Role of the polycomb protein EED in the propagation of repressive histone marks. Nature *461*, 762–767.

Marras, S.A.E., Kramer, F.R., and Tyagi, S. (2002). Efficiencies of fluorescence resonance energy transfer and contact-mediated quenching in oligonucleotide probes. Nucleic Acids Res. *30*, e122.

Mavrich, T.N., Ioshikhes, I.P., Venters, B.J., Jiang, C., Tomsho, L.P., Qi, J., Schuster, S.C., Albert, I., and Pugh, B.F. (2008). A barrier nucleosome model for statistical positioning of nucleosomes throughout the yeast genome. Genome Res. *18*, 1073–1083.

Mazurkiewicz, J., Kepert, J.F., and Rippe, K. (2006). On the mechanism of nucleosome assembly by histone chaperone NAP1. J. Biol. Chem. *281*, 16462–16472.

McDowall, A.W., Smith, J.M., and Dubochet, J. (1986). Cryo-electron microscopy of vitrified chromosomes in situ. EMBO J. *5*, 1395–1402.

McGinty, R.K., and Tan, S. (2015). Nucleosome Structure and Function. Chem. Rev. *115*, 2255–2273.

McGinty, R.K., Henrici, R.C., and Tan, S. (2014). Crystal structure of the PRC1 ubiquitylation module bound to the nucleosome. Nature *514*, 591–596.

McKnight, J.N., Jenkins, K.R., Nodelman, I.M., Escobar, T., and Bowman, G.D. (2011). Extranucleosomal DNA Binding Directs Nucleosome Sliding by Chd1. Mol. Cell. Biol. *31*, 4746–4759.

Mizuguchi, G., Shen, X., Landry, J., Wu, W.H., Sen, S., and Wu, C. (2004). ATP-Driven Exchange of Histone H2AZ Variant Catalyzed by SWR1 Chromatin Remodeling Complex. Science (80-.). *303*, 343–348.

Morgan, M.T., Haj-Yahya, M., Ringel, A.E., Bandi, P., Brik, A., and Wolberger, C. (2016). Structural basis for histone H2B deubiquitination by the SAGA DUB module. Science (80-.). *351*, 725–728.

Moudrianakis, E.N., and Arents, G. (1993). Structure of the histone octamer core of the nucleosome and its potential interactions with DNA. Cold Spring Harb. Symp. Quant. Biol. *58*, 273–279.

Ngo, T.T.M., Zhang, Q., Zhou, R., Yodh, J.G., and Ha, T. (2015). Asymmetric Unwrapping of Nucleosomes under Tension Directed by DNA Local Flexibility. Cell *160*, 1135–1144.

Nodelman, I.M., Horvath, K.C., Levendosky, R.F., Winger, J., Ren, R., Patel, A., Li, M., Wang, M.D., Roberts, E., and Bowman, G.D. (2016). The Chd1 chromatin remodeler can sense both entry and exit sides of the nucleosome. Nucleic Acids Res. *44*.

Nodelman, I.M., Bleichert, F., Patel, A., Ren, R., Horvath, K.C., Berger, J.M., and Bowman, G.D. (2017). Interdomain Communication of the Chd1 Chromatin Remodeler across the DNA Gyres of the Nucleosome. Mol. Cell *65*, 447–459.e6.

North, J.A., Shimko, J.C., Javaid, S., Mooney, A.M., Shoffner, M.A., Rose, S.D., Bundschuh, R., Fishel, R., Ottesen, J.J., and Poirier, M.G. (2012). Regulation of the nucleosome unwrapping rate controls DNA accessibility. Nucleic Acids Res. *40*, 10215–10227.

Olins, D.E., and Olins, A.L. (2003). Chromatin history: our view from the bridge. Nat. Rev. Mol. Cell Biol. *4*, 809–814.

Ong, M.S., Richmond, T.J., and Davey, C.A. (2007). DNA Stretching and Extreme Kinking in the Nucleosome Core. J. Mol. Biol. *368*, 1067–1074.

Ou, H.D., Phan, S., Deerinck, T.J., Thor, A., Ellisman, M.H., and O'Shea, C.C. (2017). ChromEMT: Visualizing 3D chromatin structure and compaction in interphase and mitotic cells. Science (80-.). *357*, eaag0025-15.

Patel, A., McKnight, J.N., Genzor, P., and Bowman, G.D. (2011). Identification of residues in chromodomain helicase DNA-binding protein 1 (Chd1) required for coupling ATP hydrolysis to nucleosome sliding. J. Biol. Chem. *286*, 43984–43993.

Patel, A., Chakravarthy, S., Morrone, S., Nodelman, I.M., McKnight, J.N., and Bowman, G.D. (2013). Decoupling nucleosome recognition from DNA binding dramatically alters the properties of the Chd1 chromatin remodeler. Nucleic Acids Res. *41*, 1637–1648.

Pavri, R., Zhu, B., Li, G., Trojer, P., Mandal, S., Shilatifard, A., and Reinberg, D. (2006). Histone H2B monoubiquitination functions cooperatively with FACT to regulate elongation by RNA polymerase II. Cell *125*, 703–717.

Pennings, S., Meersseman, G., and Bradbury, E.M. (1991). Mobility of positioned nucleosomes on 5 S rDNA. J. Mol. Biol. *220*, 101–110.

Pointner, J., Persson, J., Prasad, P., Norman-Axelsson, U., Strålfors, A., Khorosjutina, O., Krietenstein, N., Peter Svensson, J., Ekwall, K., and Korber, P. (2012). CHD1 remodelers regulate nucleosome spacing in vitro and align nucleosomal arrays over gene coding regions in S. pombe. EMBO J. *31*, 4388–4403.

Qiu, Y., Levendosky, R.F., Chakravarthy, S., Patel, A., Bowman, G.D., and Myong, S. (2017). The Chd1 Chromatin Remodeler Shifts Nucleosomal DNA Bidirectionally as a Monomer. Mol. Cell *68*, 76–88.e6.

Racki, L.R., Yang, J.G., Naber, N., Partensky, P.D., Acevedo, A., Purcell, T.J., Cooke, R., Cheng, Y., and Narlikar, G.J. (2009). The chromatin remodeller ACF acts as a dimeric motor to space nucleosomes. Nature *462*, 1016–1021.

Radman-Livaja, M., Quan, T.K., Valenzuela, L., Armstrong, J.A., van Welsem, T., Kim, T., Lee, L.J., Buratowski, S., van Leeuwen, F., Rando, O.J., et al. (2012). A Key Role for Chd1 in Histone H3 Dynamics at the 3′ Ends of Long Genes in Yeast. PLoS Genet. *8*, e1002811-10.

Ramachandran, S., Zentner, G.E., and Henikoff, S. (2015). Asymmetric nucleosomes flank promoters in the budding yeast genome. Genome Res. *25*, 381–390.

Rasnik, I., McKinney, S.A., and Ha, T. (2006). Nonblinking and long-lasting single-molecule fluorescence imaging. Nat. Methods *3*, 891–893.

Reinke, H., Gregory, P.D., and Hörz, W. (2001). A transient histone hyperacetylation signal marks nucleosomes for remodeling at the PHO8 promoter in vivo. Mol. Cell *7*, 529–538.

Rhee, H.S., Bataille, A.R., Zhang, L., and Pugh, B.F. (2014). Subnucleosomal Structures and Nucleosome Asymmetry across a Genome. Cell *159*, 1377–1388.

Robinson, P.J.J., Fairall, L., Huynh, V.A.T., and Rhodes, D. (2006). EM measurements define the dimensions of the "30-nm" chromatin fiber: Evidence for a compact, interdigitated structure. Proc. Natl. Acad. Sci. *103*, 6506–6511.

Roussel, L., Erard, M., Cayrol, C., and Girard, J.P. (2008). Molecular mimicry between IL-33 and KSHV for attachment to chromatin through the H2A-H2B acidic pocket. EMBO Rep. *9*, 1006–1012.

Ruthenburg, A.J., Li, H., Patel, D.J., and Allis, C.D. (2007). Multivalent engagement of chromatin modifications by linked binding modules. Nat. Rev. Mol. Cell Biol. *8*, 983–994.

Ryan, D.P., Sundaramoorthy, R., Martin, D., Singh, V., and Owen-Hughes, T. (2011). The DNA-binding domain of the Chd1 chromatin-remodelling enzyme contains SANT and SLIDE domains. EMBO J. *30*, 2596–2609.

Saha, A., Wittmeyer, J., and Cairns, B.R. (2005). Chromatin remodeling through directional DNA translocation from an internal nucleosomal site. Nat. Struct. Mol. Biol. *12*, 747–755.

Sanborn, M.E., Connolly, B.K., Gurunathan, K., and Levitus, M. (2007). Fluorescence Properties and Photophysics of the Sulfoindocyanine Cy3 Linked Covalently to DNA. J. Phys. Chem. B *111*, 11064–11074.

Schalch, T., Duda, S., Sargent, D.F., and Richmond, T.J. (2005). X-ray structure of a tetranucleosome and its implications for the chromatin fibre. Nature *436*, 138–141.

Schiessel, H., Widom, J., Bruinsma, R.F., and Gelbart, W.M. (2001). Polymer reptation and nucleosome repositioning. Phys. Rev. Lett. *86*, 4414–4417.

Schwanbeck, R., Xiao, H., and Wu, C. (2004). Spatial contacts and nucleosome step movements induced by the NURF chromatin remodeling complex. J. Biol. Chem. *279*, 39933–39941.

Schwarz, P.M., and Hansen, J.C. (1994). Formation and stability of higher order chromatin structures. Contributions of the histone octamer. J. Biol. Chem. *269*, 16284–16289.

Schwarz, P.M., Felthauser, A., Fletcher, T.M., and Hansen, J.C. (1996). Reversible oligonucleosome self-association: dependence on divalent cations and core histone tail domains. Biochemistry *35*, 4009–4015.

Shahian, T., and Narlikar, G.J. (2012). Analysis of changes in nucleosome conformation using fluorescence resonance energy transfer. Methods Mol. Biol. *833*, 337–349.

Shogren-Knaak, M., Ishii, H., Sun, J.-M., Pazin, M.J., Davie, J.R., and Peterson, C.L. (2006). Histone H4-K16 Acetylation Controls Chromatin Structure and Protein Interactions. Science (80-.). *311*, 844–847.

Shrestha, D., Jenei, A., Nagy, P., Vereb, G., and Szöllősi, J. (2015). Understanding FRET as a research tool for cellular studies.

Simic, R., Lindstrom, D.L., Tran, H.G., Roinick, K.L., Costa, P.J., Johnson, A.D., Hartzog, G.A., and Arndt, K.M. (2003). Chromatin remodeling protein Chd1 interacts with transcription elongation factors and localizes to transcribed genes. EMBO J. *22*, 1846–1856.

Simon, M., North, J.A., Shimko, J.C., Forties, R.A., Ferdinand, M.B., Manohar, M., Zhang, M., Fishel, R., Ottesen, J.J., and Poirier, M.G. (2011). Histone fold modifications control nucleosome unwrapping and disassembly. Proc. Natl. Acad. Sci. 1–6.

Smolle, M., Venkatesh, S., Gogol, M.M., Li, H., Zhang, Y., Florens, L., Washburn, M.P., and Workman, J.L. (2012). Chromatin remodelers Isw1 and Chd1 maintain chromatin structure during transcription by preventing histone exchange. Nat. Struct. Mol. Biol. *19*, 884–892.

Song, F., Chen, P., Sun, D., Wang, M., Dong, L., Liang, D., Xu, R.-M., Zhu, P., and Li, G. (2014). Cryo-EM Study of the Chromatin Fiber Reveals a Double Helix Twisted by Tetranucleosomal Units. Science. *344*, 376–380.

Stennett, E.M.S., Ciuba, M.A., Lin, S., and Levitus, M. (2015). Demystifying PIFE: The Photophysics Behind the Protein-Induced Fluorescence Enhancement Phenomenon in Cy3. J. Phys. Chem. Lett. *6*, 1819–1823.

Stockdale, C., Flaus, A., Ferreira, H., and Owen-Hughes, T. (2006). Analysis of nucleosome repositioning by yeast ISWI and Chd1 chromatin remodeling complexes. J. Biol. Chem. *281*, 16279–16288.

Sundaramoorthy, R., Hughes, A.L., Singh, V., Wiechens, N., Ryan, D.P., El-Mkami, H., Petoukhov, M., Svergun, D.I., Treutlein, B., Quack, S., et al. (2017). Structural reorganization of the chromatin remodeling enzyme Chd1 upon engagement with nucleosomes. Elife *6*, 1405.

Sundaramoorthy, R., Hughes, A.L., El-Mkami, H., Norman, D.G., Ferreira, H., and Owen-Hughes, T. (2018). Structure of the chromatin remodelling enzyme Chd1 bound to a ubiquitinylated nucleosome. Elife *7*, 1–28.

Sundstroem, V., and Gillbro, T. (1982). Viscosity-dependent isomerization yields of some cyanine dyes. A picosecond laser spectroscopy study. J. Phys. Chem. *86*, 1788–1794.

Tee, W.-W., and Reinberg, D. (2014). Chromatin features and the epigenetic regulation of pluripotency states in ESCs. Development *141*, 2376–2390.

Tims, H., and Widom, J. (2007). Stopped-flow fluorescence resonance energy transfer for analysis of nucleosome dynamics. Methods *41*, 296–303.

Tims, H.S., Gurunathan, K., Levitus, M., and Widom, J. (2011). Dynamics of nucleosome invasion by DNA binding proteins. J. Mol. Biol. *411*, 430–448.

Tokuda, J.M., Ren, R., Levendosky, R.F., Tay, R.J., Yan, M., Pollack, L., and Bowman, G.D. (2018). The ATPase motor of the Chd1 chromatin remodeler stimulates DNA unwrapping from the nucleosome. Nucleic Acids Res. *46*, 4978–4990.

Tremethick, D.J. (2007). Higher-Order Structures of Chromatin: The Elusive 30 nm Fiber. Cell *128*, 651–654.

Tsukiyama, T., Palmer, J., Landel, C.C., Shiloach, J., and Wu, C. (1999). Characterization of the imitation switch subfamily of ATP-dependent chromatin-remodeling factors in Saccharomyces cerevisiae. Genes Dev. *13*, 686–697.

Venkatesh, S., and Workman, J.L. (2015). Histone exchange, chromatin structure and the regulation of transcription. Nat. Publ. Gr. *16*, 178–189.

Vogler, C., Huber, C., Waldmann, T., Ettig, R., Braun, L., Izzo, A., Daujat, S., Chassignet, I., Lopez-Contreras, A.J., Fernandez-Capetillo, O., et al. (2010). Histone H2A C-Terminus Regulates Chromatin Dynamics, Remodeling, and Histone H1 Binding. PLoS Genet. *6*, e1001234-12.

Voigt, P., LeRoy, G., Drury III, W.J., Zee, B.M., Son, J., Beck, D.B., Young, N.L., Garcia, B.A., and Reinberg, D. (2012). Asymmetrically Modified Nucleosomes. Cell *151*, 181–193.

Voigt, P., Tee, W.W., and Reinberg, D. (2013). A double take on bivalent promoters. Genes Dev. *27*, 1318–1338.

Weiner, A., Hughes, A., Yassour, M., Rando, O.J., and Friedman, N. (2010). High-resolution nucleosome mapping reveals transcription-dependent promoter packaging. Genome Res. *20*, 90–100.

Wiechens, N., Singh, V., Gkikopoulos, T., Schofield, P., Rocha, S., and Owen-Hughes, T. (2016). The Chromatin Remodelling Enzymes SNF2H and SNF2L Position Nucleosomes adjacent to CTCF and Other Transcription Factors. PLoS Genet. *12*, e1005940.

Winger, J., and Bowman, G.D. (2017). The Sequence of Nucleosomal DNA Modulates Sliding by the Chd1 Chromatin Remodeler. J. Mol. Biol. *429*, 808–822.

Winger, J., Nodelman, I.M., Levendosky, R.F., and Bowman, G.D. (2018). A twist defect mechanism for ATP-dependent translocation of nucleosomal DNA. Elife *7*, 1–23.

Wozniak, G.G., and Strahl, B.D. (2014). Hitting the "mark": Interpreting lysine methylation in the context of active transcription. Biochim. Biophys. Acta - Gene Regul. Mech. *1839*, 1353–1361.

Xiao, T., Kao, C.-F., Krogan, N.J., Sun, Z.-W., Greenblatt, J.F., Osley, M.A., and Strahl, B.D. (2005). Histone H2B ubiquitylation is associated with elongating RNA polymerase II. Mol. Cell. Biol. *25*, 637–651.

Yan, L., Wang, L., Tian, Y., Xia, X., and Chen, Z. (2016). Structure and regulation of the chromatin remodeller ISWI. Nature.

Yang, J., and Narlikar, G. (2007). FRET-based methods to study ATP-dependent changes in chromatin structure. Methods *41*, 291–295.

Yang, J.G., Madrid, T.S., Sevastopoulos, E., and Narlikar, G.J. (2006). The chromatin-remodeling enzyme ACF is an ATP-dependent DNA length sensor that regulates nucleosome spacing. Nat. Struct. Mol. Biol. *13*, 1078–1083.

Yen, K., Vinayachandran, V., Batta, K., Koerber, R.T., and Pugh, B.F. (2012). Genome-wide nucleosome specificity and directionality of chromatin remodelers. Cell *149*, 1461–1473.

Zhang, Z., Wippo, C.J., Wal, M., Ward, E., Korber, P., and Pugh, B.F. (2011). A packing mechanism for nucleosome organization reconstituted across a eukaryotic genome. Science (80-.). *332*, 977–980.

Zofall, M., Persinger, J., and Bartholomew, B. (2004). Functional Role of Extranucleosomal DNA and the Entry Site of the Nucleosome in Chromatin Remodeling by ISW2. Mol. Cell. Biol. *24*, 10047–10057.

Zofall, M., Persinger, J., Kassabov, S.R., and Bartholomew, B. (2006). Chromatin remodeling by ISW2 and SWI/SNF requires DNA translocation inside the nucleosome. Nat. Struct. Mol. Biol. *13*, 339–346.

CURRICULUM VITAE

Robert F. Levendosky

Born September 3rd, 1977 in Silver Spring, Maryland

Education

Ph.D. **Johns Hopkins University** Program in Cell, Molecular, Developmental Biology and Biophysics
Completed in Winter 2019

B.S. **Northeastern Illinois University** Biology major and Chemistry minor.
Graduated Summa Cum Laude in 2013

Experience

- **Graduate researcher** in the Laboratory of Gregory D. Bowman at Johns Hopkins University 2014-present
    - Used biochemical and biophysical methods to elucidate the activity and regulation of the Chd1 chromatin remodeler. Extensively studied the nucleosome structure and how that relates to nucleosome sliding by Chd1.
    - Participated in experimental design and preparation of figures and manuscripts for publication.
    - Helped in developing novel tools within the field. This includes producing nucleosomes with defined asymmetrically placed modifications, generating novel sites for histone mapping, and development of novel FRET labeling schemes to track nucleosome movement.
    - Helped bring outside techniques to the lab. This included site-specific covalent crosslinking to add protein modifications to histones, hydroxyl radical foot-printing
    - Refined established lab protocols. This includes eliminating inefficient parts of a site-specific histone mapping protocol and expanding that protocol to provide greater time resolution.
    - Developed tools for streamlining data analysis.
    - Participated in fruitful collaborations with outside labs.
    - Helped manage and maintain lab equipment.
    - Trained new students and acted as mentor for student projects.
    - Provided thoughtful feedback, ideas, and encouragement to all members of the lab and department, demonstrating a positive scientific philosophy.
- **Volunteer researcher** in the Laboratory of Michael Schirmer at Northeastern 2012-2013

Illinois University

- Investigated the role of Cryptochrome 1 (Cry1) in the circadian molecular clock.
- Helped with animal care and genotyping
- Transfected mammalian cell cultures with Cry1, imaged cells with bright-field microscopy and quantified cellular morphology.

- **Co-owner/Manager** of Square Design and Fine Woodworking 2004-2011
  - Produced custom woodwork, furniture and cabinetry
  - Directed sales and bookkeeping
  - Managed fabrication and engineering

Publications/Presentations

Journal Articles

- Sebanstev, A., **Levendosky, R. F.**, Bowman, G. D., Deindl, S. (2019 *under review*). Direct observation of coordinated DNA movements on the nucleosome during chromatin remodeling. *Nature Communications* Under Review
  - First two authors should be considered co-first authors
- Winger, J., Nodelman, I. M., Levendosky, R. F., & Bowman, G. D. (2018). A twist defect mechanism for ATP-dependent translocation of nucleosomal DNA. *eLife*, *7*, 391. http://doi.org/10.7554/eLife.34100 2018
- Tokuda, J. M., Ren, R., **Levendosky, R. F.**, Tay, R. J., Yan, M., Pollack, L., & Bowman, G. D. (2018). The ATPase motor of the Chd1 chromatin remodeler stimulates DNA unwrapping from the nucleosome. *Nucleic Acids Research*, *37*, 54. http://doi.org/10.1093/nar/gky206 2018
  - First three authors should be considered co-first authors
- Qiu, Y., **Levendosky, R. F.**, Chakravarthy, S., Patel, A., Bowman, G. D., & Myong, S. (2017). The Chd1 Chromatin Remodeler Shifts Nucleosomal DNA Bidirectionally as a Monomer. *Molecular Cell*. http://doi.org/10.1016/j.molcel.2017.08.018 2017
- **Levendosky, R. F.**, Sabantsev, A., Deindl, S., & Bowman, G. D. (2016). The Chd1 chromatin remodeler shifts hexasomes unidirectionally. *eLife*, *5*, 3302. http://doi.org/10.7554/eLife.21356 2016
- Nodelman, I. M., Horvath, K. C., **Levendosky, R. F.**, Winger, J., Ren, R., Patel, A., et al. (2016). The Chd1 chromatin remodeler can sense both entry and exit sides of the nucleosome. *Nucleic Acids Research*, *44*(16), 7580–7591. http://doi.org/10.1093/nar/gkw406 2016

Presentations

- Talk presented at the semi-annual Johns Hopkins Chromatin Workshop "Chd1 induces nucleotide-dependent unwrapping of nucleosomal DNA" 2017
- Poster presented at Biophysics Department recruitment weekend "The Chd1 chromatin remodeler shifts hexasomes unidirectionally" 2017
- Poster presented at the NCI Symposium on Chromatin Biology "The Chd1 chromatin remodeler shifts hexasomes unidirectionally" 2016
- Talk presented at the Johns Hopkins Bi-Monthly Chromatin Meeting "Recognition of the H2A/H2B heterodimer regulates nucleosome sliding by Chd1" 2016
- Talk presented to the Johns Hopkins Biophysics Department Student Series "Recognition of the H2A/H2B heterodimer regulates nucleosome sliding by Chd1" 2016
- Progress report talk presented to the Johns Hopkins Biology Department "Recognition of the H2A/H2B heterodimer regulates nucleosome sliding by Chd1" 2016
- Poster presented at the Johns Hopkins Biophysics Department retreat: "Hexasome remodeling by Chd1" 2015
- Poster presented at the Meeting of the Biophysical Society: "Using FRET to monitor nucleosome movement by the Chd1 chromatin remodeler" 2015
- Poster presented at the Johns Hopkins Biology Department retreat: "Monitoring nucleosome movement by Chd1 using FRET" 2014
- Poster presented at the Johns Hopkins Biophysics Department retreat: "Monitoring nucleosome movement by Chd1 using FRET" 2014

Teaching Experience

- Teachers Assistant for Intro to Computing at Johns Hopkins University Fall 2016
    - Assisted with in-class guidance.
    - Helped prepare homework questions.
    - Graded homework and exams.
- Teachers Assistant for Cell Biology at Johns Hopkins University Spring 2015
    - Conducted laboratory instruction.
    - Graded laboratory reports and exams.
- Teachers Assistant for Biochemistry at Johns Hopkins University Fall 2014
    - Conducted laboratory instruction.

- Graded laboratory reports and exams.

- Teachers Assistant for Cell Biology at Northeastern Illinois University — Spring 2013
  - Prepared and taught lectures in membrane transport, action potentials and muscle contraction.
  - Prepared and taught an original laboratory session.
  - Assisted with grading assignments and exams.

Students Trained

- Mentored rotating graduate student investigating how DNA propagates around the nucleosome during remodeling. — Spring 2018
  - Trained student in generation of single stranded gaps in DNA, large scale PCR, DNA purification, nucleosome purification, site-specific histone mapping assays, running DNA sequencing gels.
- Mentored undergraduate/post-baccalaureate student in a project to develop additional histone crosslinking sites to track DNA movement on additional regions of the nucleosome. — Fall 2016-Fall 2017
  - Trained student in mutagenesis, denaturing protein purification from inclusion bodies, native protein purification, large scale PCR, DNA purification, nucleosome purification, site-specific histone mapping assays and running DNA sequencing gels.
- Mentored rotating graduate student investigating how Chd1 slides nucleosomes containing modified/mutated histones. — Fall 2015
  - Trained student in protein purification, large scale PCR, DNA purification, nucleosome purification, site-specific histone mapping assays, running DNA sequencing gels, fluorescence assays to measure nucleosome sliding kinetics and data analysis.
- Mentored rotating graduate student investigating how Chd1 binds to hexasomes as compared to nucleosomes. — Spring 2015
  - Trained student in protein purification, large scale PCR, DNA purification, nucleosome purification, site-specific histone mapping assays, running DNA sequencing gels, fluorescence binding assays and data analysis.

Affiliations/Memberships

- Alpha Chi National Honor Society 2012-present
- SACNAS (Society for the Advancement of Chicanos and Native Americans in Science) member 2012-2013

Skills

Laboratory Skills

- Molecular cloning and mutagenesis
- Exonuclease and endonuclease digestions
- Polymerase chain reaction
- Protein Purification
    - Fast Protein Liquid Chromatography
    - Native and denaturing purifications
    - Affinity, ion exchange and size exclusion chromatography
- Native acrylamide DNA and nucleosome purification
- Native and SDS-PAGE
- Urea denaturing PAGE
- Sanger Sequencing
- Protein-DNA crosslinking
- Protein-protein site-specific covalent crosslinking
- Hydroxyl radical foot-printing
- NADH ATPase assay
- Fluorescent labeling of protein and DNA
- Fluorescence Resonance Energy Transfer (FRET) design, experimentation and data analysis
- Fluorescence binding assays
- Western blotting

Computer Programs

- Mathematica: programing, data fitting and analysis optimization, figure design
- PyMOL: molecular visualization design, movie design, assemble and dock molecules using python scripts
- Python: basic programing for data extraction, manipulation and analysis
- MATLAB: familiar with use for data analysis
- Adobe Illustrator: generation of cartoons to visually explain complex scientific ideas. Generation of final figures for publications and presentations.
- Adobe Photoshop
- Microsoft Word, Power Point and Excel

Interests

- Music: guitar, vocals, songwriting, improvisation and teaching my children music
- Sports: Tennis, Golf, Soccer
- Outdoors: Hiking, Camping, Climbing